NASA Contractor Report 191581

ICASE Report No. 93-93

ICASE

20 Years of Excellence

THE NONLINEAR GALERKIN METHOD: A MULTI-SCALE METHOD APPLIED TO THE SIMULATION OF HOMOGENEOUS TURBULENT FLOWS

A. Debussche

T. Dubois

R. Temam

NASA Contract No. NAS1-19480
December 1993

Institute for Computer Applications in Science and Engineering
NASA Langley Research Center
Hampton, Virginia 23681-0001

Operated by the Universities Space Research Association

National Aeronautics and
Space Administration

Langley Research Center
Hampton, Virginia 23681-0001

ICASE Fluid Mechanics

Due to increasing research being conducted at ICASE in the field of fluid mechanics, future ICASE reports in this area of research will be printed with a green cover. Applied and numerical mathematics reports will have the familiar blue cover, while computer science reports will have yellow covers. In all other aspects the reports will remain the same; in particular, they will continue to be submitted to the appropriate journals or conferences for formal publication.

The Nonlinear Galerkin Method : A multi-scale method applied to the simulation of homogeneous turbulent flows

A.Debussche, T.Dubois and R.Temam[1]

Laboratoire d'Analyse Numérique
Bât. 425, *Université Paris-Sud, 91405 Orsay*
and
The Institute for Applied Mathematics and Scientific Computing,
Indiana University, Bloomington, Indiana 47405

ABSTRACT

Using results of DNS in the case of two-dimensional homogeneous isotropic flows, we first analyze in detail the behavior of the small and large scales of Kolmogorov like flows at moderate Reynolds numbers. We derive several estimates on the time variations of the small eddies and the nonlinear interaction terms; those terms play the role of the Reynolds stress tensor in the case of LES. Since the time step of a numerical scheme is determined as a function of the energy-containing eddies of the flow, the variations of the small scales and of the nonlinear interaction terms over one iteration can become negligible by comparison with the accuracy of the computation. Based on this remark, we propose a multilevel scheme which treats differently the small and the large eddies. Using mathematical developments, we derive estimates of all the parameters involved in the algorithm, which then becomes a completely self-adaptive procedure. Finally, we perform realistic simulations of (Kolmorov like) flows over several eddy-turnover times. The results are analyzed in detail and a parametric study of the nonlinear Galerkin method is performed.

[1] Part of the work was done while the second and third authors were visiting the Institute for Computer Applications in Science and Engineering (ICASE), NASA Langley Research Center, Hampton, VA 23681.

Introduction

A turbulent flow can be characterized by a spatial and temporal chaotic behaviour. Indeed, strong gradients may appear and, in the physical space, several structures with various sizes are generated by the external force and by the flow itself. The structures are convected by the mean flow. In the case of viscous incompressible flows in dimension two, thin and elongated sheets of vorticity appear. These structures are characteristic of incompressible flows. The phenomenological theory of turbulence, introduced by Kolmogorov in dimension three and Kraichnan in dimension two, predicts that the size of the smallest scales of a flow decreases while the nondimensional Reynolds number grows. So, the number of degrees of freedom required to describe the motion can be estimated in terms of the Reynolds number ($\sim cRe$ in space dimension two).
Hence, a Direct Numerical Simulation, i.e. the resolution of all physically relevant scales, can not be achieved when the Reynolds number becomes too high and then, when the turbulence is fully developed. A model is then used in many simulations ; i.e. the small scales are not exactly integrated but their interaction with the large ones are taken into account in a simplified way. Basically, the aim of these models is to recover the large eddies of the flow (or their statistic) without explicitly computing all the scales of motion.

In relation with recent developments in the theory of dynamical systems and its application to turbulence phenomena, new objects have been introduced (exact or approximate inertial manifolds, see Foias, Manley and Temam [1]) and new numerical methods have been proposed (the nonlinear Galerkin methods, see Marion and Temam [2] and [3], the incremental unknown method, see Temam [4]). These objects and methods are based on a decomposition of the unknown, such as the velocity field, into its small scale component and its large scale one, and essential in the nonlinear Galerkin method is a systematically differentiated treatment of the small and large scales.

These approximate inertial manifolds are subsets of the phase space and consist in an approximate form of the small scale equations. They provide an adiabatic law modeling the interaction between the low and the high fre-

quency components of the flow ; the small eddies are in fact expressed as a nonlinear function of the large ones, they are slaved by the large ones. Moreover, these manifolds enjoy the property that they attract all the orbits exponentially fast in time and that they contain the attractor in a thin neighborhood. In that sense, they provide a good way to approximate the solutions of the Navier–Stokes equations. The nonlinear Galerkin method, proposed by Marion and Temam [2], consists in looking for a solution lying on these specific subsets of the phase space. Several implementations of this scheme have previously been done by Jauberteau, Rosier and Temam ([5] and [6]), and Dubois, Jauberteau and Temam ([7]). Results presented in these papers were mainly feasibility tests involving exact solutions (analytical), where the authors tried to recover known velocity and pressure fields. These tests provided good indications on computational feasibility and performances, but had no physical relevance. In the present article we intend to develop further the study of the numerical implementation of the nonlinear Galerkin method for flow problems. We have several objectives which we describe hereafter in some details. Firstly, we would like to compute physically more relevant flows, namely here Kolmogorov type flows. Secondly, the effective implementation of the nonlinear Galerkin method involves several parameters (such as the cut–off wavelength between low and high frequencies, and the time during which the high frequencies are allowed to be frozen) ; and another of our aims is to conduct a parametric study of the method, and to develop simple self–adaptive methods for the determination of these parameters.

Here, we consider two–dimensional periodic flows governed by the incompressible Navier–Stokes equations. Of course, such flows correspond more to an idealized situation rather than a physical one. Nevertheless, this model contains several difficulties which occur when simulating turbulent flows, and then it provides a good test to implement a numerical algorithm. More physically relevant situations, such as three–dimensional flows, will be presented elsewhere. In a parallel effort, we are also treating the case of a flow driven by a constant pressure gradient between two infinite parallel plates, namely the channel flow (see for instance [8]).
In the first section of the paper, we introduce the equations and several notations. Then, we define the decomposition of the velocity field into large scale components and small scale structures. This decomposition depends on a cut–off value, corresponding to a wave–number of the Fourier decomposition

of the unknowns, and provides two grids in the physical space. In previous theoretical works (see for instance [1] and [9]), the authors have rigorously proved that, for a sufficiently large wavenumber, the large scale components contain most of the energy of the flow. The small scale structures represent then small quantities, which have to be taken into account in order to correctly compute the large scales of motion. After recalling these results and comparing them with numerical simulations, we show, based on both theoretical and numerical investigations, that the time variation of the small eddies over one time step can be smaller than the energy carried by these scales themselves, when the cut–off value is chosen sufficiently large. A similar result is also proved for the nonlinear interaction terms expressing the action of the small eddies over the large ones. Then, introducing the expected accuracy of the computation ε as a parameter, we deduce that there exists a level such that the one–step time variation of the small scale components is smaller than ε. We note here that this result is not in contradiction with the fact that the small eddies evolve faster than the large ones. In fact, their time scales are smaller but their order of magnitude also decreases for large wavenumbers.
Hence, the time variations of part of the spectrum can be locally neglected. We have also proved that the interaction terms enjoy the same property. These two fundamental results are one of the keys of the numerical algorithm proposed in the following sections.

Based on these results, we have implemented a spatial and temporal multilevel adaptative method ; i.e. the level of refinement, which define the separation of the flow into low and high frequencies, evolves in time undergoing successive multilevel V–cycles ; moreover, it follows the dynamic of the small and the large scales of the motion. Moreover, some part of the spectrum are frozen, as well as the interaction terms, during short time periods. After a complete description of this multilevel procedure, we derive several estimates of characteristic time scales for the small structures and for the terms involving their interactions with the large scale components. These estimates provide an efficient way to evaluate the length of the time interval during which the small scales, corresponding to several levels of refinement, as well as the corresponding interaction terms are allowed to be frozen without introducing an error larger than the accuracy ε. Hence, we obtain a completely self–adaptative procedure which depend on only one parameter,

namely ε. At the end of each frozen period, the velocity field is projected on an Approximate Inertial Manifold (AIM), which provides a simple and efficient way to directly compute the high frequencies. We analyze here the perturbation introduced by using first order Approximate Inertial Manifolds and we deduce in which range of the spectrum the manifold can be used to compute the small scales.

The last section is devoted to the description and the analysis of several numerical simulations performed with the multiscale (Nonlinear Galerkin) method. The integral scale Reynolds number Re_L was successively set to 784 and to 6,328 for spatial resolutions of respectively $(256)^2$ and $(512)^2$. In these cases, a full dissipation range is resolved as the larger wavenumber is at least 6 times larger than the dissipation wavenumber. The Reynolds numbers are not sufficiently large for the solutions to have a k^{-3} energy spectrum power range ; indeed, the computed velocities have an intermediate energy spectrum between k^{-4} and k^{-3}. Nevertheless, the different scale components are strongly time dependent, and they provide interesting tests for the multilevel adaptative procedure. More physically relevant situations, eg simulations with larger Reynolds number, will be treated and presented elsewhere. For each simulation, the code has run during more than 50,000 time iterations, which represents $10s$ of unit hours on a Cray-2.
In this last section, we first compare the results obtained with a previous version of the algorithm with those obtained with the multiscale procedure described in subsection 2.4. For this comparison a Direct Numerical Simulation performed with a standard pseudo–spectral Galerkin approximation is used as a reference. In the previous versions of the algorithm ([7], [10]), there was no control of the variations of the small eddies. Hence, the cut–off wavelengths as well as the length of the period during which the variations of the small scales are frozen were not properly evaluated. This led to an accumulation of perturbations and a loss of the accuracy ; this is no more the case.
Finally, in order to study the effect of the cut–off wavelength on the numerical results, we perform several simulations with decreasing cut–off values. In fact, we show that the separation wavenumber can be taken of the order of the dissipation wavenumber k_η ; as k_η is of the order of 20, in our computation, the cut–off value can not reasonably take smaller value. Nevertheless, the standard Galerkin pseudo–spectral method, with a larger wavelength of

the order of the dissipation one, does not provide a sufficient resolution : the large scales of motion are not recovered in that case. Hence, the multiscale method provides an efficient way to simulate the enstrophy dissipation and the energy dissipation ranges. In order to describe the effect of the multiscale procedure inside the power range, simulations with larger Reynolds number have to be performed. Such study will be presented elsewhere.

1 Motivations.

1.1 Preliminary.

We consider here two–dimensional viscous incompressible flows driven by an external volume force $\mathbf{f}$, and governed by the Navier-Stokes equations :

$$\begin{cases} \dfrac{\partial \mathbf{u}}{\partial t} - \nu \Delta \mathbf{u} + (\mathbf{u} \cdot \boldsymbol{\nabla})\mathbf{u} + \boldsymbol{\nabla} p \;=\; \mathbf{f}, \\ \\ \boldsymbol{\nabla} \cdot \mathbf{u} \;=\; 0, \\ \\ \mathbf{u}(\mathbf{x}, t = 0) \;=\; \mathbf{u}_0(\mathbf{x}), \end{cases} \tag{1}$$

where $\mathbf{u}(\mathbf{x}, t) = (u_1(\mathbf{x}, t), u_2(\mathbf{x}, t))$ is the velocity field, $p(\mathbf{x}, t)$ the pressure ($\mathbf{x} = (x_1, x_2)$), ν is the kinetic viscosity and the density is set to unity. Equation (1) is supplemented with boundary conditions, namely $\mathbf{u}$ and p are periodic of period L_1 (resp. L_2) in the direction x_1 (resp. x_2). We denote by $\Omega = (0, L_1) \times (0, L_2)$ the period and we assume that the average of the external force over the period Ω vanishes, i.e. :

$$\frac{1}{\mid \Omega \mid} \int_\Omega \mathbf{f}(\mathbf{x}, t)\, d\mathbf{x} \;=\; 0, \quad \forall t.$$

Taking the average over the whole domain Ω of the momentum equation in (1) and using the periodicity of $\mathbf{u}$ and p, we obtain :

$$\frac{d}{dt} \left(\frac{1}{\mid \Omega \mid} \int_\Omega \mathbf{u}(\mathbf{x}, t)\, d\mathbf{x} \right) \;=\; 0.$$

Assuming now that the average of the initial condition is also zero, we conclude that the average of the velocity field vanishes :

$$\frac{1}{\mid \Omega \mid} \int_\Omega \mathbf{u}(\mathbf{x}, t)\, d\mathbf{x} \;=\; 0, \quad \forall t.$$

We now denote by $\boldsymbol{\omega} = \boldsymbol{\nabla} \times \mathbf{u}$ the vorticity and as usual we rewrite the conservation of momentum equation in (1) as :

$$\frac{\partial \mathbf{u}}{\partial t} - \nu \Delta \mathbf{u} + (\boldsymbol{\omega} \times \mathbf{u}) + \boldsymbol{\nabla} P \;=\; \mathbf{f}, \tag{2}$$

where $P = p + \frac{1}{2} \mid \mathbf{u} \mid^2$. This choice is motivated by two facts. First, it is important to note that a pseudo–spectral evaluation of $(\boldsymbol{\omega} \times \mathbf{u})$ requires three Fast Fourier Transforms (FFT) fewer than the usual form $(\mathbf{u} \cdot \boldsymbol{\nabla})\mathbf{u}$. Also, this form of the equations semi-conserves the kinetic energy for inviscid flows, when a collocation or pseudo-spectral discretization is used (see [11]) and ensures numerical stability, while the original form does not.

Since the unknowns $\mathbf{u}$ and p are space periodic functions, they can be expanded in Fourier series :

$$\begin{aligned} \mathbf{u}(\mathbf{x},t) &= \sum_{\mathbf{k}\in\mathbf{Z}^2} \hat{\mathbf{u}}(\mathbf{k},t)\, w_{\mathbf{k}}(\mathbf{x}), \\ p(\mathbf{x},t) &= \sum_{\mathbf{k}\in\mathbf{Z}^2} \hat{p}(\mathbf{k},t)\, w_{\mathbf{k}}(\mathbf{x}), \end{aligned} \tag{3}$$

where $w_{\mathbf{k}}(\mathbf{x}) = e^{2i\pi \mathbf{k}_L \cdot \mathbf{x}}$, $\mathbf{k}_L = (k_1/L_1, k_2/L_2)$ and $\mathbf{k}_L \cdot \mathbf{x} = (k_1 x_1/L_1 + k_2 x_2/L_2)$. The Fourier coefficients $\hat{\mathbf{u}}(\mathbf{k},t) = (\hat{u}_1(k_1,t), \hat{u}_2(k_2,t))$ (resp. $\hat{p}(\mathbf{k},t)$) are complex numbers and we recall that :

$$\begin{aligned} \hat{u}_i(-\mathbf{k},t) &= \bar{\hat{u}}_i(\mathbf{k},t), \quad i = 1 \text{ or } 2, \\ \hat{p}(-\mathbf{k},t) &= \bar{\hat{p}}(\mathbf{k},t), \end{aligned} \tag{4}$$

where $\bar{c}$ denotes the complex conjugate of c. This property is very important in practice ; it allows to store twice fewer coefficients in the second direction of the spectral space, when we look for a finite approximation of $\mathbf{u}(\mathbf{x},t)$ and $p(\mathbf{x},t)$, i.e. by storing $\hat{\mathbf{u}}(\mathbf{k},t)$ for $\mathbf{k}$ such that $k_2 \geq 0$, (4) allows us to recover the Fourier coefficients $\hat{\mathbf{u}}(\mathbf{k},t)$ for $k_2 < 0$.

Let us now introduce P_{div} the projection operator onto the divergence free space ; P_{div} can be easily expressed as :

$$P_{\text{div}}\boldsymbol{\varphi}(\mathbf{x}) = \sum_{\mathbf{k}\in\mathbf{Z}^2} \left(\hat{\boldsymbol{\varphi}}_{\mathbf{k}} - \frac{\mathbf{k}}{\mid \mathbf{k} \mid^2} (\mathbf{k} \cdot \hat{\boldsymbol{\varphi}}_{\mathbf{k}}) \right) w_{\mathbf{k}}(\mathbf{x}).$$

Assuming that $\mathbf{u}$ and p lie in the proper Hilbert spaces (see for instance [12], [13]) and applying P_{div} to the Navier-Stokes equations, we obtain

$$\frac{\partial \mathbf{u}}{\partial t} - \nu \Delta \mathbf{u} + B(\mathbf{u},\mathbf{u}) = \mathbf{g}, \tag{5}$$

where $\mathbf{g} = P_{\text{div}}\mathbf{f}$ and $B(\mathbf{u},\mathbf{u})$ is a bilinear form defined by :

$$\begin{aligned} B(\mathbf{u},\mathbf{u}) &= P_{\text{div}}(\boldsymbol{\omega}\times\mathbf{u}) \\ &= \sum_{\mathbf{k}\in\mathbf{Z}^2}\left((\widehat{\boldsymbol{\omega}\times\mathbf{u}})_{\mathbf{k}} - \frac{\mathbf{k}}{|\,\mathbf{k}\,|^2}(\mathbf{k}\cdot(\widehat{\boldsymbol{\omega}\times\mathbf{u}})_{\mathbf{k}})\right) w_{\mathbf{k}}\,(\mathbf{x}) \end{aligned} \tag{6}$$

As we shall see later, the numerical procedures are directly applied to this last form of the Navier–Stokes equations.

1.2 Separation of scales.

1.2.1 Small and large scales equations.

Let us choose an integer N. We introduce P_N the orthogonal projector onto the space spanned by the first N^2 Fourier modes. A pseudo–spectral Galerkin approximation $\mathbf{u}_N$ of the velocity field $\mathbf{u}$ is given by

$$\mathbf{u}_N(\mathbf{x},t) = \sum_{\mathbf{k}\in I_N}\hat{\mathbf{u}}(\mathbf{k},t)w_{\mathbf{k}}(\mathbf{x}),$$

where $I_N = [1-N/2, N/2]\times[0, N/2]$, and $\mathbf{u}_N$ satisfies the following equation

$$\frac{d\mathbf{u}_N}{dt} - \nu\Delta\mathbf{u}_N + P_N B(\mathbf{u}_N,\mathbf{u}_N) = P_N\mathbf{g}. \tag{7}$$

Here we only consider external force with no high wavenumber coefficients, namely :

$$\hat{\mathbf{g}}(\mathbf{k}) = 0, \text{ for } \mathbf{k}\in I_N\backslash I_{m_0}, \text{ for some } m_0. \tag{8}$$

Instead of (8), we can also assume that the spectrum of the external force has an exponential decay for wavenumbers larger than a given one.
We now introduce the decomposition

$$\mathbf{u}_N = \mathbf{y}_{N_1} + \mathbf{z}_{N_1}, \text{ with } m_0 \le N_1 \le N, \tag{9}$$

where

$$\mathbf{y}_{N_1} = P_{N_1}\mathbf{u}_N = \sum_{\mathbf{k}\in I_N}\hat{\mathbf{u}}(\mathbf{k},t)w_{\mathbf{k}} \tag{10}$$

and

$$\mathbf{z}_{N_1} \;=\; Q_{N_1}^N \mathbf{u}_N \;=\; \sum_{\mathbf{k}\in I_{N_1}^N = I_N \setminus I_{N_1}} \hat{\mathbf{u}}(\mathbf{k},t) w_{\mathbf{k}}. \tag{11}$$

We note that, in the decomposition (9), $\mathbf{y}_{N_1}$ represents the large-scale structures of the flow, and $\mathbf{z}_{N_1}$ corresponds to the small-scale components, or in other words, the fine structures of the flow. Since, the operators P_{N_1} and $Q_{N_1}^N$ commute with the differentiation operators, we have :

$$P_{N_1}(\Delta \mathbf{u}_N) \;=\; \Delta(P_{N_1}\mathbf{u}_N) \;=\; \Delta \mathbf{y}_{N_1},$$

and

$$Q_{N_1}^N(\Delta \mathbf{u}_N) \;=\; \Delta(Q_{N_1}^N \mathbf{u}_N) \;=\; \Delta \mathbf{z}_{N_1}.$$

By projecting (7) with respect to P_{N_1} and $Q_{N_1}^N$, we obtain the following coupled system of ordinary differential equations (ODE) :

$$\left\{ \begin{array}{l} \dfrac{\partial \mathbf{y}_{N_1}}{\partial t} - \nu \Delta \mathbf{y}_{N_1} + P_{N_1} B(\mathbf{y}_{N_1} + \mathbf{z}_{N_1}, \mathbf{y}_{N_1} + \mathbf{z}_{N_1}) \;=\; P_{N_1}\mathbf{g}, \\ \\ \dfrac{\partial \mathbf{z}_{N_1}}{\partial t} - \nu \Delta \mathbf{z}_{N_1} + Q_{N_1}^N B(\mathbf{y}_{N_1} + \mathbf{z}_{N_1}, \mathbf{y}_{N_1} + \mathbf{z}_{N_1}) \;=\; 0. \end{array} \right. \tag{12}$$

The initial conditions associated with (12) are $P_{N_1}\mathbf{u}_0$ and $Q_{N_1}^N \mathbf{u}_0$. In (12), as well as in the following, we will only use the projection operator P_{N_1} with N_1 larger than m_0.

We now introduce two norms :

$$|\, \boldsymbol{\varphi} \,|_2 = \left(\int_\Omega |\, \boldsymbol{\varphi}(\mathbf{x},t) \,|^2 \, d\mathbf{x} \right)^{1/2},$$

and

$$||\, \boldsymbol{\varphi} \,|| = \left(\int_\Omega |\, \boldsymbol{\nabla}\boldsymbol{\varphi}(\mathbf{x},t) \,|^2 \, d\mathbf{x} \right)^{1/2},$$

for any given field $\boldsymbol{\varphi}(\mathbf{x},t) = (\varphi_1(\mathbf{x},t), \varphi_2(\mathbf{x},t))$. We note that these norms are related to well-known physical quantities. Indeed, with the above definitions, the kinetic energy $e(\mathbf{u})$ of the velocity field $\mathbf{u}$ is related to $|\, - \,|_2$ by

$$e(\mathbf{u}) \;=\; \frac{1}{2} |\, \mathbf{u} \,|_2^2,$$

and in the case considered here of periodic boundary conditions, the enstrophy, $ens(\mathbf{u})$ is :

$$ens(\mathbf{u}) = \frac{1}{2}|| \mathbf{u} ||^2 = \frac{1}{2} | \boldsymbol{\omega} |_2^2 .$$

We now recall theoretical results, constituting the basis of this framework ; they were established by Foias, Manley and Temam in [1] and [9]. In [1], the authors proved that for sufficiently large values of N and N_1, namely N and $N_1 \simeq G^2$, where G designates the Grashoff number $G = \frac{|\mathbf{g}|_2}{\nu^2 \lambda_1}$ ($\lambda_1 \simeq 1/L^2$ where L is a characteristic length of the domain), and after a transient time, depending only on the data, the small scale components $\mathbf{z}_{N_1}(t)$ remain small in both norms introduced above, while the large scales $\mathbf{y}_{N_1}(t)$ are of the order of $\mathbf{u}(t)$. We do not know how close to the inertial range the corresponding cut–off eigenvalue $\lambda_{N_1} = cN_1^2$ can be, and it is one of our objectives in this work to explore this point. In [9], the authors derived other estimates of the ratios

$$\frac{| \mathbf{z}_{N_1}(t) |_2}{| \mathbf{y}_{N_1}(t) |_2} \quad \text{and} \quad \frac{|| \mathbf{z}_{N_1}(t) ||}{|| \mathbf{y}_{N_1}(t) ||}$$

in terms of the Grashoff number at appropriate powers of $1/(N_1+1)$, when the cut-off value N_1 is still of the order of G^2. Moreover, by using the analyticity in time of the solutions of the Navier–Stokes equations and invoking the Cauchy formula, one can show that $| \frac{\partial \mathbf{z}_{N_1}}{\partial t} |_2$, as well as $|| \frac{\partial \mathbf{z}_{N_1}}{\partial t} ||$, are respectively of the order of $| \mathbf{z}_{N_1} |_2$ and $|| \mathbf{z}_{N_1} ||$, for N_1 sufficiently large, corresponding to a wavenumber in the dissipation range. Even if these results do not provide fine estimates on the norms of the time derivative of the small–scale components, they show that the time derivatives of the velocity field $\mathbf{u}$ have also a decaying spectrum, which is not the case of course in the inertial range.

This behavior of the small-scale $\mathbf{z}_{N_1}$ is very important and is one of the keys of the numerical implementation of the multilevel method, as we will see in the following sections. Although, these results were proved theoretically only when N_1 is of the order of G^2, and λ_{N_1} is far in the dissipation range, numerical results show that $\mathbf{z}_{N_1}$ is small compared to $\mathbf{y}_{N_1}$ for much smaller values of N_1, and the same is true for their time derivative. From the phenomenological theory of two-dimensional turbulence point of view, due in part to Kraichman (cf [14] and [15]), the energy spectrum of a de-

veloped turbulent flow is expected to display a power–law inertial range and an exponential decay for wavenumbers larger than the Kraichnan's dissipation wavenumber (see Figure 1). So, the theoretical results mentioned above are in agreement with this assumption in the sense that for sufficiently large wavenumbers, the energy spectrum has a decaying behaviour. The exponential range is generally referred as the dissipation range.

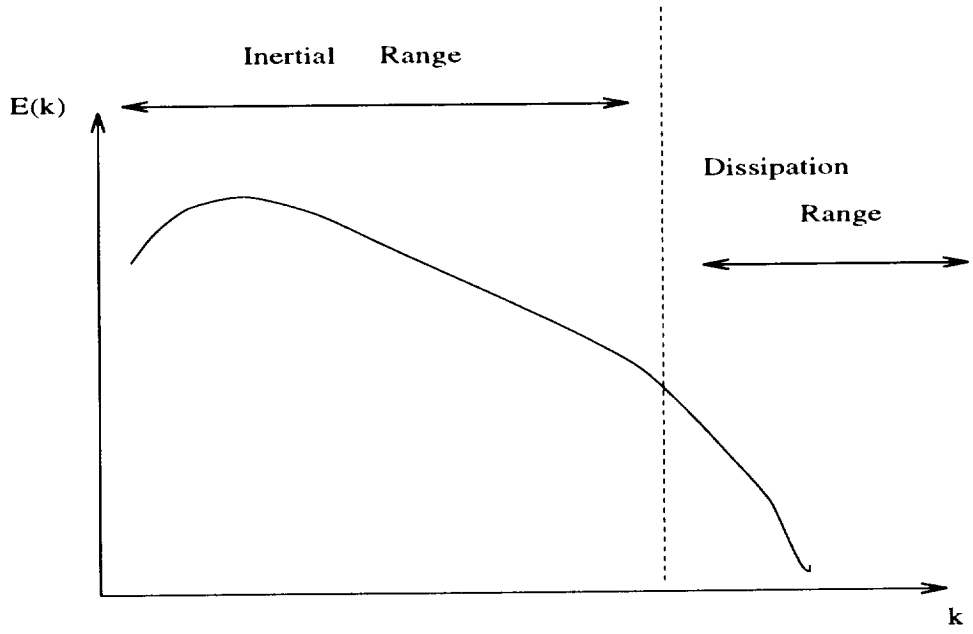

Figure 1: Energy Spectrum $E(k)$.

Due to the bilinearity of B, we can split $B(\mathbf{u}_N, \mathbf{u}_N)$ into

$$\begin{aligned} B(\mathbf{u}_N, \mathbf{u}_N) &= B(\mathbf{y}_{N_1} + \mathbf{z}_{N_1}, \mathbf{y}_{N_1} + \mathbf{z}_{N_1}) \\ &= B(\mathbf{y}_{N_1}, \mathbf{y}_{N_1}) + B_{\text{int}}(\mathbf{y}_{N_1}, \mathbf{z}_{N_1}), \end{aligned} \tag{13}$$

where

$$B_{\text{int}}(\mathbf{y}_{N_1}, \mathbf{z}_{N_1}) = B(\mathbf{y}_{N_1}, \mathbf{z}_{N_1}) + B(\mathbf{z}_{N_1}, \mathbf{y}_{N_1}) + B(\mathbf{z}_{N_1}, \mathbf{z}_{N_1}).$$

It represents the interaction between the small and the large structures and the interaction of the small structures among them. We now recall that a

classical (Galerkin) approximation of $\mathbf{u}$ based on the first N_1^2 Fourier coefficients consists in setting $\mathbf{z}_{N_1}$ to zero in (12), so that $P_{N_1} B_{\text{int}}(\mathbf{y}_{N_1}, \mathbf{z}_{N_1})$ is neglected. If $\mathbf{z}_{N_1}$ represents a small part of the kinetic energy, namely

$$e(\mathbf{z}_{N_1}) \ll e(\mathbf{y}_{N_1}),$$

then, we can expect that

$$| P_{N_1} B_{\text{int}}(\mathbf{y}_{N_1}, \mathbf{z}_{N_1}) |_2 \ll | P_{N_1} B(\mathbf{y}_{N_1}, \mathbf{y}_{N_1}) |_2 .$$

Therefore, the contribution of the interaction terms is much smaller than the component of the nonlinear terms, involving only the large scales $\mathbf{y}_{N_1}$. This argument can be justified when comparing Figures 4 and 5. More precisely, we have the following

$$\begin{array}{ccc} | P_{N_1} B_{\text{int}}(\mathbf{y}_{N_1}, \mathbf{z}_{N_1}) |_2 & \ll & | P_{N_1} B(\mathbf{y}_{N_1}, \mathbf{y}_{N_1}) |_2 \\ \simeq & & \simeq \\ \nu \mid \Delta \mathbf{y}_{N_1} \mid_2 & & \mid \dfrac{d\mathbf{y}_{N_1}}{dt} \mid_2 \end{array}$$

However, the interactions terms can not be neglected in the first equation (12) unless N_1 is taken very large. Indeed, their effects on long time computations can modify the behavior of the large scale components. Since the evaluation of these terms at each time step is very expansive, we try to take their effects into account in a simplified manner. We will see that the time variations of $\mathbf{z}_{N_1}$ and $P_{N_1} B_{\text{int}}(\mathbf{y}_{N_1}, \mathbf{z}_{N_1})$ are locally negligible, and this will allow us to freeze them during some parts of the iterations.

1.2.2 Time variations of $\mathbf{z}_{N_1}$ and $P_{N_1} B_{\text{int}}(\mathbf{y}_{N_1}, \mathbf{z}_{N_1})$.

We now aim to derive an estimate of the variations of $\mathbf{z}_{N_1}$ over one time iteration. This quantity can be represented by

$$\Delta_{N_1} = \Delta t \mid \dot{\mathbf{z}}_{N_1} \mid_2,$$

where the dot represents the differentiation with respect to t. The time step Δt is given by the CFL stability condition :

$$\Delta t \; N \mid \mathbf{u}_N \mid_{L^\infty} < \alpha, \text{ with } \alpha < 1. \tag{14}$$

We recall that N is the total number of modes in each direction. We assume that the smallest scale $\ell_N = 1/k_N$, $k_N = N/2$, is smaller than the Kraichnan dissipation scale $\ell_\eta = 1/k_\eta$. Let us first consider the case where $\ell_{N_1} = 1/k_{N_1}$ is lying between ℓ_η and ℓ_N, and ℓ_N, ℓ_{N_1}, ℓ_η are of the same order of magnitude :

$$\ell_N \leq \ell_{N_1} \leq \ell_\eta.$$

Let us assume, as shown in Figure 6, that the time derivative $\dot{\mathbf{z}}_{N_1}$ is of the order of the dissipation term (remember we are in the dissipation range),

$$| \dot{\mathbf{z}}_{N_1} |_2 \sim \nu | \Delta \mathbf{z}_{N_1} |_2 .$$

Due to the exponential decay of the velocity spectrum in the dissipation range, we can write

$$\nu | \Delta \mathbf{z}_{N_1} |_2 \leq c_1 \nu k_{N_1}^2 | \mathbf{z}_{N_1} |_2, \tag{15}$$

where c_1 is a nondimensional constant of the order of unity. It follows by (14) that :

$$\begin{aligned} \Delta_{N_1} = \Delta t | \dot{\mathbf{z}}_{N_1} |_2 &\leq c_2 \nu \Delta t \, k_{N_1}^2 | \mathbf{z}_{N_1} |_2 \\ &\leq c_2 \frac{\alpha}{N | \mathbf{u}_N |_{L^\infty}} \nu k_{N_1}^2 | \mathbf{z}_{N_1} |_2 . \end{aligned} \tag{16}$$

Then, using the estimate of k_η obtained in [16] namely

$$k_\eta \simeq k_0 G^{1/3} = \frac{k_0 | \mathbf{g} |_2^{1/3}}{\nu^{2/3} \lambda_1^{1/3}},$$

we obtain :

$$\Delta_{N_1} \leq c_2 \frac{\alpha k_0 | \mathbf{g} |_2^{1/3}}{\sqrt{2} \lambda_1^{1/3} | \mathbf{u}_N |_{L^\infty}} \left(\frac{k_{N_1}^2}{k_N k_\eta} \right) \nu^{1/3} | \mathbf{z}_{N_1} |_2 .$$

As $k_{N_1} \leq k_N$, we obtain :

$$\Delta_{N_1} \leq c_3 \frac{| \mathbf{g} |_2^{1/3}}{| \mathbf{u}_N |_{L^\infty}} \left(\frac{k_{N_1}}{k_\eta} \right) \nu^{1/3} | \mathbf{z}_{N_1} |_2 .$$

Since $k_{N_1} \sim k_\eta$, then for sufficiently small values of the viscosity ν, the variations of $\mathbf{z}_{N_1}$ over one time iteration are much smaller than $| \mathbf{z}_{N_1} |_2$.

We now try to derive a similar estimate when

$$\ell_\eta \leq \ell_{N_1},$$

i.e. when ℓ_{N_1} is in the inertial range. In that case, we assume as shown on Figure 7, that the time derivative $\dot{\mathbf{z}}_{N_1}$ is of the order of the interaction nonlinear terms

$$| \dot{\mathbf{z}}_{N_1} |_2 \sim | Q_{N_1}^N B_{\text{int}}(\mathbf{y}_{N_1}, \mathbf{z}_{N_1}) |_2 .$$

We recall that

$$\begin{aligned} & | Q_{N_1}^N B_{\text{int}}(\mathbf{y}_{N_1}, \mathbf{z}_{N_1}) |_2 \\ & \quad = | Q_{N_1}^N B(\mathbf{y}_{N_1}, \mathbf{z}_{N_1}) + Q_{N_1}^N B(\mathbf{z}_{N_1}, \mathbf{y}_{N_1}) + Q_{N_1}^N B(\mathbf{z}_{N_1}, \mathbf{z}_{N_1}) |_2 \\ & \quad \leq | Q_{N_1}^N B(\mathbf{y}_{N_1}, \mathbf{z}_{N_1}) |_2 + | Q_{N_1}^N B(\mathbf{z}_{N_1}, \mathbf{y}_{N_1}) |_2 \\ & \qquad + | Q_{N_1}^N B(\mathbf{z}_{N_1}, \mathbf{z}_{N_1}) |_2 . \end{aligned} \tag{17}$$

As $Q_{N_1}^N$ is a projection operator, we have

$$| Q_{N_1}^N B(\mathbf{y}_{N_1}, \mathbf{z}_{N_1}) |_2 \leq | B(\mathbf{y}_{N_1}, \mathbf{z}_{N_1}) |_2 .$$

The bilinear form B can be estimated as follows (see for instance [12] and [13])

$$| B(\mathbf{y}_{N_1}, \mathbf{z}_{N_1}) |_2 \leq c_4 | \mathbf{y}_{N_1} |_{L^\infty} || \mathbf{z}_{N_1} || .$$

As $| \mathbf{y}_{N_1} |_{L^\infty} \simeq | \mathbf{u}_N |_{L^\infty}$, for sufficiently large values of N_1, we obtain

$$| B(\mathbf{y}_{N_1}, \mathbf{z}_{N_1}) |_2 \leq c_4 | \mathbf{u}_N |_{L^\infty} || \mathbf{z}_{N_1} || .$$

The decay of the velocity Fourier components implies that

$$\| \mathbf{z}_{N_1} \| \leq c_5 k_{N_1} | \mathbf{z}_{N_1} |_2, \text{ where } c_5 \sim 1,$$

so that

$$| Q_{N_1}^N B(\mathbf{y}_{N_1}, \mathbf{z}_{N_1}) |_2 \leq c_4 \, c_5 \, k_{N_1} | \mathbf{u}_N |_{L^\infty} | \mathbf{z}_{N_1} |_2 .$$

We also have

$$| Q_{N_1}^N B(\mathbf{z}_{N_1}, \mathbf{y}_{N_1}) |_2 \leq | B(\mathbf{z}_{N_1}, \mathbf{y}_{N_1}) |_2,$$

which can be estimated by (see [12], [13])

$$| B(\mathbf{z}_{N_1}, \mathbf{y}_{N_1}) |_2 \leq c_6 | \mathbf{z}_{N_1} |_2^{1/2} | \Delta \mathbf{z}_{N_1} |_2^{1/2} \| \mathbf{y}_{N_1} \| .$$

In fact, the norm $\| \mathbf{y}_{N_1} \|$ and the infinity norm $| \mathbf{y}_{N_1} |_{L^\infty}$ are of the same order. We then obtain

$$| B(\mathbf{z}_{N_1}, \mathbf{y}_{N_1}) |_2 \leq c_7 | \mathbf{z}_{N_1} |_2^{1/2} | \Delta \mathbf{z}_{N_1} |_2^{1/2} | \mathbf{y}_{N_1} |_{L^\infty} .$$

From the inequality (15), we deduce that

$$| Q_{N_1}^N B(\mathbf{z}_{N_1}, \mathbf{y}_{N_1}) |_2 \leq c_8 \, k_{N_1} | \mathbf{y}_{N_1} |_{L^\infty} | \mathbf{z}_{N_1} |_2 .$$

A similar estimate can be derived for the third term $Q_{N_1}^N B(\mathbf{z}_{N_1}, \mathbf{z}_{N_1})$. We finally obtain

$$| Q_{N_1}^N B_{\text{int}}(\mathbf{y}_{N_1}, \mathbf{z}_{N_1}) |_2 \leq c_9 \, k_{N_1} | \mathbf{u}_N |_{L^\infty} | \mathbf{z}_{N_1} |_2 .$$

Then,

$$\Delta_{N_1} \leq c_9 \, k_{N_1} \Delta t | \mathbf{u}_N |_{L^\infty} | \mathbf{z}_{N_1} |_2 .$$

As

$$\Delta t \leq \frac{\alpha}{| \mathbf{u}_N |_{L^\infty} \; N} = \frac{\alpha}{| \mathbf{u}_N |_{L^\infty} \sqrt{2} \, k_N},$$

we find

$$\Delta_{N_1} \leq c_9 \, \frac{\alpha}{\sqrt{2}} \left(\frac{k_{N_1}}{k_N} \right) | \mathbf{z}_{N_1} |_2,$$

which also implies that $\Delta_{N_1} < | \mathbf{z}_{N_1} |_2$ in the inertial range as well. Figure 8 supports the theoretical estimates derived above. We want to note, at this point, that these results will remain valid if energy is injected in the small scales by a given external force, having a decaying spectrum ; i.e. if $\hat{\mathbf{g}}(\mathbf{k}) \sim | \mathbf{k} |^a \, e^{-\alpha |\mathbf{k}|}$, for $| \mathbf{k} |$ larger than a given wavenumber.

Let us now introduce ε the accuracy of the computations ; ε represents here an energy error. We assume that ε is a given parameter, which can be chosen under several considerations ; examples will be given in Section 3 devoted to the description of the numerical results. The accuracy ε can be associated with a small scale, i.e.

$$\begin{gathered} \text{there exists a level } N_1(\varepsilon) \; (\leq N) \text{ such that} \\ | \mathbf{z}_{N_1(\varepsilon)} |_2 \sim \varepsilon. \end{gathered} \tag{18}$$

According to the estimate previously derived, $\Delta_{N_1(\varepsilon)}$ is much smaller than ε. From the previous estimates we can deduce that there exists several levels of discretization N_1 lower that $N_1(\varepsilon)$, for which Δ_{N_1} is also smaller than ε. Let us denote by $N_1'(\varepsilon)$ the lowest level of refinement satisfying $\Delta_{N_1'(\varepsilon)} \leq \varepsilon$. The above result means that the small scales can be integrated with a larger time step, even if their time scales are smaller than the ones of the large eddies. By definition and due to the behavior of $\mid \dot{\mathbf{z}}_{N_1} \mid_2$, with respect to N_1, the quantity Δ_{N_1} increases for decreasing values of N_1. Hence, the appropriate time step for $\ell_{N_1(\varepsilon)}$ is larger than the appropriate one for $\ell_{N_1'(\varepsilon)}$. Moreover, on Figure 4, we note that $\mid \dot{\mathbf{z}}_{N_1} \mid_2$ presents strong variations during the time evolution. Consequently, the levels $N_1(\varepsilon)$ and $N_1'(\varepsilon)$ are not constant in time. To take into account this specific dynamics of the small scales, we propose, as it was done in [10], [7] and [17], to use multigrid technics. The integration of the intermediate scales ℓ_{N_1}, $\ell_{N_1(\varepsilon)} < \ell_{N_1} < \ell_{N_1'(\varepsilon)}$, consists in performing a succession of multigrid V–cycles during which some parts of the spectrum are frozen during the time evolution. Hence, we use here a property of the first order term of the evolution equation of the small scales.

On Figures 11, we can see that the variations of $P_{N_1} B_{\text{int}}(\mathbf{y}_{N_1}, \mathbf{z}_{N_1})$ and of $\mathbf{z}_{N_1}$ are correlated. Therefore, we deduce that the variations of $P_{N_1} B_{\text{int}}(\mathbf{y}_{N_1}, \mathbf{z}_{N_1})$ over one time iteration is smaller than $P_{N_1} B_{\text{int}}(\mathbf{y}_{N_1}, \mathbf{z}_{N_1})$; in fact, one can show that :

$$\Delta'_{N_1} \;=\; \Delta t \mid P_{N_1} \dot{B}_{\text{int}}(\mathbf{y}_{N_1}, \mathbf{z}_{N_1}) \mid_2 \leq\; c_{10} \left(\frac{k_{N_1}}{k_N}\right) \mid P_{N_1} B_{\text{int}}(\mathbf{y}_{N_1}, \mathbf{z}_{N_1}) \mid_2 .$$

The nonlinear interaction term $P_{N_1} B_{\text{int}}(\mathbf{y}_{N_1}, \mathbf{z}_{N_1})$ represents a small part of the large scales time derivative $\dot{\mathbf{y}}_{N_1}$. Hence, its variation over one time iteration can be neglected without a lost of the accuracy on the large scale approximation. We use here a property of the time evolution of $P_{N_1} B_{\text{int}}(\mathbf{y}_{N_1}, \mathbf{z}_{N_1})$ which is a second order term of the large scale evolution. As the time scale of $\mathbf{z}_{N_1}$ is much smaller than the one of $\mathbf{z}_{N_1}$, the time derivative $P_{N_1} \dot{B}_{\text{int}}(\mathbf{y}_{N_1}, \mathbf{z}_{N_1})$ behaves as $\dot{\mathbf{z}}_{N_1}$ and then is very oscilating with the time. From the previous inequality, it appears that the quantity Δ'_{N_1} can be controlled by the term $P_{N_1} B_{\text{int}}(\mathbf{y}_{N_1}, \mathbf{z}_{N_1})$; hence, we estimate the level $N_1'(\varepsilon)$ by imposing that the ratio

$$\frac{\mid P_{N_1'(\varepsilon)} B_{\text{int}}(\mathbf{y}_{N_1'(\varepsilon)}, \mathbf{z}_{N_1'(\varepsilon)}) \mid_2}{\mid P_{N_1'(\varepsilon)} B(\mathbf{y}_{N_1'(\varepsilon)}, \mathbf{y}_{N_1'(\varepsilon)}) \mid_2}$$

remains smaller than a given constant. As the computation of the nonlinear terms requires several calls to the FFT routines, the evaluation of the above ratio is expensive and then prohibitive. So, we have looked for another form of it. In the numerical results, we have noted that

$$\frac{\mid P_{N_1} B_{\rm int}(\mathbf{y}_{N_1}, \mathbf{z}_{N_1}) \mid_2}{\mid P_{N_1} B(\mathbf{y}_{N_1}, \mathbf{y}_{N_1}) \mid_2} \simeq \frac{\|\mathbf{z}_{N_1}\|}{\|\mathbf{y}_{N_1}\|} = \left(\frac{\mathrm{ens}(\mathbf{z}_{N_1})}{\mathrm{ens}(\mathbf{y}_{N_1})}\right)^{1/2},$$

as we can see on Figures 13. Hence, we use the ratio of the enstrophy of the small scales over the enstrophy of the large ones to evaluate the level $N_1'(\varepsilon)$. As we have seen before, the notion of variation of the scales is intrinsic to the definition of $N_1'(\varepsilon)$. More sophisticated criteria will be derived in Section 2.2. Finally, we want to note that controlling the size of $P_{N_1} B_{\rm int}(\mathbf{y}_{N_1}, \mathbf{z}_{N_1})$ and its time variation ensures that the interaction of the small scales over the large ones is negligible, in the sense that this interaction can be locally neglected from a numerical point of view.

2 Description of the multiscale method.

As it was shown in Section 1.2.2, the small scales of the flow as well as the terms involving their nonlinear interactions can be fixed in time during a few time steps. Nevertheless, their order of magnitude may change drastically over a period of time ; so, the cut–off value N_1 defining the separation between the small and the large eddies can not be let fixed in time. Hence, we propose a multilevel adaptative procedure evaluating the appropriate level of refinement as time evolves. Using partly theoretical arguments, we show in this section that we can derive estimates for the variations of the small scales and of the transfer terms to the largest scales. We then deduce estimates for the length of the frozen periods. Finally, we introduce these estimates in the algorithm and we derive a dynamic procedure allowing an a priori and an a posteriori control of the length of the quasi–static time intervals. In the first subsection, we describe the multilevel adaptive procedure ; secondly, we derive time scales estimates of the fine structures and of the transfer terms. In the third part, we give an explicit approximation law used to compute the small scale components of the flow and we derive error estimates for this Approximate Inertial Manifold. Finally, we describe the whole algorithm including the modifications previously discussed.

2.1 The multilevel adaptive procedure

As in the preceeding Section 1.2.1, we choose an integer N larger than m_0 (cf (8)), which represents the total number of modes retained in the truncation and we denote by

$$\mathbf{u}_N = \sum_{\mathbf{k} \in I_N} \hat{u}(\mathbf{k}, t)\, w_{\mathbf{k}},$$

an approximation of $\mathbf{u}$. We associate with N the largest wave number of $\mathbf{u}_N$, namely $k_N = N/2$. Hence, the smallest scale in the computation is $\ell_N = 1/k_N$.

We are now given a sequence of levels N_i satisfying

$$N_1 < N_2 < \ldots < N_i < N_{i+1} < \ldots < N. \tag{19}$$

As we want to perform pseudo-spectral approximations of equations (12) on these different levels of refinement, the elements N_i of these sequences have to satisfy the restrictions imposed by the Fast Fourier Transforms (FFT) ; namely, the N_i's must be of the form $2^p\, 3^q\, 5^r$, where $p \geq 2$ and $q,\ r \geq 0$. Such an algorithm enables us to define a suitable sequence of levels N_i. Examples of sequences will be given in Section 3, where the numerical results will be described. We note that an FFT allowing only decompositions in powers of 2 is not efficient for this purpose.

Let us now assume that the approximation $\mathbf{u}_N(\mathbf{x}, t)$ is known at a time t_j. As it was suggested in the previous section, we define two levels of discretization $N_{i_1}(t_j)$ and $N_{i_2}(t_j)$ by the following procedure :

$$\begin{cases} \underline{i_1 \text{ is defined by the condition that}} \\ \text{for every } i \geq i_1, \\ \qquad \dfrac{ens(\mathbf{z}_{N_i}(t_j))}{ens(\mathbf{y}_{N_i}(t_j))} < \theta_1. \end{cases} \tag{20}$$

$$\begin{cases} \underline{i_2 \text{ is defined by the condition that}} \\ \text{for every } i \geq i_2, \\ \qquad \dfrac{e(\mathbf{z}_{N_i}(t_j))}{e(\mathbf{y}_{N_i}(t_j))} < \theta_2. \end{cases} \tag{21}$$

where θ_1 and θ_2 are two given constants ; θ_2 is chosen so that $e(\mathbf{z}_{N_{i_2}})$ is of the order of the accuracy ε^2. In the previous versions of the algorithm, the parameter θ_1 was arbitrary fixed ; we will derive an estimate of θ_1 in section 2.4. . In order to be sure that $N_{i_1} < N_{i_2}$, we impose the additional condition that $(i_2 - i_1)$ has to be larger than a given constant. This is motivated by the fact that, as we described in the previous section, the intermediate region of the spectrum between $N_{i_1}(t_j)$ and $N_{i_2}(t_j)$ is a transition zone between the large scales and the static (frozen) small scales.

We now introduce the quantities

$$\theta_1(t_j) \;=\; \left(\frac{ens(\mathbf{z}_{N_{i_1}}(t_j))}{ens(\mathbf{y}_{N_{i_1}}(t_j))}\right)^{1/2} \tag{22}$$

and

$$\theta_2(t_j) \;=\; \left(\frac{e(\mathbf{z}_{N_{i_2}}(t_j))}{e(\mathbf{y}_{N_{i_2}}(t_j))}\right)^{1/2} \tag{23}$$

Let $\tau_c(t_j)$ be the length of the time interval during which the scales smaller than $\ell_{N_{i_2}}$, i.e. $\mathbf{z}_{N_{i_2}}$, can be frozen without loosing the order of approximation on the larger scales ; estimates for the characteristic length $\tau_c(t_j)$ will be derived in Section 2.2. In previous works, see for instance [8], $\tau_c(t_j)$ was estimated by the characteristic relaxation time of the viscous term, namely :

$$\tau_c(t_j) \;=\; (\nu k_{N_{i_2}}^2)^{-1}.$$

As we will see in Section 3, this estimate is not fine enough and may induce strong errors in the approximation of the velocity field. The available levels of refinement, lying between $N_{i_1}(t_j)$ and $N_{i_2}(t_j)$, are

$$N_{i_1} < N_{i_1+1} < \ldots < N_i < \ldots < N_{i_2-1} < N_{i_2},$$

which correspond to $(i_2 - i_1 + 1)$ levels. For the sake of simplicity, we omit here the dependence on t_j for the levels N_{i_1} and N_{i_2}.

As in classical multigrid methods, we use the concept of V-cycle to perform the integration of (12) on the interval $[t_j, t_j + \tau_c]$. Let us define a V-cycle starting at time t_j. Such a V-cycle is constituted of two phases described as follows :

- phase 1 : on the interval $[t_j, t_j + (i_2 - i_1)\Delta t]$, the current level $N_i(t)$ is defined by :

$$N_i(t) \;=\; N_{i_2 - j}, \quad \text{for } j = 0, ..., i_2 - i_1,$$

hence $N_i(t)$ decreases from $N_{i_2}(t_j)$ to $N_{i_1}(t_j)$.

- phase 2 : on the interval $[t_j + (i_2 - i_1)\Delta t, t_j + (2(i_2 - i_1) + 1)\Delta t]$, the current level $N_i(t)$ is defined by :

$$N_i(t) = N_{i_1 + (j - i_2 + i_1 - 1)}, \quad \text{for } j = i_2 - i_1 + 1, ..., 2(i_2 - i_1) + 1,$$

hence $N_i(t)$ increases from $N_{i_1}(t_j)$ to $N_{i_2}(t_j)$.

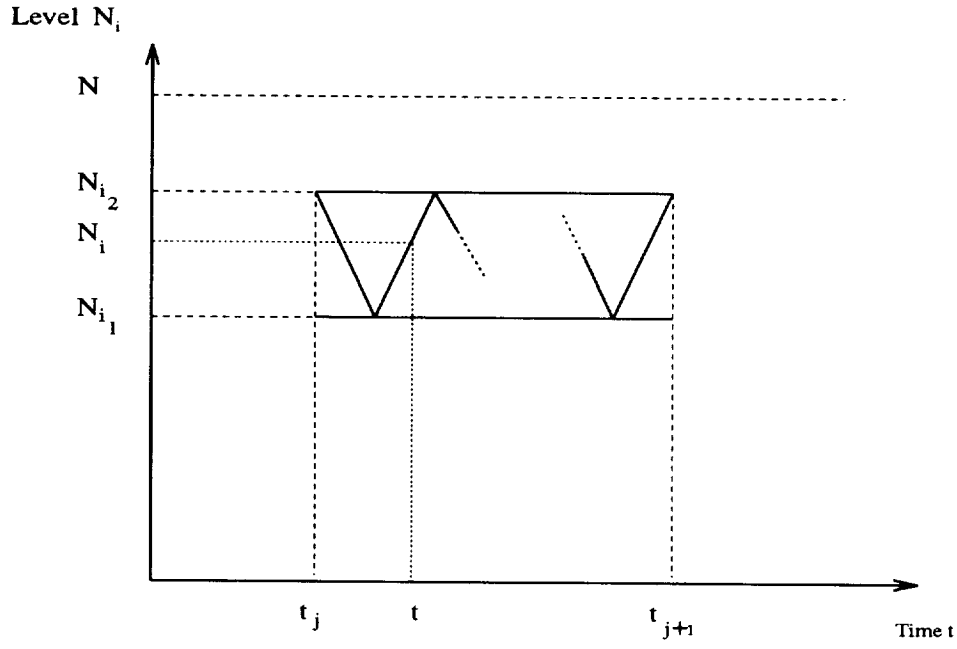

Figure 2: Evolution of $N_i(t)$.

Then, a V-cycle consists in $[2(i_2 - i_1) + 1]$ time iterations. The quantity $\tau_c(t_j)$ is adjusted so that the time interval $[t_j, t_j + \tau_c]$ can be divided into a fixed

number of such cycles. Figure 2 summarizes this process.

Let t be an intermediate time on the interval $[t_j, t_j + \tau_c]$; according to the previous procedure, the current level $N_i(t)$ is given by :

$$N_i(t) \;=\; \begin{cases} N_{i_2-r+1}, & \text{if} \quad 1 \le r \le (i_2 - i_1), \\ N_{i_1+(r-(i_2-i_1+1))} & \\ & \text{if} \quad (i_2 - i_1 + 1) \le r \le 2(i_2 - i_1), \end{cases} \tag{24}$$

where r is given by :

$$t - t_j = (2p\ (i_2 - i_1) + r)\ \Delta t.$$

Knowing the size N_i of the coarse grid at time t, we decompose $\mathbf{u}_N(t)$ into :

$$\mathbf{u}_N(t) \;=\; \mathbf{y}_{N_i}(t) + \mathbf{z}_{N_i}(t),$$

where $\mathbf{y}_{N_i}(t)$ represents the scales larger than ℓ_{N_i}, and $\mathbf{z}_{N_i}(t)$ the scales smaller than ℓ_{N_i} and larger than ℓ_N. The computation of both components $\mathbf{y}_{N_i}(t)$ and $\mathbf{z}_{N_i}(t)$ are performed as follows :

- **computation of $\mathbf{z}_{N_i}(t)$:**

$$\mathbf{z}_{N_i}(t) \;=\; \mathbf{z}_{N_i}(t - \Delta t),$$

  i.e. $\mathbf{z}_{N_i}(t)$ is frozen and set to its last value.

- **computation of $\mathbf{y}_{N_i}(t)$** : in order to evaluate $\mathbf{y}_{N_i}(t)$, we integrate equation (12) over the interval $[t - \Delta t,\ t]$; then it follows that

$$\begin{aligned} \hat{u}(\mathbf{k}, t) \;&=\; e^{-\nu|\mathbf{k}|^2 \Delta t} \hat{u}(\mathbf{k}, t - \Delta t) \\ &+ \int_{t-\Delta t}^{t} e^{-\nu|\mathbf{k}|^2 (t-\tau)} B_{\mathbf{k}}(\mathbf{y}_{N_i}(\tau), \mathbf{y}_{N_i}(\tau))\ d\tau \\ &+ \int_{t-\Delta t}^{t} e^{-\nu|\mathbf{k}|^2 (t-\tau)} B_{\mathrm{int},\mathbf{k}}(\mathbf{y}_{N_i}(\tau), \mathbf{z}_{N_i}(\tau))\ d\tau \end{aligned} \tag{25}$$

  for every $\mathbf{k}$ in $I_{N_i} = [1 - N_i/2, N_i/2] \times [0, N_i/2]$.

The first integral is computed by an explicit Runge–Kutta scheme of order 3 (see [7]). With this scheme the interval $[t-\Delta t, t]$ is split into three sub–intervals of the form $[t_i, t_{i+1}]$, where $t_0 = t - \Delta t$ and $t_3 = t$. On each of these sub–intervals, the second integral is approximated as follows :

$$\begin{aligned} &\int_{t_i}^{t_{i+1}} e^{-\nu|\mathbf{k}|^2(t_{i+1}-\delta)} B_{\mathrm{int},\mathbf{k}}(\mathbf{y}_{N_i}(\delta), \mathbf{z}_{N_i}(\delta))\, d\delta \\ &\qquad \simeq \Delta t\; e^{-\nu|\mathbf{k}|^2(t_{i+1}-t_i)}\; B_{\mathrm{int},\mathbf{k}}(\mathbf{y}_{N_i}(t_j), \mathbf{z}_{N_i}(t_j)) \end{aligned} \tag{26}$$

We note here that this approximation is an explicit Euler scheme on the interval $[t_i, t_{i+1}]$, where the following approximation is performed

$$B_{\mathrm{int},\mathbf{k}}(\mathbf{y}_{N_i}(t_i), \mathbf{z}_{N_i}(t_i)) \sim B_{\mathrm{int},\mathbf{k}}(\mathbf{y}_{N_i}(t_j), \mathbf{z}_{N_i}(t_j)).$$

This integration requires the storage of $P_{N_i} B_{\mathrm{int}}(\mathbf{y}_{N_i}(t_j), \mathbf{z}_{N_i}(t_j))$, at the beginning of the cycle, for each coarse grid N_i between N_{i_1} and N_{i_2}, i.e. for $(i_2 - i_1 + 1)$ levels.

As the time $\tau_c(t_j)$ is adjusted to be a multiple of a complete V–cycle, the current level at time $t_j + \tau_c(t_j)$ is equal to N_{i_2}, the highest coarse level. Referring to the integration process described above, the large scales $\mathbf{y}_{N_{i_2}}$ are known at the end of the cycle, i.e. at time $t_j + \tau_c(t_j)$. The smallest scales $\mathbf{z}_{N_{i_2}}$ are then updated by projecting the approximate solution $\mathbf{u}_N(t_j + \tau_c(t_j))$ on an approximate form of the small scales equation (12), for instance

$$\mathbf{z}_{N_{i_2}}(t_j + \tau_c(t_j)) \;=\; \phi(\mathbf{y}_{N_{i_2}}(t_j + \tau_c(t_j)), \mathbf{z}_{N_{i_2}}(t_j), \tau_c(t_j)). \tag{27}$$

(27) is the equation of an Approximate Inertial Manifold. Such manifolds were first derived in [1] ; (27) provides an interaction law between the small and the large scale components of the flow, and expresses $\mathbf{z}_{N_{i_2}}$ as a function of $\mathbf{y}_{N_{i_2}}$. Further information on such law can be found in [18], [19], and [7]. Other kinds of approximate inertial manifolds are derived in [20] and [21] ; the implementation of an Approximate Inertial Manifolds of first order will be discussed in Section 2.3. In Section 2.3, we will discuss on the efficiency of these nonlinear forms and derive some estimates which explain in which range of the spectrum they can be implemented. From a strictly computational point of view, an approximate inertial manifold is efficient in the sense that this equation allows us to estimate the small scales as an explicit

function of the large ones. Moreover, a first order law only requires one evaluation of the nonlinear terms, on the fine grid (see Section 2.3).

Finally, at $t_{j+1} = t_j + \tau_c(t_j)$, i.e. at the end of a whole cycle, we have an approximation of $\mathbf{u}_N(t_{j+1})$ by :

$$\mathbf{u}_N(t_{j+1}) \;=\; \mathbf{y}_{N_{i_2}}(t_{j+1}) + \mathbf{z}_{N_{i_2}}(t_{j+1}).$$

We start the full procedure again by computing two new levels $N_{i_1}(t_{j+1})$ and $N_{i_2}(t_{j+1})$. Then, we perform new V-cycles on the time interval $[t_{j+1}, t_{j+1} + \tau_c(t_{j+1})]$, and so on.

Basically, we can summarize this process by saying that the full time interval $[0, T]$ of the whole computation is split into several small time intervals $[t_j, t_j + \tau_c(t_j)]$ and, on each of these intervals the velocity spectrum is split into three fundamental regions :

- the dynamical range, corresponding to wavenumbers smaller than $k_{N_{i_1}}$. It represents the large scale structures of the flow – i.e. the scales containing most of the energy and the enstrophy of the flow. The modes lying in this part of the spectrum are integrated at each time step of the time interval $[t_j, t_j + \tau_c(t_j)]$.

- a transition range, corresponding to wavenumbers between $k_{N_{i_1}}$ and $k_{N_{i_2}}$. An up and down oscillation process is used, i.e. the current level of discretization $N_i(t)$ undergoes all the intermediate levels between $N_{i_1}(t)$ and $N_{i_2}(t)$, while the time evolves.

- a quasi–static range, i.e. for wavenumbers larger than $k_{N_{i_2}}$. It represents the smallest scales, which are numerically negligible ; i.e. their energy and their variations are smaller than the expected accuracy.

Figure 3 represents these three different regions of the spectrum.

Now we want to make some remarks on the effect of the integration procedure previously described on the smale scale components of the flow. One of the crucial points concerns the technic used to update the small structures $\mathbf{z}_{N_1}(t)$ lying in the transition range.

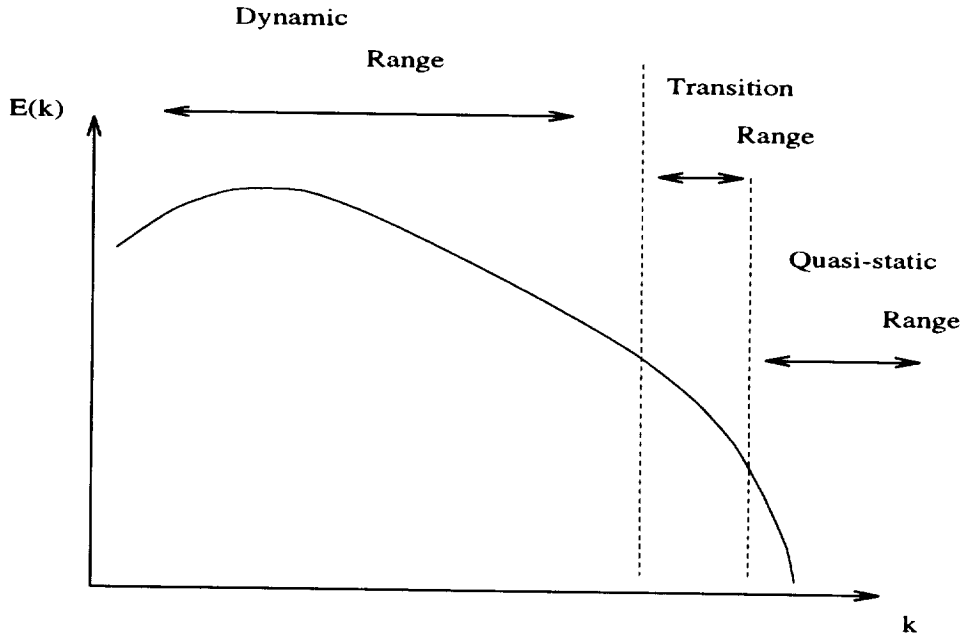

Figure 3: The multilevel procedure.

Let us first recall the equation satisfied by the $k^{\underline{\text{th}}}$ coefficient of the Fourier decomposition of $\mathbf{u}_N$:

$$\begin{aligned} \frac{d\hat{\mathbf{u}}(\mathbf{k})}{dt} + \nu \mid \mathbf{k} \mid^2 \hat{\mathbf{u}}(\mathbf{k}) \quad & + \hat{B}_{\mathbf{k}}(\mathbf{y}_{N_1}, \mathbf{y}_{N_1}) \\ & + \hat{B}_{\text{int},\mathbf{k}}(\mathbf{y}_{N_1}, \mathbf{z}_{N_1}) \;=\; 0. \end{aligned} \tag{28}$$

We assume here that $\mathbf{k}$ is such that $\mid \mathbf{k} \mid \geq m_0$ and hence (see (8)) :

$$\hat{\mathbf{g}}(\mathbf{k}) \;=\; 0.$$

We can then write (28) in the following form

$$\frac{d}{dt}\left(e^{\nu|\mathbf{k}|^2 t}\hat{u}(\mathbf{k})\right) \;=\; -e^{\nu|\mathbf{k}|^2 t}\left[\hat{B}_{\mathbf{k}}(\mathbf{y}_{n_1}, \mathbf{y}_{n_1}) - \hat{B}_{\text{int},\mathbf{k}}(\mathbf{y}_{n_1}, \mathbf{z}_{n_1})\right]. \tag{29}$$

Integration of (29) over a time interval $[t, t+\tau]$ leads to :

$$\begin{aligned} \hat{\mathbf{u}}(\mathbf{k}, t+\tau) = \; & e^{-\nu|\mathbf{k}|^2\tau}\hat{\mathbf{u}}(\mathbf{k}, t) \\ & - \int_t^{t+\tau} e^{\nu|\mathbf{k}|^2(\theta-(t+\tau))}\left[\hat{B}_{\mathbf{k}}(\mathbf{y}_{n_1}, \mathbf{y}_{n_1}) + \hat{B}_{\text{int},\mathbf{k}}(\mathbf{y}_{n_1}, \mathbf{z}_{n_1})\right] d\theta \end{aligned} \tag{30}$$

We note that if $\mathbf{k}$ is large enough, $\hat{\mathbf{u}}(\mathbf{k})$ is a component of the small scales. For instance, we assume that :

$$| \mathbf{k} | \geq N_{i_1}(t).$$

Then, $\mathbf{k}$ lies either in the transition or quasi–static range. According to the implementation of the multilevel method in (30), $\hat{\mathbf{u}}(\mathbf{k}, t)$ is replaced by an approximation close to the actual value, as the perturbations are smaller than the accuracy ε. If $\mathbf{k}$ lies far enough in the dissipation range, then the dissipative terms are quasi–dominent, namely :

$$| \dot{\mathbf{z}}_{N_1} |_2 \simeq | \nu \Delta \mathbf{z}_{N_1} |_2 \simeq | Q_{N_1}^N B_{\text{int}}(\mathbf{y}_{N_1}, \mathbf{z}_{N_1}) |_2,$$

as we can see on Figure 12. In that case, the errors introduced by the quasi–static integration are quickly damped by the effects of the operator $-\Delta$: few corrected iterations are needed. If $\mathbf{k}$ is not as large, i.e. if it is closer to the inertial range, then the coupled nonlinear terms become the most important terms of equation (30). In that case, the error is convected by nonlinear effects in the largest wavenumbers, and are finally damped by viscous effects.

During the V–cycles, the modes closer to $N_{i_1}(t)$ are more often integrated than the ones close to $N_{i_2}(t)$. The structure of the V–cycles is thus well–adapted to the integration of the small scales. As we will see in Section 3, devoted to the description of the numerical results, there is no accumulation of errors in the intermediate scales and there is no energy pile–up in the high wavenumbers of the Fourier decomposition. The enstrophy cascades are well described by the V–cycle technic.

2.2 Time scale estimates for the small eddies and for the nonlinear interaction terms.

Time scale estimates for $\mathbf{z}_{N_1}$.

From now on and for the sake of simplicity, we omit the subscripts N_1 in the notations. We then denote by $\mathbf{z}(t)$ the small scale components of the flow. As the Navier–Stokes equations are analytic in time (see [1]), we can write a Taylor expansion of $\mathbf{z}(t)$:

$$\mathbf{z}(t+\tau) = \mathbf{z}(t) + \tau \dot{\mathbf{z}}(t) + o(\tau^2). \tag{31}$$

As we saw in Section 1.2.2, the quantity $\tau\dot{\mathbf{z}}(t)$ can be much smaller than $\mathbf{z}(t)$. We can then assume that the higher order terms, in the Taylor expansion are negligible by comparison with the first order ones.

As in the previous section, we denote by ε the accuracy, i.e. the solution is approximated with an error of the order of ε. Let us assume that, on an interval $[t, t+\tau]$, we tolerate an error of the order of ε on the approximation of the small scale components. From (31), we then derive an estimate on τ, namely :

$$\tau \leq \frac{K\varepsilon}{\mid \dot{\mathbf{z}}(t) \mid_2}. \tag{32}$$

We denote $\tau(\varepsilon) = K\varepsilon/\mid \dot{\mathbf{z}}(t) \mid_2$, where K is a nondimensional real constant of the order of the unity. As the time derivative $\mid \dot{\mathbf{z}}(t) \mid_2$ has a decaying spectrum, the quantity $\tau(\varepsilon)$ then decreases with decreasing values of the level N_i. Estimate (32) then provides a restriction on the available level on which the modes can be frozen, i.e. there exists a level N_i such that $\tau(\epsilon)$ becomes smaller than the time step Δt. On Figure 14, we have plotted the ratio $\tau(\varepsilon)$ for different values of N_i. These results are obtained from the computation presented in Section 3. In this case, the accuracy is given by the temporal discretization and is of the order of Δt^3. As the time step Δt is of the order of 10^{-3}, we can estimate $K\varepsilon \simeq 10^{-8}$. So, for a fixed given value of the level N_i, the corresponding time scale $\tau(\varepsilon)$ presents very strong variations. In a previous version of the algorithm, τ was estimated by $(\nu k_{N_{i_2}}^2)^{-1}$ and then was constant in time ; this choice is obviously inappropriate. Deriving an estimate on $\tau(\varepsilon)$ is essential to insure the efficiency of the algorithm. Indeed, we can imagine a situation where the procedure (20) and (21) allows the choice of a level N_{i_1} while the condition (32) is violated, i.e. that τ is much smaller than the time step. Hence, the constraint (32) provides an additional way to determine N_{i_1} and N_{i_2}.

In the transition range $[N_{i_1}(t_j), N_{i_2}(t_j)]$, we have a time estimate $\tau_{N_i}(\varepsilon)$, given by (32), for level N_i :

$$\tau_{N_i}(\varepsilon) \;=\; \frac{K\varepsilon}{\mid \dot{\mathbf{z}}_{N_i}(t) \mid_2}.$$

As we have noted above, the quantity $\tau_{N_i}(\varepsilon)$ decreases when N_i decreases.

According to the definition of a V–cycle, on the lower level $N_{i_1}(t_j)$, the characteristic time scale has to satisfy :

$$\tau_{N_{i_1}}(\varepsilon) \geq \Delta t. \tag{33}$$

We recall that (33) is motivated by the fact that the scales $\mathbf{z}_{N_{i_1}}$ will be frozen over only one time iteration during a complete V–cycle ; (33) is then a constraint that $N_{i_1}(t_j)$ has to satisfy. As we have previously remarked, the time derivative can be evaluated by the nonlinear terms, i.e. :

$$| \dot{\mathbf{z}}_{N_{i_1}} |_2 \simeq | Q^N_{N_{i_1}} B(\mathbf{u}_N, \mathbf{u}_N) |_2 .$$

At time t_j, $B_{int}(\mathbf{y}_{N_{i_1}}, \mathbf{z}_{N_{i_1}})$ is obtained by using the following relation :

$$B_{int}(\mathbf{y}_{N_{i_1}}, \mathbf{z}_{N_{i_1}}) \;=\; B(\mathbf{u}_N, \mathbf{u}_N) - B(\mathbf{y}_{N_{i_1}}, \mathbf{y}_{N_{i_1}}).$$

Hence, $B(\mathbf{u}_N, \mathbf{u}_N)$ will be computed at that time. Then, the computation of the quantity

$$\tau_{N_{i_1}}(\varepsilon) \;=\; \frac{K\varepsilon}{| \dot{\mathbf{z}}_{N_{i_1}}(t_j) |_2} \simeq \frac{K\varepsilon}{| Q^N_{N_{i_1}} B(\mathbf{u}_N, \mathbf{u}_N) |_2} \tag{34}$$

will not add extra cost. With (33), we are sure that on all levels N_i higher than N_{i_1}, the corresponding scales can be frozen during more than one time iteration.

The characteristic time $\tau_{N_{i_2}}(\varepsilon)$ provides an estimate of the global time length $\tau_c(t_j)$ of the whole cycle $[t_j, t_j + \tau_c(t_j)]$; $\tau_{N_{i_2}}(\varepsilon)$ can be evaluated as in (34), i.e. :

$$\tau_{N_{i_2}}(\varepsilon) \;\simeq\; \frac{K\varepsilon}{| Q^N_{N_{i_2}} B(\mathbf{u}_N, \mathbf{u}_N) |_2}. \tag{35}$$

Remark 1 : if N_{i_2} lies in the quasi–static range, another estimate can be derived ; as we have seen before, we have :

$$| \dot{\mathbf{z}}_{N_{i_2}}(t_j) |_2 \simeq \; \nu \, | \Delta \mathbf{z}_{N_{i_2}}(t_j) |_2 .$$

Then, we can write :

$$| \dot{\mathbf{z}}_{N_{i_2}}(t_j) |_2 \geq \; c_{11} \nu \, | \Delta \mathbf{z}_{N_{i_2}}(t_j) |_2,$$

where c_{11} is a constant of the order of unity. From the definition of the norm $|-|_2$ and of $\mathbf{z}_{N_{i_2}}$, we can obtain :

$$\nu \mid \Delta \mathbf{z}_{N_{i_2}}(t_j) \mid_2 \geq \nu \, (k_{N_{i_2}})^2 \mid \mathbf{z}_{N_{i_2}}(t_j) \mid_2 .$$

We then obtain the following estimate of $\tau_{N_{i_2}}(\varepsilon)$:

$$\tau_{N_{i_2}}(\varepsilon) \leq \frac{K\varepsilon}{c_{11}\nu \, (k_{N_{i_2}})^2 \mid \mathbf{z}_{N_{i_2}}(t_j) \mid_2}.$$

Moreover, we recall that, by definition :

$$\mid \mathbf{z}_{N_{i_2}}(t_j) \mid_2 = \theta_2(t_j) \mid \mathbf{y}_{N_{i_2}}(t_j) \mid_2 .$$

We finally have an a priori estimate for $\tau_{N_{i_2}}$:

$$\tau_{N_{i_2}}(\varepsilon) \leq \frac{K\varepsilon}{\nu \, {k_{N_{i_2}}}^2 \theta_2(t_j) \mid \mathbf{y}_{N_{i_2}}(t_j) \mid_2} . \tag{36}$$

If ε is the accuracy of the time scheme, we recall that K corresponds to a high order derivative of $\mathbf{u}_N$ versus time. Hence, we can reasonably assume that K is at least of the order of $\mid \mathbf{y}_{N_{i_2}}(t_j) \mid_2$. This case occurs when a Direct Numerical Simulation is performed.

Time scale estimate for the transfer terms.

Let us denote by $\mathbf{y}$ instead of $\mathbf{y}_{N_i}$ the large scale component of the flow. We recall that $\mathbf{y}$ is governed by the equation :

$$\dot{\mathbf{y}} - \nu\Delta\mathbf{y} + PB(\mathbf{y},\mathbf{y}) + PB_{\text{int}}(\mathbf{y},\mathbf{z}) = P\mathbf{g}.$$

Here, P denotes P_{N_i} and $\dot{\mathbf{y}} = \frac{\partial \mathbf{y}}{\partial t}$. Let us rewrite the previous equation under the form :

$$\dot{\mathbf{y}} = \nu\Delta\mathbf{y} + P\mathbf{g} - PB(\mathbf{y},\mathbf{y}) - PB_{\text{int}}(\mathbf{y},\mathbf{z}).$$

We introduce the function F defined by

$$F(\mathbf{y}) = \nu\Delta\mathbf{y} + P\mathbf{g} - PB(\mathbf{y},\mathbf{y}),$$

so that :

$$\dot{\mathbf{y}} = F(\mathbf{y}) - PB_{\text{int}}(\mathbf{y},\mathbf{z}). \tag{37}$$

In this form, it clearly appears that the transfer terms $PB_{\rm int}(\mathbf{y},\mathbf{z})$ is a correction to the time derivative of the large scale components. As it was done before for the small structures, we derive a Taylor expansion of $\mathbf{y}(t)$:

$$\mathbf{y}(t+\tau) \;=\; \mathbf{y}(t) + \tau\dot{\mathbf{y}}(t) + \frac{\tau^2}{2}\ddot{\mathbf{y}}(t) + o(\tau^3). \tag{38}$$

We assume here that the terms of order larger than three are negligible. From (37), we can derive :

$$\ddot{\mathbf{y}}(t) \;=\; \dot{F}(\mathbf{y}) - P\dot{B}_{int}(\mathbf{y},\mathbf{z}).$$

Reporting this expression into (38), we obtain :

$$\mathbf{y}(t+\tau) \;=\; \mathbf{y}(t) + \tau\dot{\mathbf{y}}(t) + \frac{\tau^2}{2}\dot{F}(\mathbf{y}) - \frac{\tau^2}{2}P\dot{B}_{int}(\mathbf{y},\mathbf{z}) + o(\tau^3).$$

As we tolerate an error of the order of ε on $\mathbf{y}(t+\tau)$, the coupled nonlinear terms $PB_{\rm int}(\mathbf{y},\mathbf{z})$ can be frozen during a time τ, if :

$$\frac{\tau^2}{2} \mid P\dot{B}_{int}(\mathbf{y},\mathbf{z}) \mid_2 \;\leq\; K\varepsilon. \tag{39}$$

Then, it follows an estimate on τ :

$$\tau \;\leq\; \left(\frac{2K\varepsilon}{\mid P\dot{B}_{int}(\mathbf{y},\mathbf{z}) \mid_2}\right)^{1/2} \;=\; \tau'(\varepsilon). \tag{40}$$

We note that, if ε is the accuracy of the scheme, condition (40) is necessary to preserve the order of the time scheme. On Figure 15, we have plotted the evolution of the ratio $\tau'(\varepsilon)$ for different levels of refinement N_i. As for $\tau(\varepsilon)$, the quantity $\tau'(\varepsilon)$ decreases when N_i decreases, which is due to the fact that $P\dot{B}_{int}(\mathbf{y},\mathbf{z})$ has a decaying spectrum, like $\dot{\mathbf{z}}(t)$. So, for the levels N_i lying in the transition range, i.e. between N_{i_1} and N_{i_2}, the value of $\tau'(\varepsilon)$ corresponding to the level N_{i_1} is the most restricted one. Hence, in order to control the variations of $P_{N_i}B_{\rm int}(\mathbf{y}_{N_i},\mathbf{z}_{N_i})$ on the different levels, a sufficient condition is to estimate $\tau'(\varepsilon)$ on the lower level N_{i_1} of the transition range. We want to note that the mathematical estimates which can be derived on the time derivative $P\dot{B}_{int}(\mathbf{y},\mathbf{z})$ of the transfer terms do not provide efficient

information ; nevertheless, the numerical experiments show a correlation between

$$\frac{\mid P\dot{B}_{int}(\mathbf{y},\mathbf{z}) \mid_2}{\mid PB_{\rm int}(\mathbf{y},\mathbf{z}) \mid_2} \text{ and } \frac{\mid \dot{\mathbf{z}}(t) \mid_2}{\mid \mathbf{z}(t) \mid_2}$$

as we can see on Figure 11. So, we deduce that

$$\frac{\tau^2}{2} \mid P\dot{B}_{int}(\mathbf{y},\mathbf{z}) \mid_2 \geq c_{12} \frac{\tau^2}{2} \mid PB_{\rm int}(\mathbf{y},\mathbf{z}) \mid_2 \frac{\mid \dot{\mathbf{z}}(t) \mid_2}{\mid \mathbf{z}(t) \mid_2},$$

where c is nondimensional constant of the order of the unity. Hence, it follows that :

$$\tau \leq \left(\frac{2K\varepsilon}{c_{12} \mid \dot{\mathbf{z}}(t) \mid_2} \frac{\mid \mathbf{z}(t) \mid_2}{\mid PB_{\rm int}(\mathbf{y},\mathbf{z}) \mid_2} \right)^{1/2} = \tau''(\varepsilon). \tag{41}$$

We then obtain with (41) an estimate of τ as a function of $\mid \dot{\mathbf{z}}(t) \mid_2$. From a computational point of view, (41) is much more efficient than (40). As it was noted before, we have to derive an estimate on $\tau''_{N_{i_1}}(\varepsilon)$ in order to control the time variations of the transfer terms which depend on the scales in the transition range. We now recall that the level N_{i_1} is defined by the evaluation of the ratio :

$$\theta_1(t_j) = \frac{\| \mathbf{z}_{N_{i_1}}(t_j) \|}{\| \mathbf{y}_{N_{i_1}}(t_j) \|}.$$

Moreover, this ratio is equivalent to the ratio of the coupled nonlinear terms of the large scales in the energy norm, namely

$$\frac{\mid P_{N_{i_1}} B_{\rm int}(\mathbf{y}_{N_{i_1}}, \mathbf{z}_{N_{i_1}}) \mid_2}{\mid P_{N_{i_1}} B(\mathbf{y}_{N_{i_1}}, \mathbf{y}_{N_{i_1}}) \mid_2} \geq c_{13} \frac{\| \mathbf{z}_{N_{i_1}}(t_j) \|}{\| \mathbf{y}_{N_{i_1}}(t_j) \|} = c_{13}\, \theta_1(t_j),$$

where c is of the order of the unity. The estimates can then be written under the new form :

$$\tau''_{N_{i_1}}(\varepsilon) \leq \left(\frac{2K\varepsilon}{\theta_1(t_j) \mid P_{N_{i_1}} B(\mathbf{y}_{N_{i_1}}, \mathbf{y}_{N_{i_1}}) \mid_2} \times \frac{\mid \mathbf{z}_{N_{i_1}}(t_j) \mid_2}{\mid \dot{\mathbf{z}}_{N_{i_1}}(t_j) \mid_2} \right)^{1/2}. \tag{42}$$

In (42), the time derivative of the small scale components $\dot{\mathbf{z}}_{N_{i_1}}(t_j)$ can be estimated as it was done previously. Finally, $\tau_{N_{i_1}}(\varepsilon)$ provides a constraint on the choice of the level N_{i_1}, while $\tau_{N_{i_2}}(\varepsilon)$ and $\tau''_{N_{i_1}}(\varepsilon)$ provides two estimates of the length of the whole cycle.

2.3 Approximate equation for the quasi–static scales $\mathbf{z}_{N_1}$: projection on an Approximate Inertial Manifold.

In this section, we intend to discuss the efficiency of the Approximate Inertial Manifolds (AIM) and show in which part of the spectrum they can be used.

We consider an approximation of the equation of the small scales (12) in which we drop the coupled nonlinear terms :

$$\frac{d\mathbf{z}}{dt} - \nu\Delta\mathbf{z} + QB(\mathbf{y},\mathbf{y}) \;=\; 0. \tag{43}$$

We now introduce an operator $e^{-\nu t\Delta}$ defined by :

$$e^{-\nu t\Delta}\mathbf{z} \;=\; \sum_{\mathbf{k}\in I_N\setminus I_{N_1}} e^{\nu|\mathbf{k}|^2 t}\hat{u}(\mathbf{k},t)\; w_{\mathbf{k}}.$$

Then by applying this operator to (43), we obtain :

$$\frac{d}{dt}\left(e^{-\nu t\Delta}\mathbf{z}\right) \;=\; -e^{-\nu t\Delta}QB(\mathbf{y},\mathbf{y}). \tag{44}$$

We assume, in agreement with the method described in Section 2.1, that $\mathbf{z}$ has been frozen on the time interval $[t_j, t_j+\tau_c(t_j)]$ where $\tau_c(t_j)$ is estimated as in the previous section. For the sake of simplicity, we write here t instead of t_j and τ_c instead of $\tau_c(t_j)$. We then integrate (44) over the interval $[t, t+\tau_c]$, which yields :

$$\mathbf{z}(t+\tau_c) \;=\; e^{\nu\tau_c\Delta}\mathbf{z}(t) - \int_t^{t+\tau_c} e^{-\nu(\sigma-t-\tau_c)\Delta}QB(\mathbf{y}(\sigma),\mathbf{y}(\sigma))\; d\sigma.$$

Consider then the following approximation of the right–hand side :

$$\begin{aligned}\int_t^{t+\tau_c} e^{-\nu(\sigma-(t+\tau_c))\Delta}QB(\mathbf{y}(\sigma),\mathbf{y}(\sigma))\; d\sigma \\ \simeq (-\nu\Delta)^{-1}(1-e^{\nu\tau_c\Delta})QB(\mathbf{y}(t+\tau_c),\mathbf{y}(t+\tau_c)).\end{aligned} \tag{45}$$

Finally, $\mathbf{z}(t+\tau_c)$ is computed by :

$$\begin{aligned}\mathbf{z}(t+\tau_c) \;&=\; e^{\nu\tau_c\Delta}\mathbf{z}(t) \\ &\quad -(-\nu\Delta)^{-1}(1-e^{\nu\tau_c\Delta})QB(\mathbf{y}(t+\tau_c),\mathbf{y}(t+\tau_c))\end{aligned} \tag{46}$$

(46) means that the small scales are slaved by the large ones. Also, from a computational point of view, (46) provides an efficient way to evaluate the small scales. In comparison to a classical time scheme, (46) presents the advantage that only one evaluation of the nonlinear terms is required. The error occuring by using (46) instead of integrating the small scales equation is constituted by two components, namely the time discretization on the approximation of the integral and the dropped terms $QB_{\text{int}}(\mathbf{y},\mathbf{z})$:

$$\begin{aligned} \mid \varepsilon(\mathbf{z}) \mid_2 \; &\leq \mid \int_t^{t+\tau_c} e^{-\nu(\delta-(t+\tau_c))\Delta} QB_{\text{int}}(\mathbf{y}(\sigma),\mathbf{z}(\sigma))\, d\sigma \mid_2 \\ &+ \mid \int_t^{t+\tau_c} e^{-\nu(\sigma-(t+\tau_c))\Delta} \left(QB(\mathbf{y}(\sigma),\mathbf{y}(\sigma)) - QB(\mathbf{y}(t+\tau_c),\mathbf{y}(t+\tau_c))\right) d\sigma \mid_2 \\ &\leq \tau_c \mid QB_{\text{int}}(\mathbf{y},\mathbf{z})_{t,\tau_c} \mid_2 + 2\,\tau_c \mid QB(\mathbf{y},\mathbf{y})_{t,\tau_c} \mid_2 \end{aligned} \tag{47}$$

where $\mid QB_{\text{int}}(\mathbf{y},\mathbf{z})_{t,\tau_c} \mid_2 = \max_{\sigma\in[t,t+\tau_c]} \mid QB_{\text{int}}(\mathbf{y}(\sigma),\mathbf{z}(\sigma)) \mid_2$, and similarly for $\mid QB(\mathbf{y},\mathbf{y})_{t,\tau_c} \mid_2$.
Considering the previous discussions,

$$\begin{aligned} \mid \dot{\mathbf{z}}(t) \mid_2 \; &\simeq \mid QB_{\text{int}}(\mathbf{y}(t),\mathbf{z}(t)) \mid_2 \\ &\simeq \mid QB_{\text{int}}(\mathbf{y},\mathbf{z})_{t,\tau_c} \mid_2 \\ &\simeq \mid QB(\mathbf{y},\mathbf{y})_{t,\tau_c} \mid_2 . \end{aligned}$$

Then, we obtain an estimate of the error :

$$\mid \varepsilon(\mathbf{z}) \mid_2 \leq \; c_{14}\; \tau_c \mid \dot{\mathbf{z}}(t) \mid_2 . \tag{48}$$

Recalling that τ_c is defined such that

$$\tau_c \mid \dot{\mathbf{z}}(t) \mid_2 \; \leq K\; \varepsilon,$$

we then have the following estimate :

$$\mid \varepsilon(\mathbf{z}) \mid_2 \leq \; c_{14}\; K\; \varepsilon.$$

Then, from the definition of the level N_{i_2} and τ_c, the error introduced by using the approximate equation (46) is always smaller than ε. We want to

note that the error $\varepsilon(\mathbf{z})$ does not depend directly on the level N_{i_2} : there is no restriction on the value of N_{i_2}. The Approximate Inertial Manifold (46) can then be used to simulate the evolution of the fine structures of the flow even for wave–numbers lying inside the inertial range of the spectrum. In the numerical simulations presented in the next subsection, (46) will be used.

Remark 2 : Let us now consider the Approximate Inertial Manifold introduced in [1], namely :

$$-\nu\Delta\mathbf{z} + QB(\mathbf{y},\mathbf{y}) \;=\; 0. \tag{49}$$

We recall that (49) consists of an approximation of the full equation of the small scale components $\mathbf{z}$, where the time derivative $\dot{\mathbf{z}}$ as well as the coupled nonlinear terms $QB_{\text{int}}(\mathbf{y},\mathbf{z})$ have been dropped. In the case considered here of periodic boundary conditions, it is easy to invert the Stokes operator $(-\Delta)$ and then $\mathbf{z}$ can be evaluated as a function of $\mathbf{y}$:

$$\mathbf{z} \;=\; (-\nu\Delta)^{-1}QB(\mathbf{y},\mathbf{y}). \tag{50}$$

At this point, we note that for large values of τ_c, (46) and (50) are equivalent. The order of magnitude of the dropped terms in the small scale equations may induce a restriction on the use of (50) to evaluate $\mathbf{z}$. In fact, we want to find criteria telling in which range of the spectrum (50) can be applied. The spatial error $\delta(\mathbf{z})$ appearing when (50) is used is exactly given by the difference between (50) and the $\mathbf{z}$ equation, i.e. :

$$\delta(\mathbf{z}) \;=\; (\nu\Delta)^{-1}(\dot{\mathbf{z}} + QB_{\text{int}}(\mathbf{y},\mathbf{z})).$$

We can then estimate

$$|\,\delta(\mathbf{z})\,|_2 \leq\; (\nu k_{N_1}^2)^{-1}\;|\,\dot{\mathbf{z}} + QB_{\text{int}}(\mathbf{y},\mathbf{z})\,|_2\;.$$

In the numerical experiments that we have conducted, we have seen that the right–hand side of the previous inequality is of the order of $(\nu k_{N_1}^2)^{-1}\;|\,\dot{\mathbf{z}}\,|_2$; hence it follows that

$$|\,\delta(\mathbf{z})\,|_2 \leq\; c_{15}\;(\nu k_{N_1}^2)^{-1}\;|\,\dot{\mathbf{z}}(t)\,|_2,$$

where c_{15} is a nondimensional constant of the order of unity. Then, the spatial error introduced by (50) mainly depends on the size of $|\,\dot{\mathbf{z}}(t)\,|_2$. Assuming

that N_1 lies in the dissipation range and that $| \dot{\mathbf{z}}(t) |_2$ can be estimated by $| \nu \Delta \mathbf{z} |_2$, we obtain :

$$| \delta(\mathbf{z}) |_2 \leq c_{16} \ | \mathbf{z} |_2,$$

by using

$$| \dot{\mathbf{z}}_{N_1} |_2 \simeq (\nu k_{N_1}^2) \ | \mathbf{z}_{N_1} |_2 .$$

Hence, in that specific case, the error $\delta(\mathbf{z})$ is of the order of $\mathbf{z}$ itself. Thus (50) can be used in the quasi–static range of the spectrum where $\mathbf{z}$ is of the order of the scheme accuracy. On Figure 16, we can see that the quantity $(\nu k_{N_1}^2)^{-1} \ | \dot{\mathbf{z}}(t) |_2$ becomes larger than $| \mathbf{z} |_2$ itself when the cut–off value N_1 decreases. Hence, it seems that if (50) is an efficient way to compute the very fine structures of the flow lying far inside the dissipation range, it is no longer the case for the scales of the order of, and immediately larger than the dissipation scale ℓ_η.

2.4 Description of the complete multilevel algorithm.

In this section, we summarize the complete multilevel method which includes the time scales derived in Section 1.2.2. We still denote by ε the accuracy of the computation ; we recall that ε is a given parameter in the following algorithm.
As in subsection 2.1, we choose a sequence of levels N_i such that :

$$N_1 < N_2 < \ldots < N_i < N_{i+1} < \ldots < N.$$

The whole time interval of the simulation, namely $[t_0, t_0 + T]$, is split into several intervals of the form

$$[t_j, t_j + \tau_c(t_j)],$$

where $t_j = t_0 + \sum_{k=1}^{j-1} \tau_c(t_k)$. Futhermore, we assume that the final time $t_0 + T$ satisfies

$$t_0 + T = t_m,$$

so that we have m intervals. Let us now assume that the approximate solution $\mathbf{u}_N(\mathbf{x}, t)$ is known at time t_j with $j < m$. As in 2.1, we compute two levels

of refinement $N_{i_1}(t_j)$ and $N_{i_2}(t_j)$ according to the procedures (20) and (21). Moreover, we impose that

$$\tau_{N_{i_1}}(\varepsilon) \;=\; \frac{K\varepsilon}{\mid \dot{\mathbf{z}}_{N_{i_1}} \mid_2} \;\geq\; \Delta t.$$

With (35) and (42), we derive an a priori estimate of respectively $\tau_{N_{i_2}}(\varepsilon)$ and $\tau''_{N_{i_1}}(\varepsilon)$; we then obtain an evaluation of the length $\tau_c(t_j)$ of the $j^{\underline{\text{th}}}$ cycle :

$$\tau_c(t_j) = \min(\tau_{N_{i_2}}(\varepsilon),\ \tau''_{N_{i_1}}(\varepsilon)). \tag{51}$$

We note here that, with this definition, $\tau_c(t_j)$ can be smaller than one V–cycle, i.e. $(2(i_2-i_1)+1)\Delta t$; in such case, levels N_{i_1} and N_{i_2} are too small and need to be reevaluated. With (51), we have an a priori estimate of the global length of the whole cycle. Finally, we have computed the three characteristic values :

$$N_{i_1}(t_j),\ N_{i_2}(t_j) \ \text{ and } \ \tau_c(t_j).$$

As in 2.1, the integration is performed on the interval $[t_j, t_j + \tau_c(t_j)]$ by a succession of V–cycles. At the end of each V–cycle, i.e. at time $t_{j+pV} = t_j + (2p(i_2 - i_1) + 1)\Delta t$, we derive an a posteriori estimate of the quantities $\tau''_{N_{i_1}}(\varepsilon)$ and $\tau_{N_{i_2}}(\varepsilon)$. Hence, we take into account the evolution of the scales lying in the transition range of the spectrum of the velocity (see Figure 3). At this time, if $(t_j+\tau_c(t_j))-t_{j+pV}$ is larger than one full V–cycle, i.e. $2(i_2-i_1)+1$ time iterations, we perform another V–cycle after reajdusting the value of $\tau_c(t_j)$ with the new values of $\tau''_{N_{i_1}}(\varepsilon)$ and $\tau_{N_{i_2}}(\varepsilon)$. Now, in the other case, i.e. if $(t_j + \tau_c(t_j)) - t_{j+pV}$ is smaller than one V–cycle, we stop the whole cycle by saying that

$$t_j + \tau_c(t_j) = t_{j+1}.$$

At $t_j + \tau_c(t_j)$, we compute the small scale components $\mathbf{z}_{Ni_2}$ of the spectrum by projecting the solution on the Approximate Inertial Manifold (46).
Then, we readjust the two levels and restart a new cycle as it was done in Section 2.1.

Before we conclude this section, we want to note that with this algorithm, in opposition with the previous ones (see for instance [10], [7] or [17]), the constants θ_1 and θ_2 of the procedures (20) and (21) can be fixed very easily.

Indeed, as we have previously seen the parameter θ_2 is chosen so that $e(\mathbf{z}_{N_{i_2}})$ is of the order of ε^2. The constant θ_1, which provides an estimate of the ratio $\| \mathbf{z}_{N_{i_1}} \| / \| \mathbf{y}_{N_{i_1}} \|$, can be evaluated at the initial state, i.e. $t = 0$, by

$$\theta_1 \simeq \frac{\varepsilon}{\Delta t \| \mathbf{y}_{N_{i_1}} \| \mid \mathbf{y}_{N_{i_1}} \mid_2}.$$

Hence, we insure that :

$$\Delta_{N_{i_1}} = \Delta t \mid \dot{\mathbf{z}}_{N_{i_1}} \mid_2 \leq c\Delta t \mid \mathbf{y}_{N_{i_1}} \mid_2 \| \mathbf{z}_{N_{i_1}} \| \leq \varepsilon.$$

Then, the condition on $\tau_{N_{i_1}(\varepsilon)}$ is satisfied i.e. $\tau_{N_{i_1}(\varepsilon)} \geq \Delta t$. Moreover, we can implement a self–adaptative procedure allowing a dynamical reevaluation of these constants during the time evolution. So, if θ_1 and θ_2 were previously fixed in an empirical way in the algorithms, we have found now a more efficient way to evaluate these constants.

Figure 4: Time evolution of the ratio $\frac{|\mathbf{z}_{N_1}|_2}{|\mathbf{y}_{N_1}|_2}$ for $N_1 = 32$, 64, 128 and $N_1 = 196$.

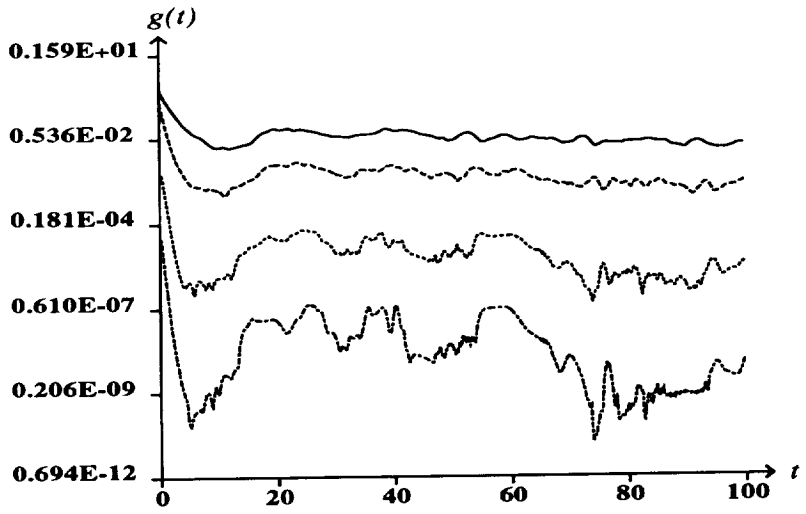

Log. Scale

Figure 5: Time evolution of the ratio $\frac{|P_{N_1} B_{\text{int}}(\mathbf{y}_{N_1}, \mathbf{z}_{N_1})|_2}{|P_{N_1} B(\mathbf{y}_{N_1}, \mathbf{y}_{N_1})|_2}$ for $N_1 = 32$, 64, 128 and $N_1 = 196$.

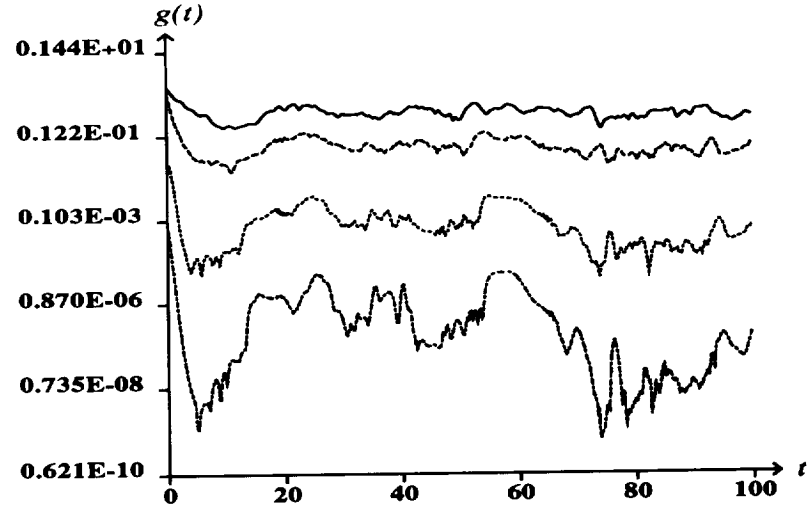

Log. Scale

Figure 6: Time evolution of $\mid \dot{\mathbf{z}}_{N_1} \mid_2$ and $\nu \mid \Delta \mathbf{z}_{N_1} \mid_2$ for $N_1 = 128$ and $N_1 = 196$.

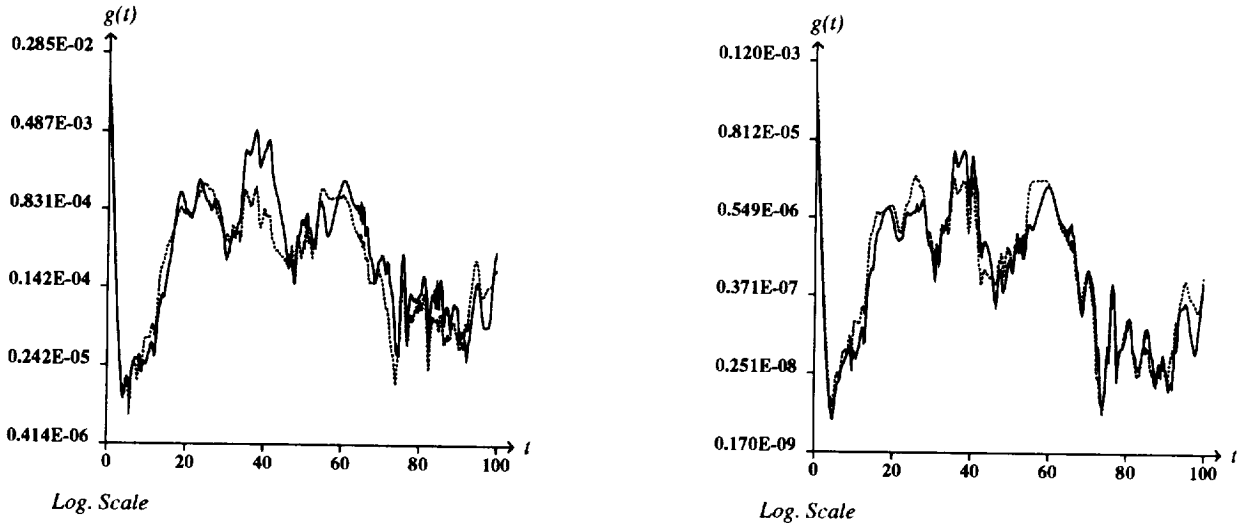

Figure 7: Time evolution of $\mid \dot{\mathbf{z}}_{N_1} \mid_2$ and $\mid Q^N_{N_1} B_{int}(\mathbf{y}_{N_1}, \mathbf{z}_{N_1}) \mid_2$, for $N_1 = 32$ and $N_1 = 64$.

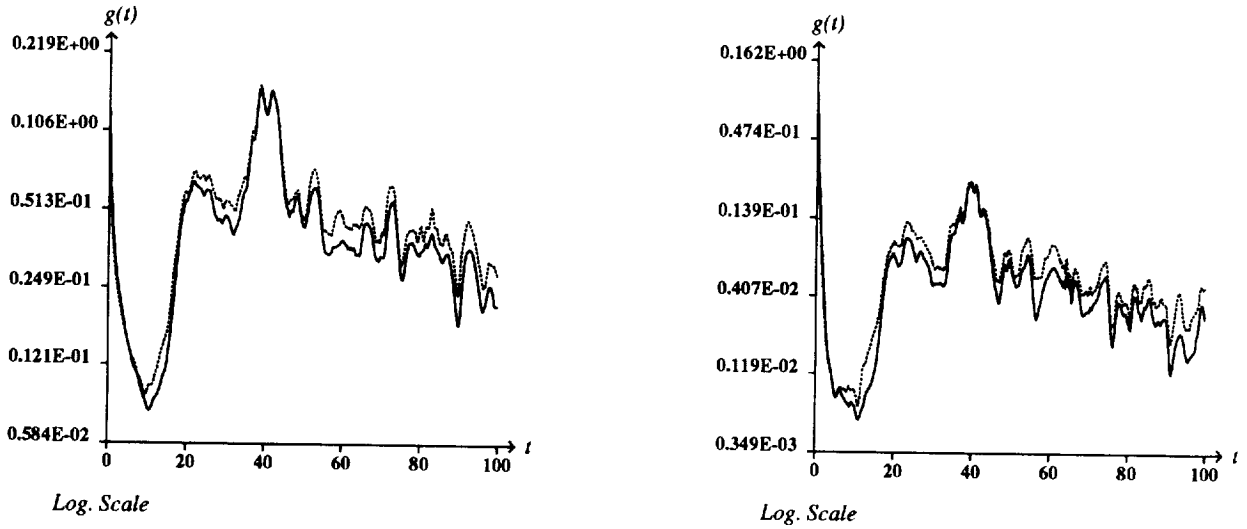

Figure 8: Time evolution of $\Delta t \mid \dot{\mathbf{z}}_{N_1} \mid_2$ and $\mid \mathbf{z}_{N_1} \mid_2$ for $N_1 = 32, 64, 128$ and 196.

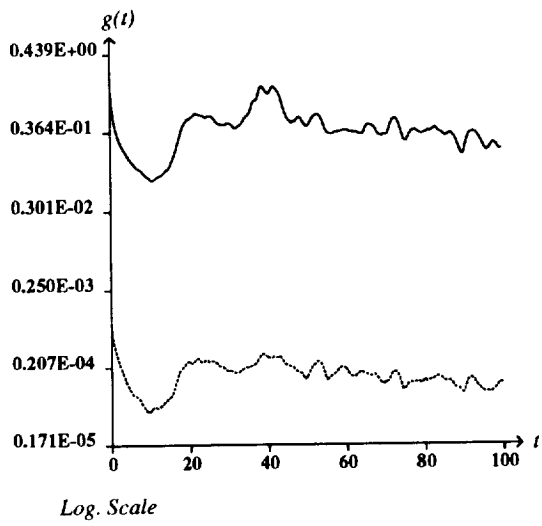

Log. Scale

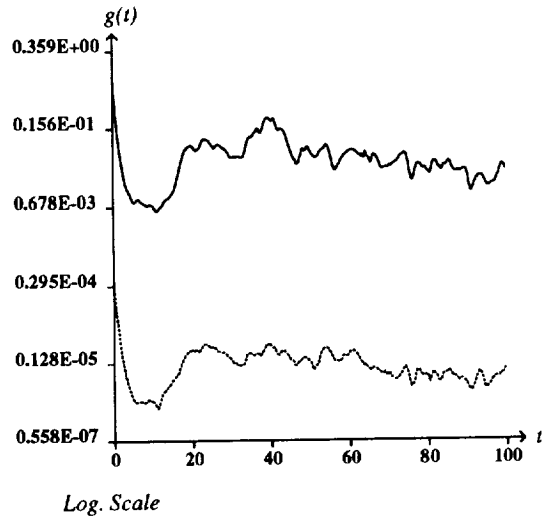

Log. Scale

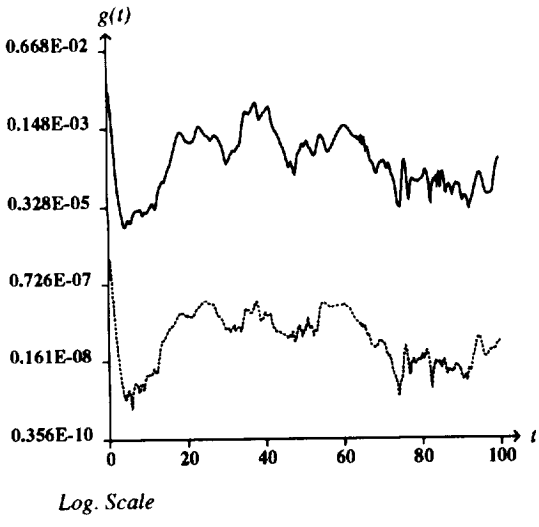

Log. Scale

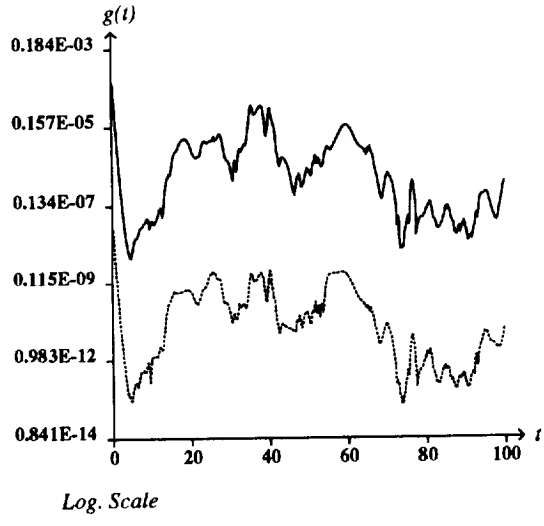

Log. Scale

Figure 9: Time evolution of $\mid \dot{\mathbf{z}}_{N_1} \mid_2$ for $N_1 = 32,\ 64,\ 128$ and $N_1 = 196$.

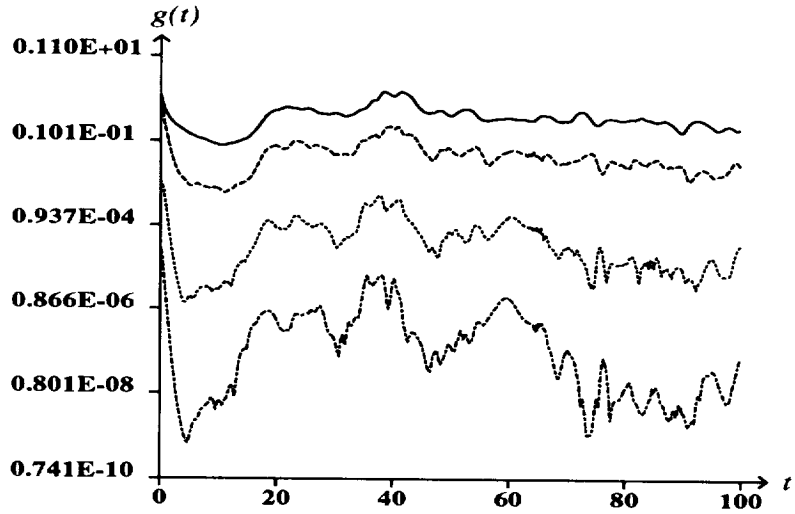

Figure 10: Time evolution of $\mid \dot{\mathbf{y}}_{N_1} \mid_2$, $\nu \mid A\mathbf{y}_{N_1} \mid_2$, $\mid P_{N_1} B(\mathbf{y}_{N_1}, \mathbf{y}_{N_1}) \mid_2$ for $N_1 = 32$.

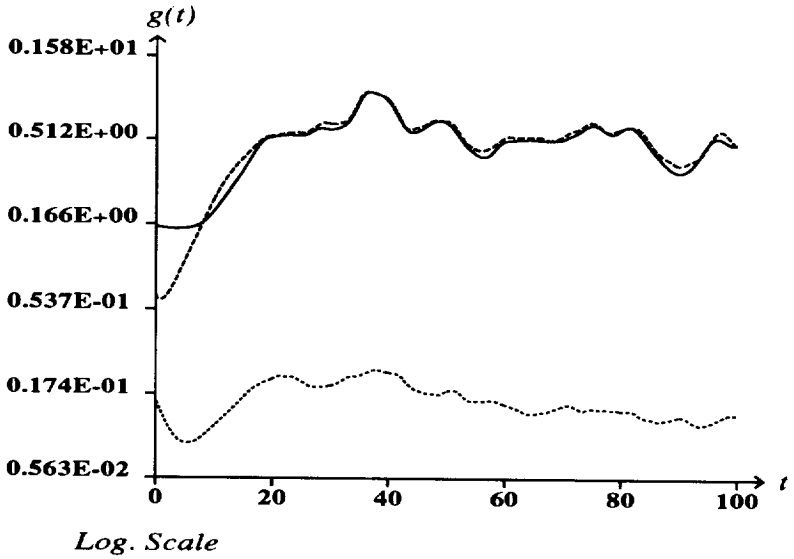

Figure 11: Time evolution of $\frac{|\dot{\mathbf{z}}_{N_1}|_2}{|\mathbf{z}_{N_1}|_2}$ and $\frac{|P_{N_1}\dot{B}_{int}(\mathbf{y}_{N_1},\mathbf{z}_{N_1})|_2}{|P_{N_1}B_{int}(\mathbf{y}_{N_1},\mathbf{z}_{N_1})|_2}$ for $N_1 =$ 32, 64, 128, and 196.

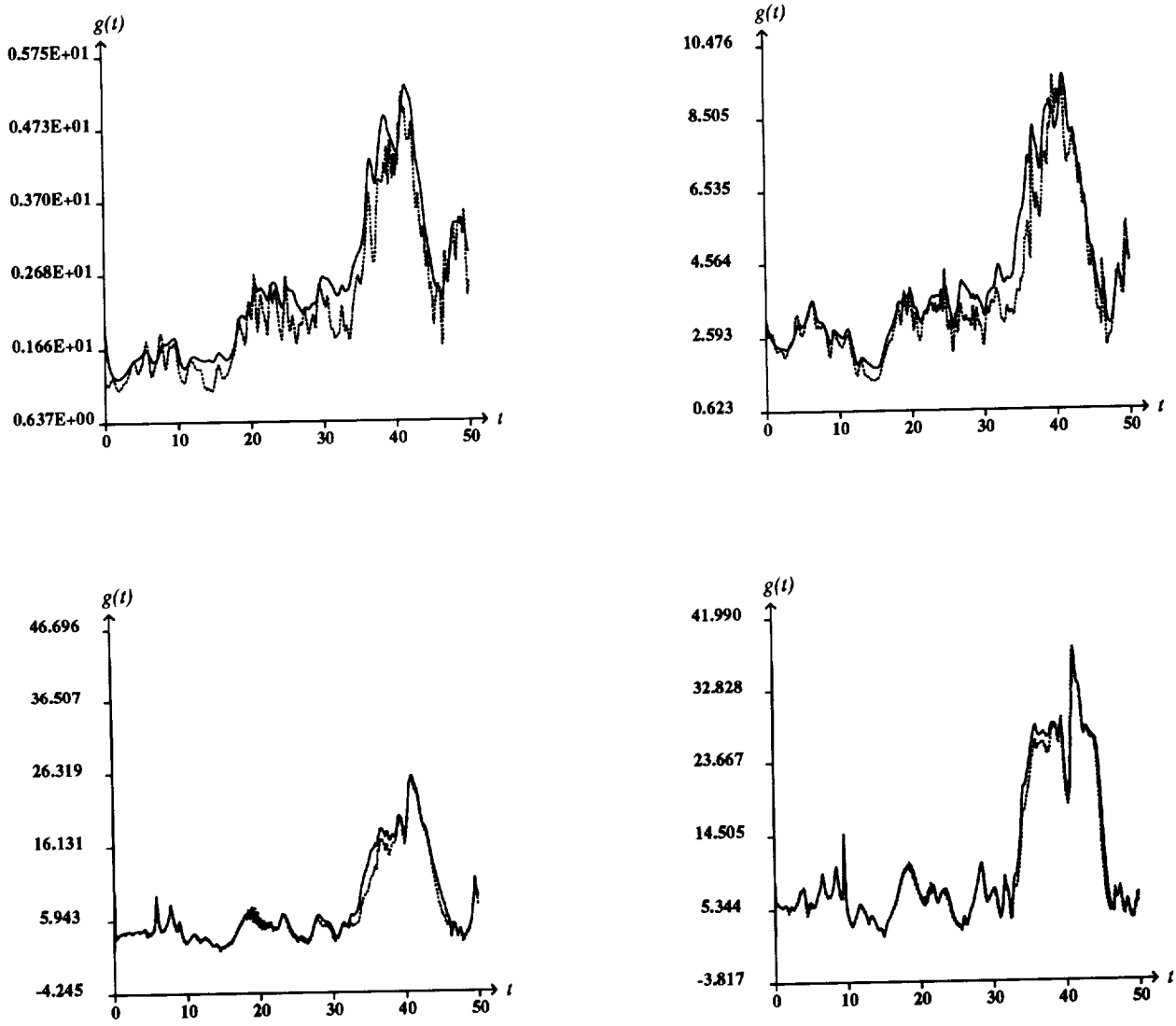

Figure 12: Time evolution of $\mid \dot{\mathbf{z}}_{N_1} \mid_2$, $\nu \mid \Delta \mathbf{z}_{N_1} \mid_2$, $\mid Q^N_{N_1} B(\mathbf{y}_{N_1}, \mathbf{y}_{N_1}) \mid_2$ and $\mid Q^N_{N_1} B_{int}(\mathbf{y}_{N_1}, \mathbf{z}_{N_1}) \mid_2$ for $N_1 = 32,\ 64,\ 128$ and 196.

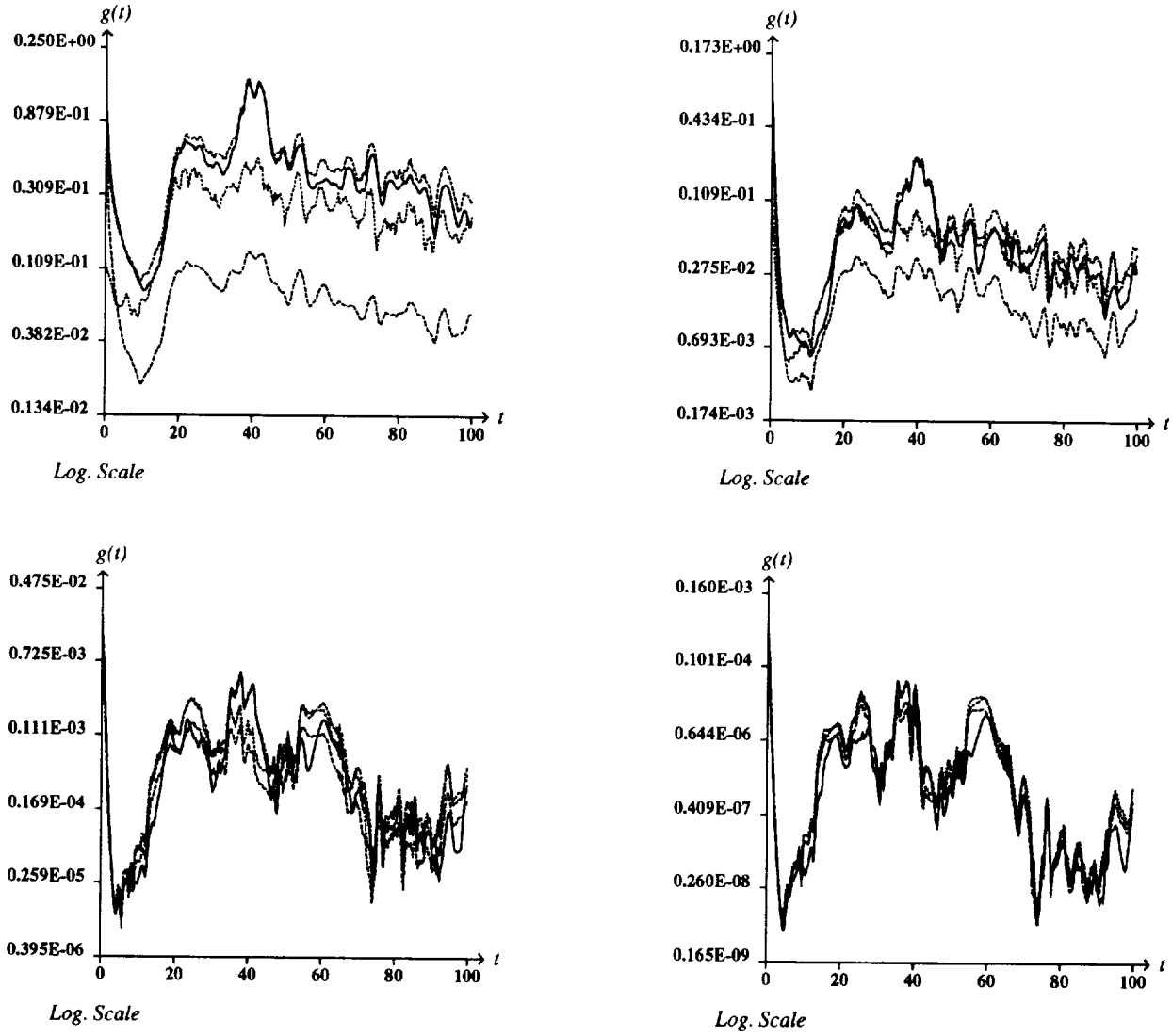

Figure 13: Time evolution of $\frac{|P_{N_1} B_{int}(\mathbf{y}_{N_1}, \mathbf{z}_{N_1})|_2}{|P_{N_1} B(\mathbf{y}_{N_1}, \mathbf{y}_{N_1})|_2}$ and $\frac{||\mathbf{z}_{N_1}||}{||\mathbf{y}_{N_1}||}$ for $N_1 =$ 32, 64, 128 and 196.

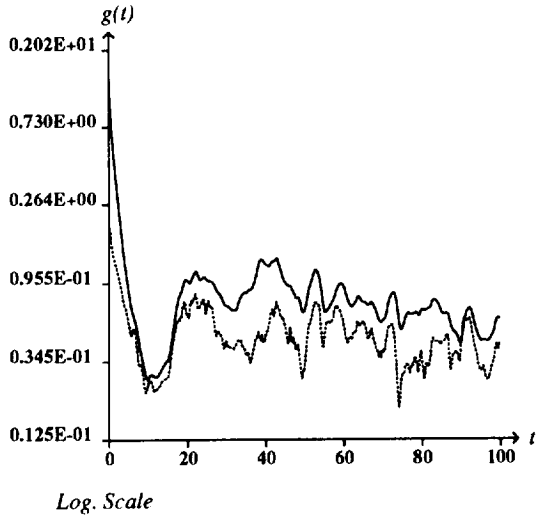

Log. Scale

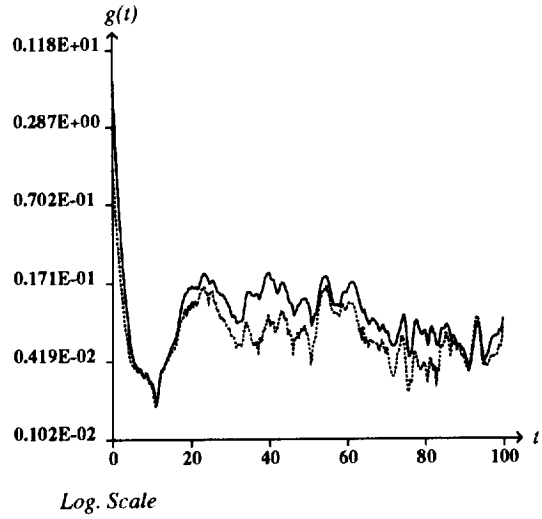

Log. Scale

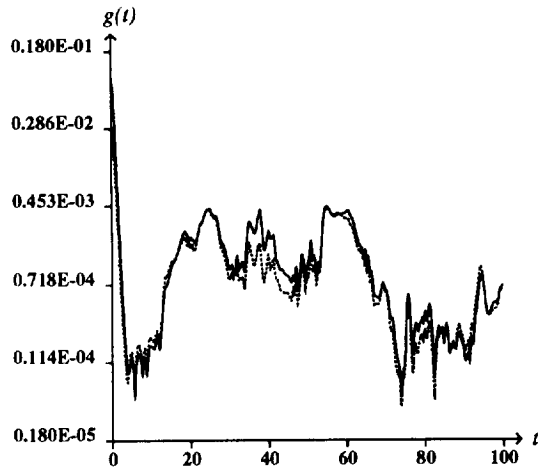

Log. Scale

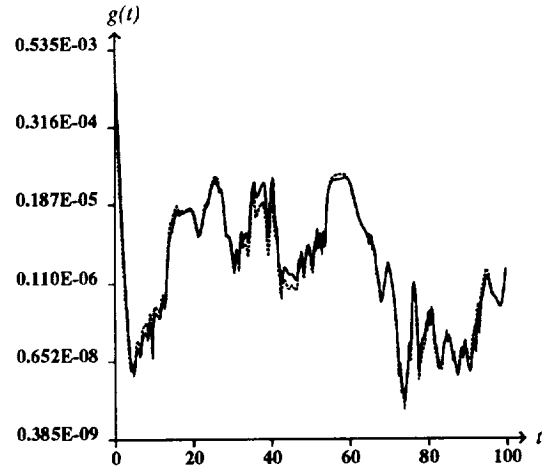

Log. Scale

Figure 14: Time evolution of $\tau(\epsilon) = \frac{K\epsilon}{|\dot{\mathbf{z}}_{N_1}(t)|_2}$ $N_1 = 32,\ 64,\ 128$ and $N_1 = 196$.

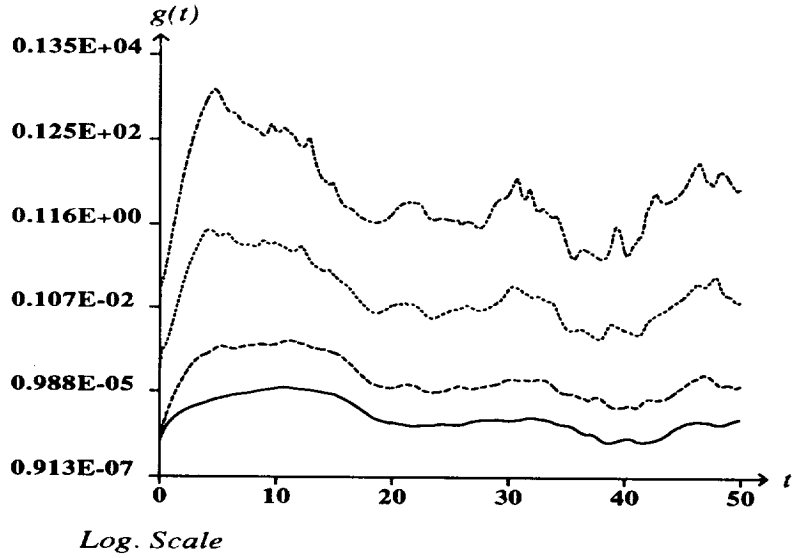

Figure 15: Time evolution of $\tau'(\epsilon) = \left(\frac{2K\epsilon}{|P_{N_1}\dot{B}_{\text{int}}(\mathbf{y}_{N_1}, \mathbf{z}_{N_1})|_2}\right)^{1/2}$ $N_1 = 32,\ 64,\ 128$ and $N_1 = 196$.

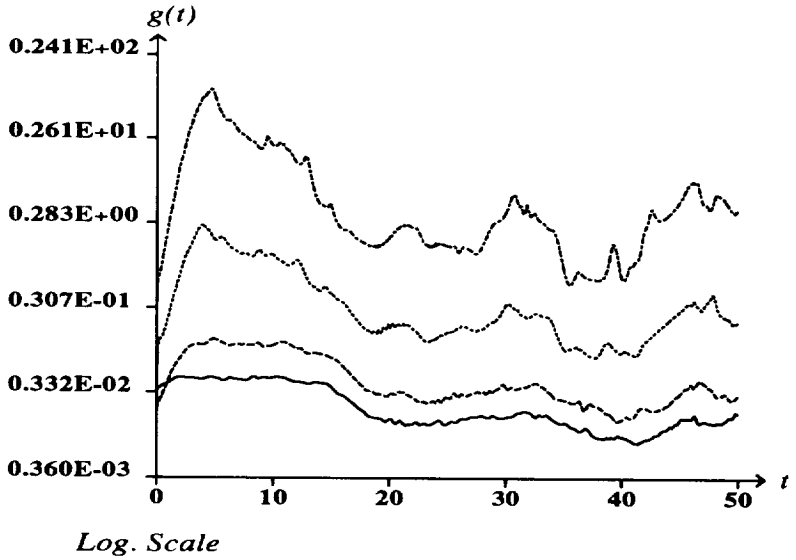

Figure 16: Time evolution of $(\nu k_{N_1}^2)^{-1}$ | $\dot{\mathbf{z}}_{N_1}$ |$_2$ and | $\mathbf{z}_{N_1}$ |$_2$ for N_1 = 32, 64, 128, and 196.

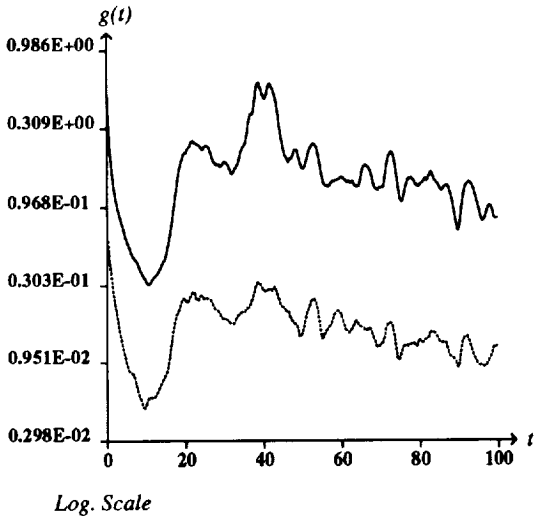

Log. Scale

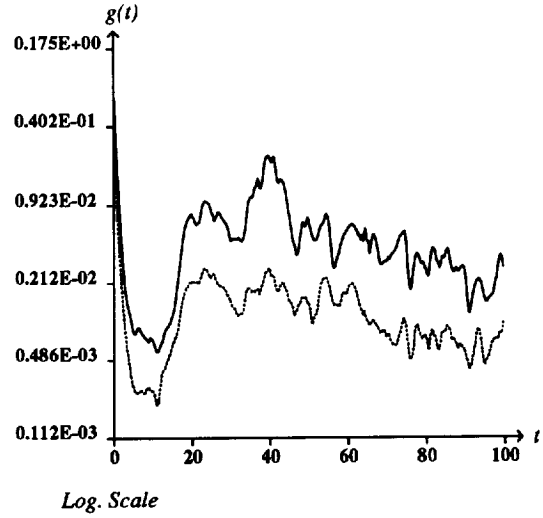

Log. Scale

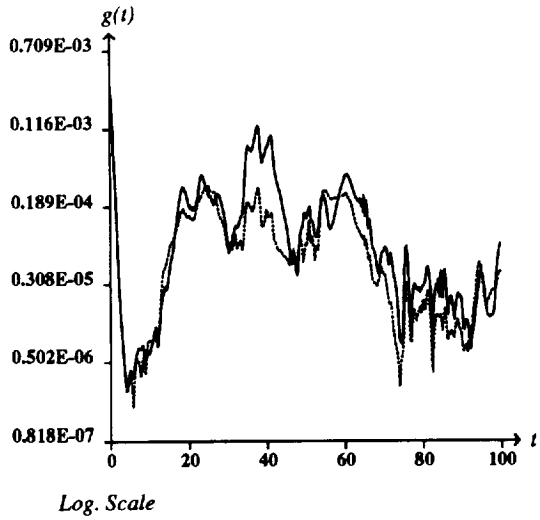

Log. Scale

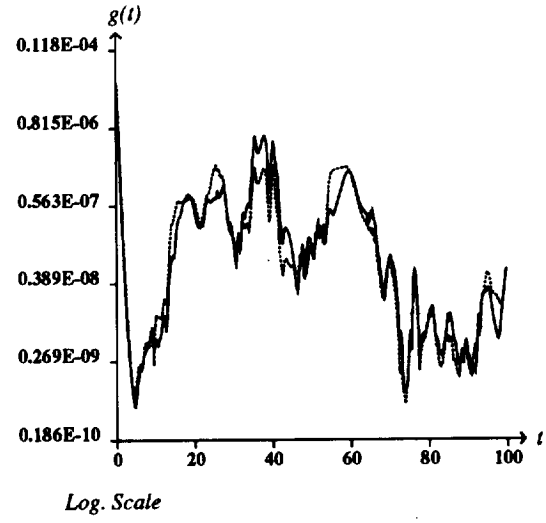

Log. Scale

3 Numerical results.

3.1 Comparison with the Galerkin method and with a previous version of the multilevel method.

In this section, we report numerical results obtained by using the nonlinear Galerkin method and a classical Galerkin projection. The flow of Kolmogorov type is forced by a time independent external force $\mathbf{f}$ which acts, in the spectral space, on only some low frequency components of the velocity field. The initial condition is chosen so that its spectrum has a specified shape but the phases of its Fourier components are randomly chosen. So, the flow at time $t = 0$ has no organized struture. We have let the flow evolve on over 10^5 time iterations, i.e. from $t = 0$ to $t = 100$; this is much longer than the integral time scale, which is of the order of the unity. We have compared the solutions obtained with both methods.

3.1.1 Description of the computation.

The initial condition here is computed from a given spectrum of the initial vorticity $\boldsymbol{\omega}_0^N = \boldsymbol{\nabla} \times \mathbf{u}_0^N$, where $\mathbf{u}_0^N$ is the following expansion :

$$\mathbf{u}_0^N(\mathbf{x}) = \sum_{\mathbf{k} \in I_N} \hat{\mathbf{u}}_{0,\mathbf{k}}(t) e^{i\mathbf{k}\cdot\mathbf{x}}, \tag{52}$$

with $\mathbf{x} = (x_1, x_2) \in \Omega$. We choose $\boldsymbol{\omega}_0^N$ by setting

$$\hat{\omega}_{0,\mathbf{k}} = \mid \hat{w}_{0,\mathbf{k}} \mid e^{i\theta_{\mathbf{k}}}, \tag{53}$$

where $\theta_{\mathbf{k}} \in [0, 2\pi]$ is generated by a random function, and :

$$\mid \hat{\omega}_{0,\mathbf{k}} \mid = \begin{cases} \dfrac{c_{17}}{(k + (\sqrt{\nu}k)^5)^{1/2}} & \text{if} \quad k = \mid \mathbf{k} \mid \leq k_\alpha, \\ \\ 0 & \text{otherwise ;} \end{cases} \tag{54}$$

c_{17} is determined such that $\mid \omega_0^N \mid_{L^\infty} = 2.0$; k_α is equal to 60. At this point, we note that if $\mid \hat{w}_{0,\mathbf{k}} \mid \sim ck^\beta$, then the energy spectrum of $\mathbf{u}_0$

$$E_0(k) = \sum_{|\mathbf{k}| = k} (\mid \hat{u}_{0,\mathbf{k}} \mid^2 + \mid \hat{v}_{0,\mathbf{k}} \mid^2)$$

is like $ck^{2\beta-2}$. So, in the case presented here $\beta = -0.5$ and we have $E_0(k) \sim k^{-3}$. On Figure 28, one can see the isovorticity lines of the initial velocity field and Figure 17 shows the energy spectrum $E(k)$.

The external force $\mathbf{f}$ is constant in time and has only a few non-zero wavenumbers, namely :

$$\hat{\mathbf{f}}_{\mathbf{k}} = (\hat{f}_{1,\mathbf{k}}, \hat{f}_{2,\mathbf{k}}),$$

with

$$\begin{cases} \mid \hat{f}_{i,\mathbf{k}} \mid = c_{18} & \text{if } \mathbf{k} \in \mathbf{Z}^2 / \mid k_1 \mid + \mid k_2 \mid = 3, \\ \mid \hat{f}_{i,\mathbf{k}} \mid = 0 & \text{otherwise,} \end{cases}$$

c_{18} is determined such that $\mid \mathbf{f} \mid_2 = 0.225$. The Fourier coefficients of $\mathbf{f}$ are finally obtained by

$$\hat{f}_{i,\mathbf{k}} = \mid \hat{f}_{i,\mathbf{k}} \mid e^{i\theta_{\mathbf{k}}},$$

where the phases $\theta_{\mathbf{k}} \in [0, 2\pi]$ are randomly generated.

In order to describe all the scales of motion, the number of modes N in each dimension of the space must be chosen so that the associated grid size $2\pi/N$ is smaller than the dissipative (Kraichnan) scales ℓ_η ; in term of wavenumber, it means that $k_N > k_\eta$. We recall that under the dissipative scales, the motion is damped by viscosity. In fact, the total number of degrees of freedom needed to describe the motion, from the dissipative scales to the large scales containing eddies, can be estimated by the ratio $(k_\eta/k_0)^2$ (see [22] and [16]). Constantin, Foias, Manley and Temam, in [16], have related this quantity to the dimension of the attrator of the Navier–Stokes equations

$$(k_\eta/k_L)^2 \sim Re_L,$$

where Re_L is the integral scale Reynolds number, which can be defined by

$$Re_L = \frac{\vartheta L}{\nu}.$$

Here $\vartheta^2 = (2/\mid \Omega \mid) e(\mathbf{u})$ and $L = 1/k_L$ is the integral length scale defined as :

$$L = \frac{\Sigma^{1/2}}{\eta^{1/3}}, \text{ where } \Sigma = (1/2)\,\vartheta^2 \text{ and } \eta = \nu \mid \Delta \mathbf{u} \mid_2^2 / \mid \Omega \mid \ (\nu = 10^{-3}).$$

L is of the order of 1.72 and ϑ is of the order of 0.45 (see Figure 19). It follows that $Re_L = 784$ and $k_\eta = 17$, which corresponds to $N_\eta = 2\ k_\eta = 34$ modes in each direction of space. In order to be sure to resolve all the scales of motion, we have chosen $N = 256$. Figures 17 show the energy spectrum $E(k)$:

$$E(k,t) \ = \sum_{|\mathbf{k}| \ = \ k} | \ \hat{\mathbf{u}}(\mathbf{k},t) \ |^2,$$

for various times. It seems that the dissipation wavenumber k_η is of the order of 20. Hence, the previous estimate based on the dimension of the attractor matches well the computational results. We note also that, if the phenomenological theory of turbulence of Kraichnan, predicts a decay of the energy spectrum like k^{-3}, results presented here seem to show a faster decay closer to k^{-4}. This results are in agreement with the ones obtained by Orszag in [23] and by Brachet et al. in [24], which show that a k^{-3} energy spectrum can only be obtained when the Reynolds number is larger than 25,000.
We also remark, that if, at $t = 0$ the small scales corresponding to a wavenumber larger than 60 are set to zero, a dissipation range appears very quickly, as we can see at $t = 5$. The enstrophy transfer from the large scales to the small ones acts on the smallest scales after a few iterations. Figure 18 indicates that the transition period is very short. The small scales are damped by viscous effect until an equilibrium between viscous and nonlinear terms appears. After that, we can see that $| \ \mathbf{z}_{N_1} \ |_2$ oscillates in time and seems to become completely independent of its initial value. Figures 28 and 30 represent the isolines of the vorticity, at different times in the interval $[0, 100]$. We can see that the very small random structures of the flow at the initial time disappear quickly. It appears that fusions of these very small structures lead to larger ones. So, after a transient period, the flow is mainly constituted by large structures.

The time step is chosen by considering the accuracy and the stability of the computation. For the stability, Δt must satisfy a CFL condition like

$$\Delta t \ N \ \ | \ \mathbf{u}_N \ |_{L^\infty} \ < \ \alpha \ (< \ 1). \tag{55}$$

From Figure 25, we can see that $| \ \mathbf{u}_N \ |_{L^\infty} < 1.25$ during all the computation, so (55) implies the following restriction on the time step :

$$\Delta t < 1.7 \ 10^{-3} \ (\alpha = 0.5).$$

We have set Δt to 10^{-3}. Here, the smallest scales (Figure 18) are of the order of 10^{-10}. Hence a time step of 10^{-3} allows to recover most of the spectrum. Indeed, the time differentiation scheme used here is a third order method, then the accuracy is of the order of 10^{-9}.

3.1.2 Comparison with a previous version of the algorithm.

In a first time, we present results obtained with a previous version of the multiscale method. In this version of the algorithm, τ_c was set to $(\nu\ k^2_{N_{i_2}})^{-1}$ and the constants θ_1, θ_2 of procedures (20) and (21) were a priori chosen (see [8]). This multiscale method is compared with the pseudo-spectral Galerkin method.

To perform this analysis, we have retained two different points of the computational domain, namely $x_1 = x_2 = \frac{2\pi}{N}\left(\frac{N}{3} - 1\right)$ and $x_1 = x_2 = \frac{2\pi}{N}\left(\frac{N}{6} - 1\right)$, and we have stored the value of the horizontal component of the velocity $u_1(x_1, x_2, t)$ at these points during the time evolution. On Figures 20 and 21, we have plotted the time history over the interval $[0, 100]$ of those two characteristic values of the flow. Results plotted here seem to be identical for both methods, but the differences between the trajectories obtained with the different algorithms are too small to appear on such graphic representation. So, we have listed below the exact values at different intermediate times for these trajectories.

In Tables 1 and 2, we have listed the values of the horizontal component of the velocity at times $t = 0, 25, 50, 75$ and 100. These results correspond to the Galerkin method for the first column. In the third column, we can see the difference between both orbits. It appears that this quantity grows as time evolves and becomes much larger than the accuracy which is of the order of $\Delta t^3 = 10^{-9}$ for this computation. On this computation, the current level $N_i(t)$ oscillates between 108 and 200. Looking backward to the results presented in section 2.2 on the estimates of the characteristic length τ_c (see Figures 22), we note that :

$$\begin{cases} \tau_{N_{i_1}} < 10^{-3} = \Delta t, \\ \tilde{\tau}''_{N_{i_1}} < 10^{-2} = 10\Delta t, \text{ for } N_{i_1} = 108. \end{cases}$$

Hence, levels N_{i1} used by the multiscale method are not appropriate.

Table 1	Galerkin	Multiscale	Difference
		Version 1	
$t = 0$	$-0.9650082490\ 10^{-2}$	———	0.000
$t = 25$	0.2980770146	0.2980770543	$3.88\ 10^{-8}$
$t = 50$	0.3592114126	0.3592114913	$7.87\ 10^{-8}$
$t = 75$	0.3819454889	0.3819452151	$2.738\ 10^{-7}$
$t = 100$	-0.1233746011	-0.1233715822	$3.0189\ 10^{-6}$

Table 2	Galerkin	Multiscale	Difference
		Version 1	
$t = 0$	0.450144224510^{-1}	———	0.000
$t = 25$	0.3879730195	0.3879729977	$2.18\ 10^{-8}$
$t = 50$	0.2458823192	0.2458824078	$9.114\ 10^{-7}$
$t = 75$	-0.3332440190	-0.3332451088	$1.091\ 10^{-6}$
$t = 100$	0.3196664945	0.3196686370	$2.142\ 10^{-6}$

Indeed, we recall that $\tau_{N_{i_1}} < \Delta t$ means that, for the level N_{i1} equal to 108, the scales smaller than $\ell_{N_{i_1}}$ can not be fixed even on one time iteration. Also,$\tau''_{N_{i_1}} < 10\Delta t$ means that the coupled nonlinear terms $P_{N_{i_1}}\tilde{B}(\mathbf{y}_{N_{i_1}}, \mathbf{z}_{N_{i_1}})$ can not be frozen on a time interval longer than $10\Delta t$. Recalling now that in this version of the multiscale algorithm, the characteristic length was estimated by $(\nu k^2_{N_{i_2}})^{-1}$, therefore the length of the frozen period oscillated between 50 Δt and 80 Δt. The constraints on the levels N_{i1} and N_{i2} imposed by the different estimates derived in section (2.2) are violated in this computation and so, the expected accuracy can not be recovered by the multiscale method.

Table 3	Galerkin	Multiscale	Difference
		Version 2	
$t = 0$	$-0.9650082490\ 10^{-2}$	———	0.0000
$t = 25$	0.2980770146	0.2980770146	$< 1.0\ 10^{-10}$
$t = 50$	0.3592114126	0.3592114126	$< 1.0\ 10^{-10}$
$t = 75$	0.3819454889	0.3819454893	$4.0\ 10^{-10}$
$t = 100$	-0.1233746011	-0.1233746004	$7.0\ 10^{-10}$

Table 4	Galerkin	Multiscale	Difference
		Version 2	
$t = 0$	0.450144224510^{-1}	———	0.000
$t = 25$	0.3879730195	0.3879729977	$2.0\ 10^{-10}$
$t = 50$	0.2458823192	0.2458824078	$< 1.0\ 10^{-10}$
$t = 75$	−0.3332440190	−0.3332451088	$2.0\ 10^{-10}$
$t = 100$	0.3196664945	0.3196686370	$< 1.0\ 10^{-10}$

3.1.3 Comparison with the improved version of the algorithm.

In Tables 3 and 4, we report results similar to those in Tables 1 and 2, but now, the second column corresponds to the version of the multiscale algorithm presented in Section 2.4. Here, the trajectories of the multiscale method remain close to the trajectories obtained with the classical method. The difference is less than $\Delta t^3 = 10^{-9}$ over the whole time interval $[0, 100]$. Here, the level N_{i1} is always larger than 128, so that the estimated limit value of τ_c is greater than Δt (see Figures 22 and 25). The levels N_{i1} and N_{i2} chosen by the new algorithm are higher than those obtained by the previous version. This fact is due to the restrictions imposed by the new criteria on τ_c. For some values of the time t, the level N_{i_1} decreases to a lower level for a short time interval and then goes up to its last value. In such a case, we have remarked that the restriction imposed on τ_c induces a restriction on the level N_{i1}. Indeed, even if a level is acceptable on a few multigrid cycles, variations of the smallest scales or of the transfers terms become too large, so that N_{i1} has to change to an upper level. Moreover, we want to mention that, during the whole computation, neither the restriction due to the small scales evolution $\tau_{N_{i_2}}$, nor the restriction due to the transfer terms evolution $\tau''_{N_{i_1}}$ is dominant. Therefore, it is necessary that both criteria be retained. Finally, we want to note that the algorithm can still be improved. Indeed, we recall that the actual choice of levels N_{i_1} and N_{i_2} are determined according two different criteria. One is based on the estimate of ratios of the kinetic energy (or enstrophy) of the small scales over the kinetic energy (or enstrophy) of the large ones, and the other one is based on the estimates of the critical characteristic time τ_c. So, it follows that τ_c may have a relatively large value, and then, the levels should be adjusted to a lower value in order to have a more reasonable estimate of τ_c. This can be viewed on Figure 27, where the time evolution of τ_c is plotted. In fact, the very strong oscillations

of τ_c are not always necessary, and, by optimising the evaluation of N_{i1} and N_{i2}, this time evolution can become smoother.
Finally, to achieve the comparison between the different algorithms, we want to note the non-negligible fact that the multiscale method requires twice less CPU time than the classical pseudospectral method. On Figure 24, the quantity :

$$\frac{T_{NLG} - T_G}{T_G}$$

is plotted, where T_{NLG} is the CPU time required by the nonlinear Galerkin method (multiscale), and T_G the CPU time required by the classical Galerkin method.
Finally, we want to mention that these simulations required more than 75 hours of CPU on a Cray2, without counting all the preliminary tests needed to the developments and improvements of the algorithm.

Figure 17: Energy spectrum at $t = 0,\ 5,\ 30,\ 50,\ 85,\ 100.$

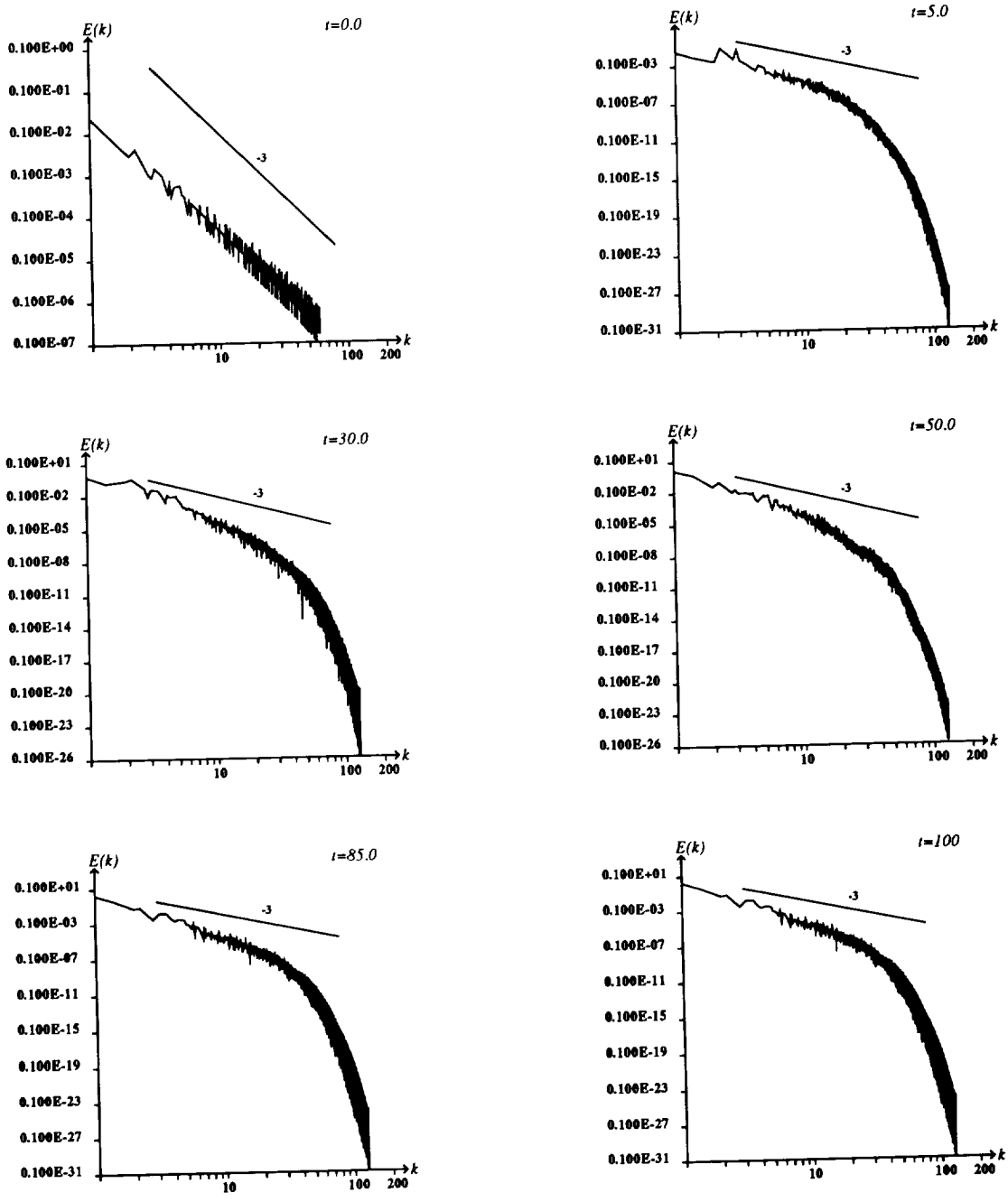

Figure 18: Time evolution of $\mid \mathbf{z}_{N_1} \mid_2$ for $N_1 = 32,\ 64,\ 128$ and $N_1 = 196$.

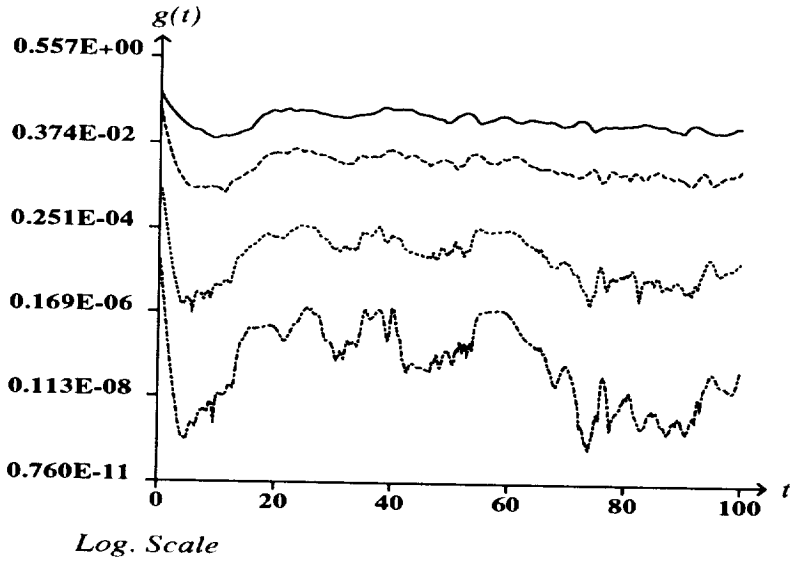

Figure 19: Time evolution of $\mid \mathbf{u}_N(t) \mid_2$.

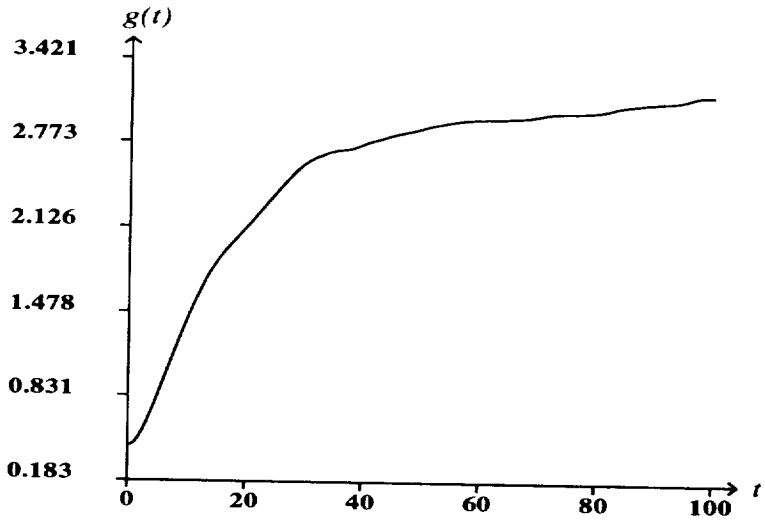

Figure 20: Time evolution of the horizontal component of the velocity $\mathbf{u_N(x, y, t)}$ at point $x = y = \frac{2\pi}{N}(\frac{N}{3} - 1)$.

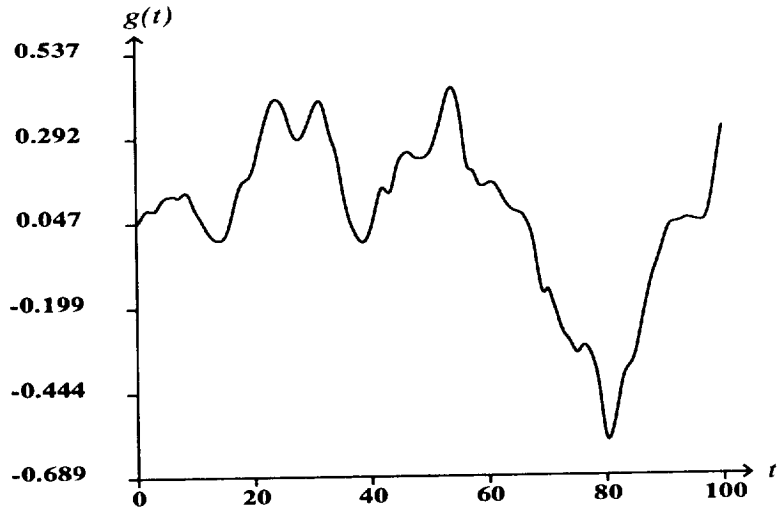

Figure 21: Time evolution of the horizontal component of the velocity $\mathbf{u}_N(x, y, t)$ at point $x = y = \frac{2\pi}{N}(\frac{N}{6} - 1)$.

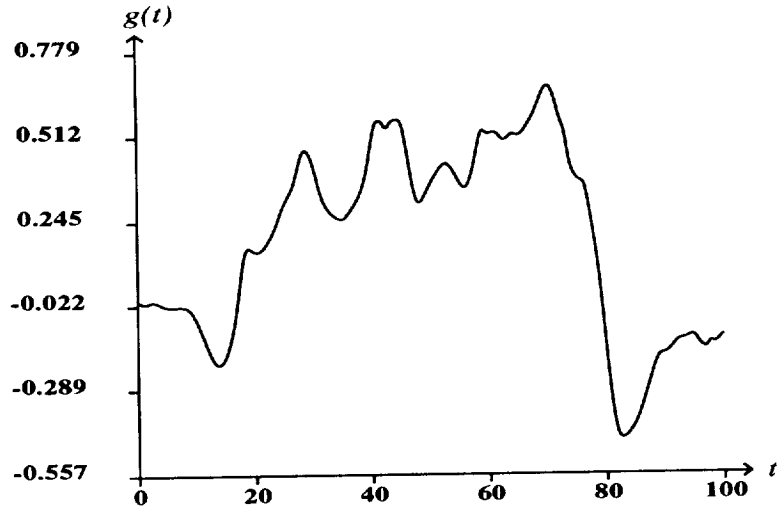

Figure 22: Time evolution of $\tau(\epsilon) = \frac{\epsilon}{|\dot{\mathbf{z}}_{N_1}(t)|_2}$ for $N_1 = 32,\ 64,\ 128$ and $N_1 = 196$.

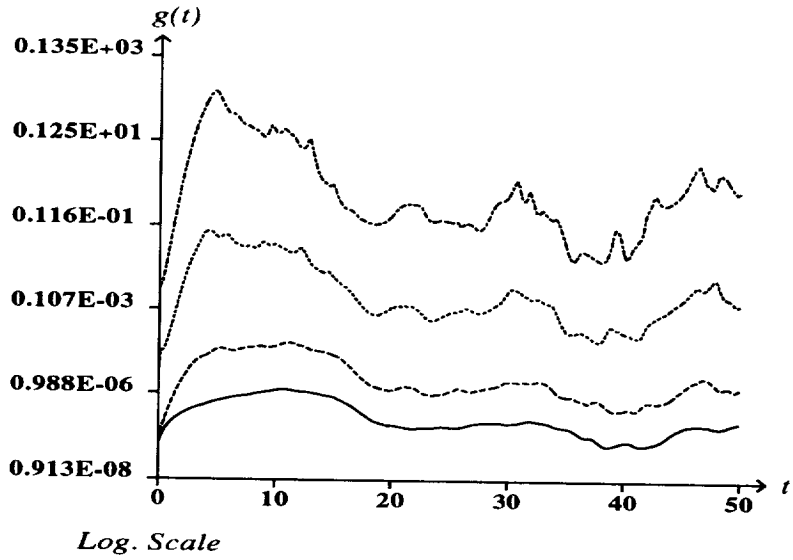

Figure 23: Time evolution of $\tau(\epsilon) = \left(\frac{2\epsilon}{|P_{N_1}\dot{B}(\mathbf{y}_{N_1}, \mathbf{z}_{N_1})|_2}\right)^{1/2}$ for $N_1 = 32,\ 64,\ 128$ and $N_1 = 196$.

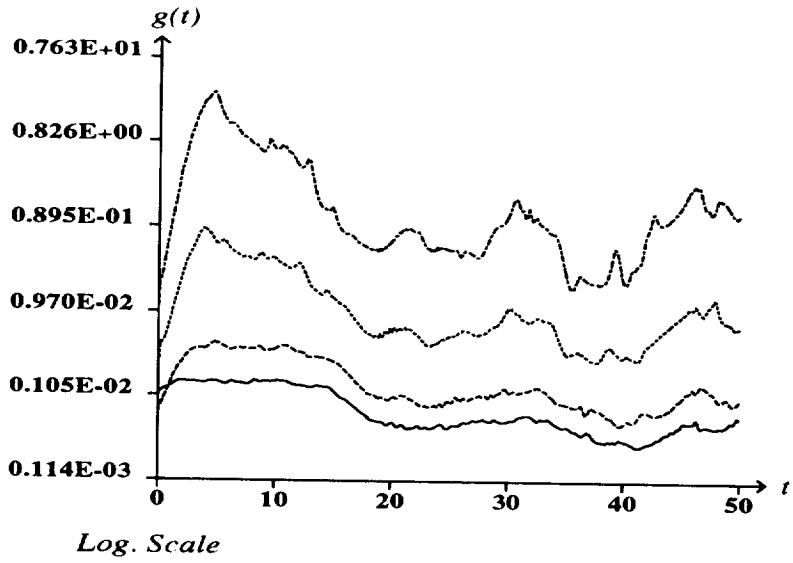

Figure 24: Time evolution of the CPU time for the classical method (full line) and for the multilevel method (dashed line).

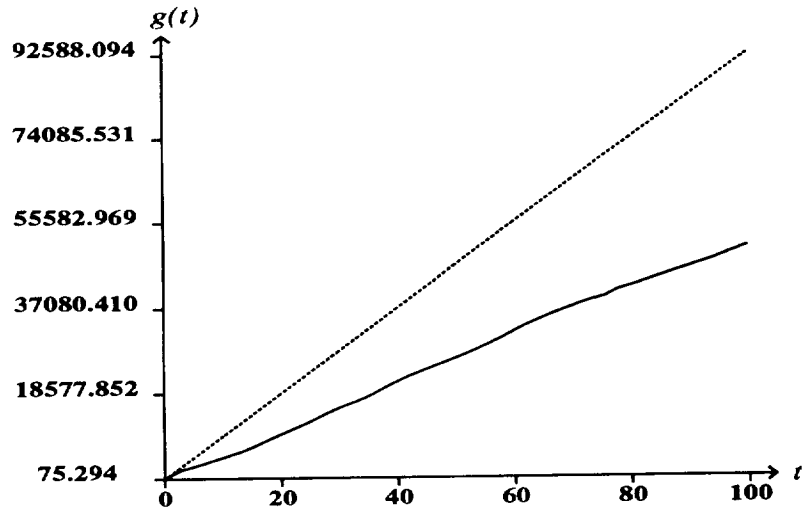

Figure 25: Time evolution of the levels $| \mathbf{u}_N(t) |_{L^\infty}$.

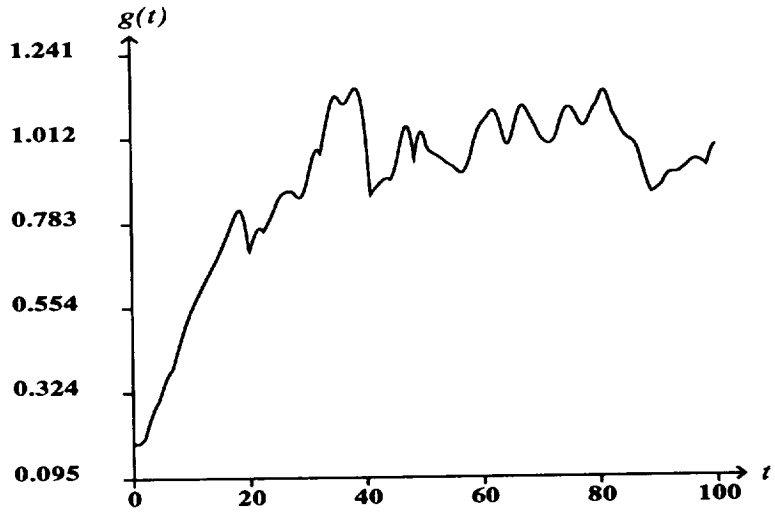

Figure 26: Time evolution of the levels $N_{i_1}(t_j)$ and $N_{i_2}(t_j)$.

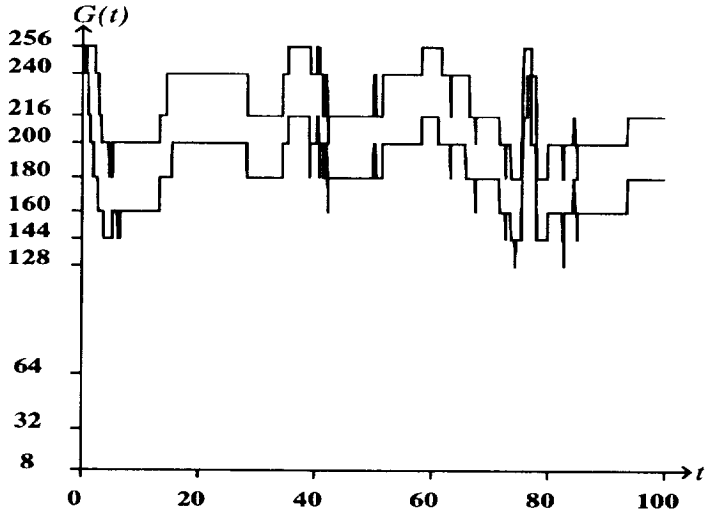

Figure 27: Time evolution of the characteristic time $\tau_c(t_j)$.

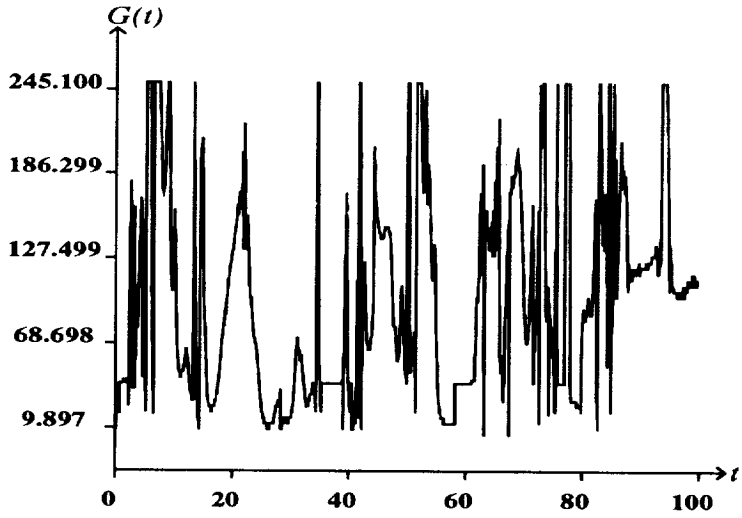

Figure 28: Vorticity structures at time $t = 0$.

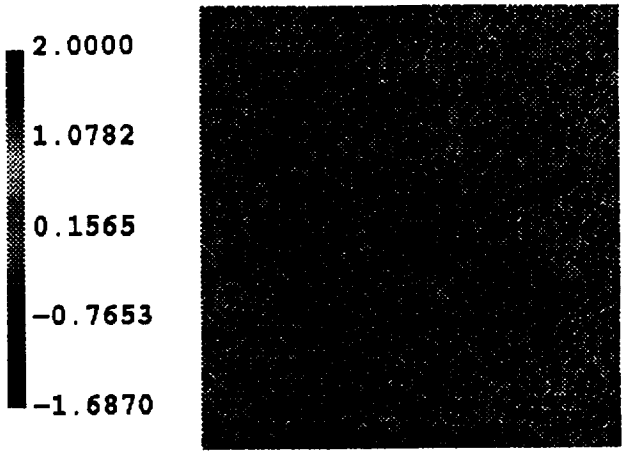

Figure 29: Vorticity structures at time $t = 30$.

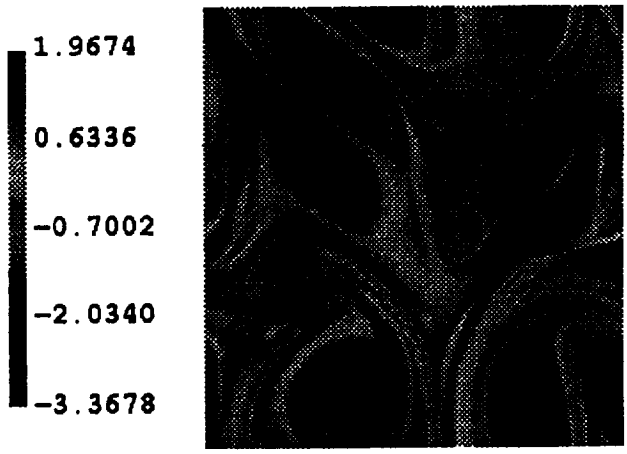

Figure 30: Vorticity structures at time $t = 60$.

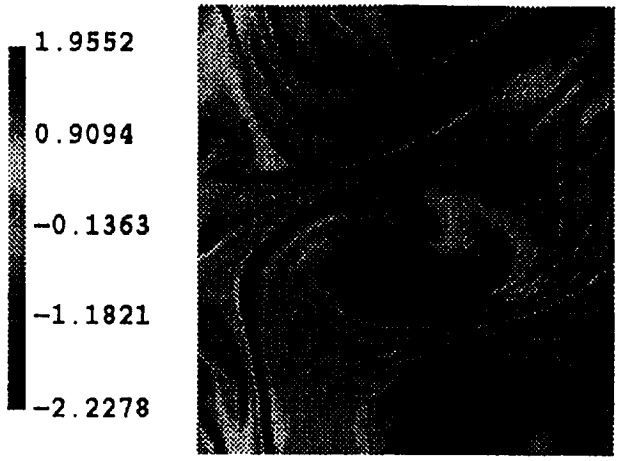

Figure 31: Vorticity structures at time $t = 100$.

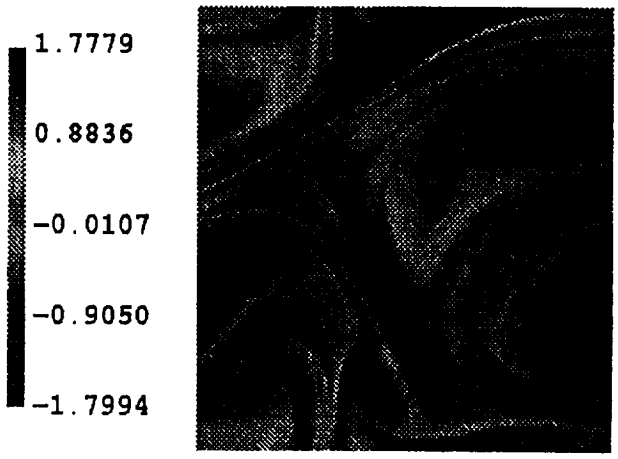

3.2 A direct numerical simulation at higher Reynolds number

We present here numerical results obtained in a numerical simulation, similar to the previous one, but with a larger value of the Reynolds number. The external force is kept the same and the viscosity is divided by 4. The initial condition is still a random field computed from a given vorticity. The computation is performed over 50,000 iterations, so that, the flow is no more dependant of its unstructured initial state. An a posteriori analysis of the behavior of the adaptative multilevel procedure confirms the previous assumptions and proves that the multiscale method is well adapted to Direct Numerical Simulations. This computation required about 50 CPU hours on a CRAY2. This total computing time includes all post-treatments done by the code, i.e. computations of different norms of several quantities related to the small and large scales. The CPU time spent to compute the velocity field is 32 hours, which corresponds to 7 10^{-6} second per mode and per iteration.

3.2.1 Description of the initial condition.

As in (3.1), the initial field $\mathbf{u}_0$ is computed in the spectral space from the coefficients of a given vorticity

$$\omega_0^N = \sum_{\mathbf{k}\in\mathbf{Z}^2, |\mathbf{k}|\leq N} \hat{\omega}_0(\mathbf{k}) e^{i\mathbf{k}\cdot\mathbf{x}}, \tag{56}$$

and the coefficients $\omega_0(\mathbf{k})$ are given by

$$\omega_0(\mathbf{k}) = \begin{cases} c_{19} \mid \mathbf{k} \mid^{-\frac{1}{2}} e^{i\theta_k} & \text{if } \mid \mathbf{k} \mid \leq k_\alpha = 60 \\ 0 & \text{otherwise} \end{cases} \tag{57}$$

where c_{19} is such that $\mid \omega_0^N \mid_{L^\infty} = 2.0$. As we can see on Figure 32, the slope of the energy spectrum at the initial time is equal to -3.
The viscosity is set to 2.5 10^{-4}, which gives a Reynolds number equal to 6,328 and the integral scale $L = 2.93$. So, the dissipative wavenumber k_η is of the order of 28 which corresponds to $N_\eta = 56$. As we want to perform a Direct Numerical Simulation a total number of modes of 512 in each direction provides a grid fine enough to resolve the scales under the dissipative ones. On Figure 32, we can see that the dissipative wavenumber obtained by the

computation is below 60. Moreover, on Figure 32 we see that the slope of the energy spectrum is smaller than -3, which is a faster decay of the energy than for a fully develloped turbulent flow.
As in the previous computation, a time step equal to 10^{-3} is small enough to insure the stability of the scheme and allows to compute all the scales with enough accuracy.

3.2.2 Analysis of the computation.

We first want to make some remarks on the behavior of the multiscale method. Figure 36 shows the time evolution of the two characteristic levels N_{i_1} and N_{i_2}, which define the transition range. As it was expected, the variations of N_{i_1} and N_{i_2} follow the variations of the ratios

$$\frac{\mid \mathbf{z}_{N_1} \mid_2}{\mid \mathbf{y}_{N_1} \mid_2} \quad \text{and} \quad \frac{\mid P_{N_1} B_{int}(\mathbf{y}_{N_1}, \mathbf{z}_{N_1}) \mid_2}{\mid P_{N_1} B(\mathbf{y}_{N_1}, \mathbf{y}_{N_1}) \mid_2}$$

for values of N_1 larger than 256, as we can see on Figures 33 and 34. On Figures 37 and 38, the variations of the characteristic times τ_{N_1} and τ''_{N_1} are plotted. We remind that τ_{N_1} is used to determine the lower level N_{i_1} and the length of the period during which the smallest scales, i.e. for $\ell < \ell_{N_{i_2}}$, can be frozen. From Figure 36, we note that the lower level of the transition range, namely N_{i_1}, has to be larger than 256. In fact, we find N_{i_1} of the order of 320, for its lowest value. Figure 35 confirms that the time derivative of the velocity has a decaying spectrum.
On Figures 39, we have plotted the time evolution of the different terms appearing in the equation of the small scale components $\mathbf{z}_{N_1}$. As we have observed in the previous computations, the time derivative $\mid \dot{\mathbf{z}}_{N_1} \mid_2$ is of the order of the coupled nonlinear terms $\mid Q^N_{N_1} B_{int}(\mathbf{y}_{N_1}, \mathbf{z}_{N_1}) \mid_2$, while the dissipative norm $\nu \mid \Delta \mathbf{z}_{N_1} \mid_2$ is much smaller for lower values of N_1. For the scales lying far inside the dissipation range, we also note that all the quantities are of the same order.
Figure 40 show the vorticity at different time of the integration interval $[0, 50]$. The unstructured initial field disappear completely after a fiew times the eddy turnover time. After a short transient period, the flow evolves by keeping the same global structures. Figure 40 represents three–dimensional views of two–dimensional maps. Lighting technics have been used, so that shadow effects allow to see the very fine structures of the flow.

Figure 32: Energy spectrum at $t = 0,\ 15,\ 30,\ 50$.

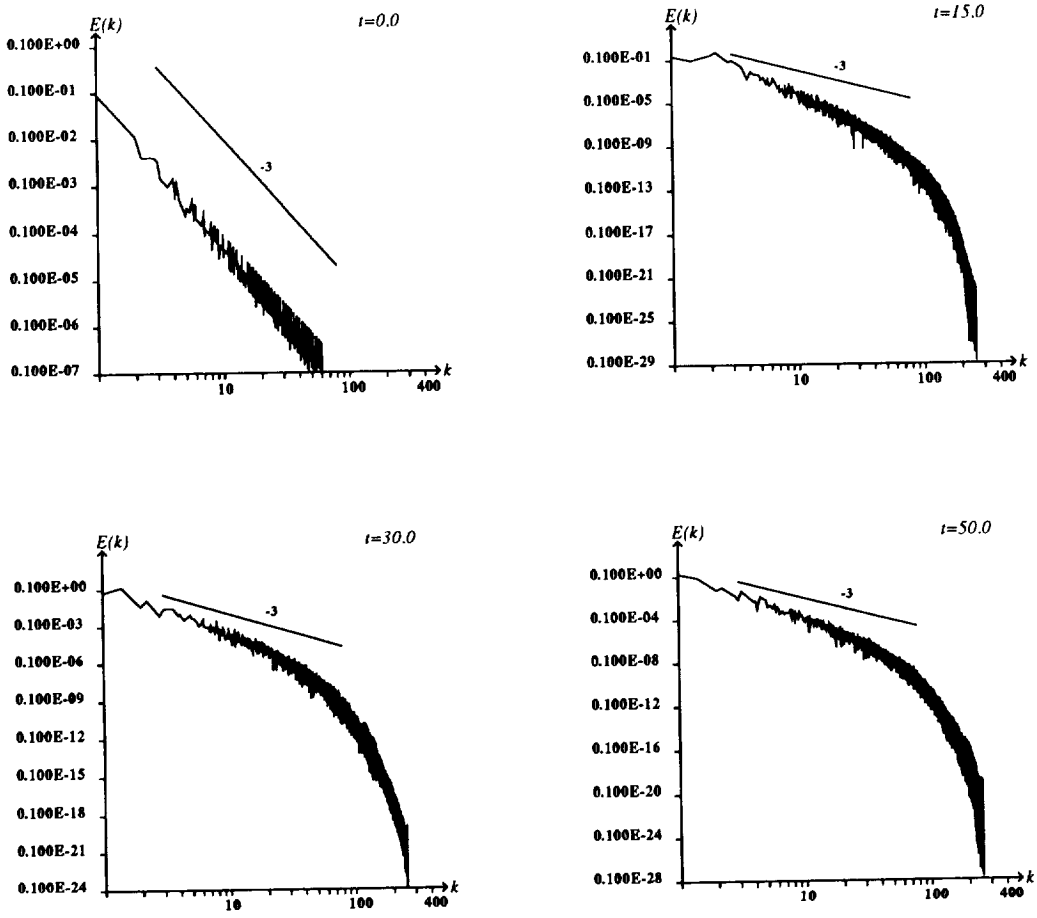

Figure 33: Time evolution of the ratio $\frac{|\mathbf{z}_{N_1}|_2}{|\mathbf{y}_{N_1}|_2}$ for $N_1 = 64$, 128, 256 and $N_1 = 480$.

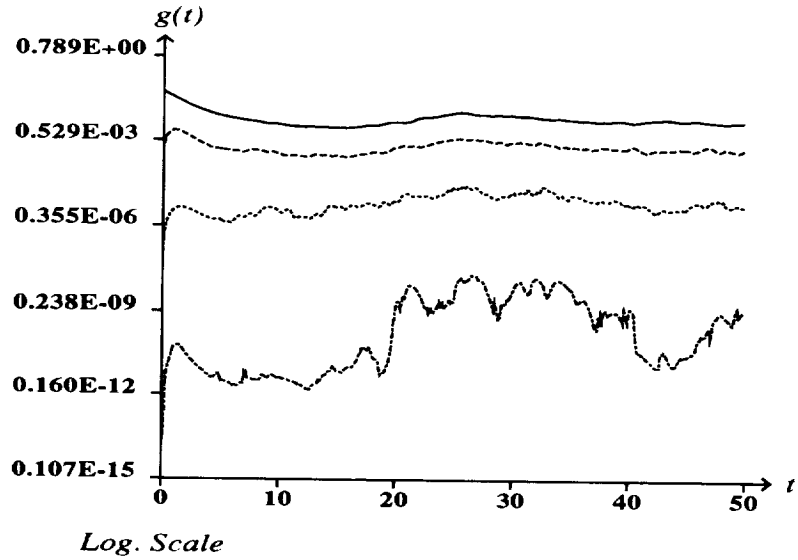

Figure 34: Time evolution of ratio $\frac{|P_{N_1} B_{\text{int}}(\mathbf{y}_{N_1}, \mathbf{z}_{N_1})|_2}{|P_{N_1} B(\mathbf{y}_{N_1}, \mathbf{y}_{N_1})|_2}$ for $N_1 = 64$, 128, 256 and $N_1 = 480$.

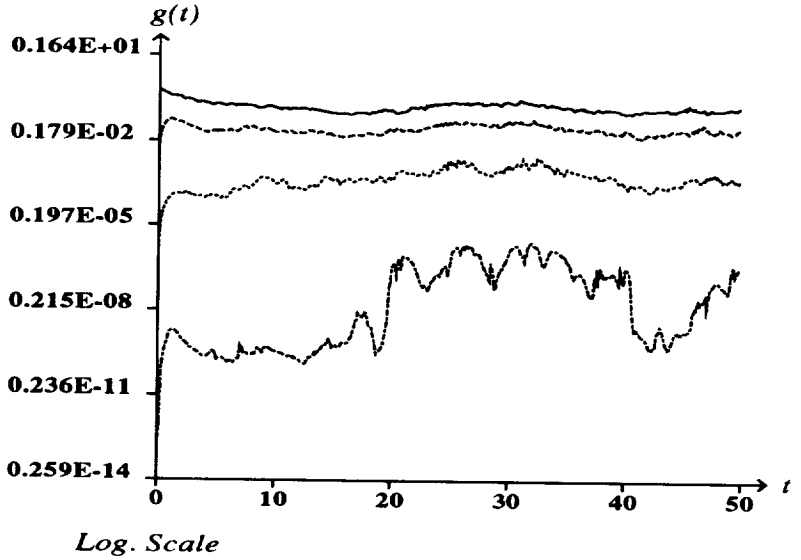

Figure 35: Time evolution of ratio $\frac{|\dot{\mathbf{z}}_{N_1}|_2}{|\dot{\mathbf{y}}_{N_1}|_2}$ for $N_1 = 64,\ 128,\ 256$ and $N_1 = 480$.

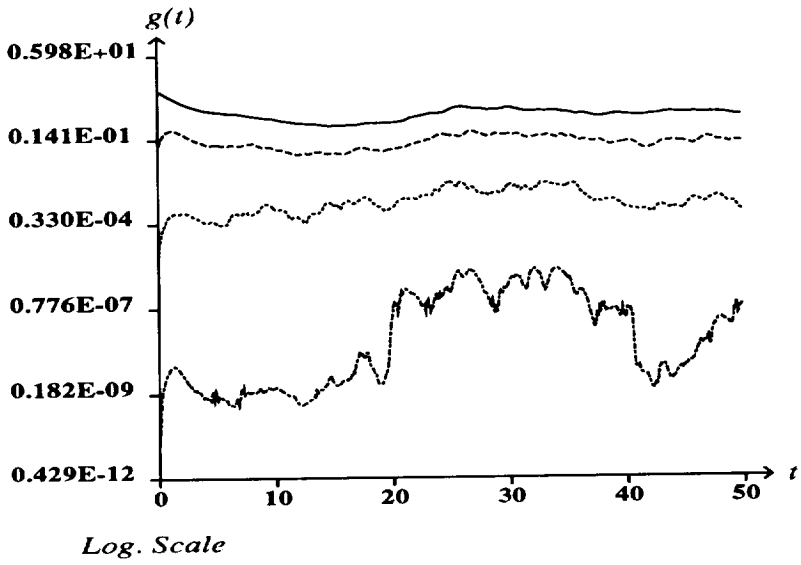

Figure 36: Time evolution of the levels N_{i_1} and N_{i_2}.

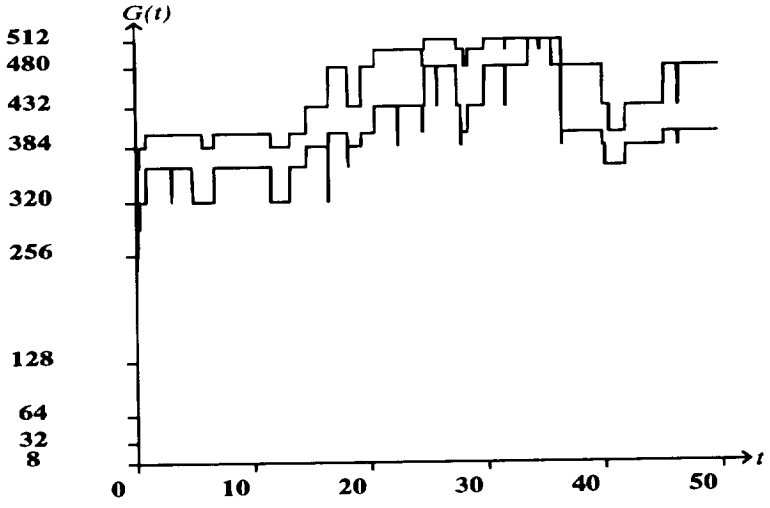

Figure 37: Time evolution of $\tau_{N_1}(\epsilon) = \frac{\epsilon}{|\dot{\mathbf{z}}_{N_1}(t)|_2}$ for $N_1 = 64,\ 128,\ 256$ and $N_1 = 480$.

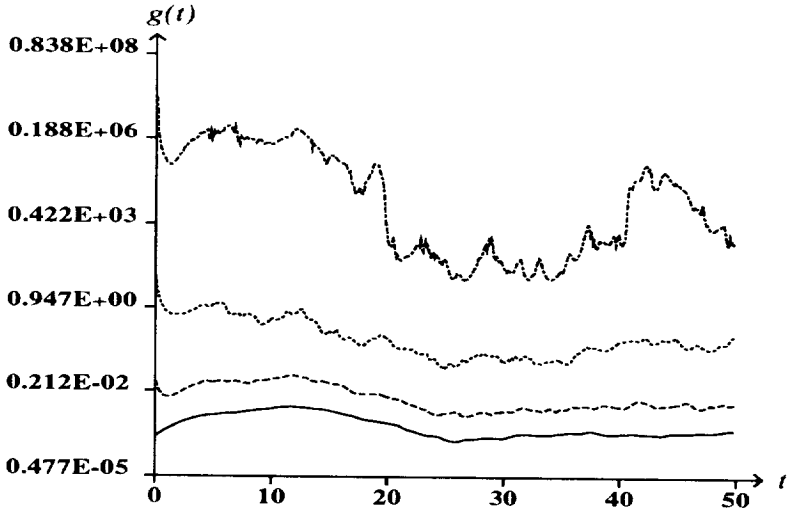

Log. Scale

Figure 38: Time evolution of $\tau''_{N_1}(\epsilon) = \left(\frac{2\epsilon}{|P_{N_1}\dot{B}(\mathbf{y}_{N_1}, \mathbf{z}_{N_1})|_2}\right)^{1/2}$ for $N_1 = 64,\ 128,\ 256$ and $N_1 = 480$.

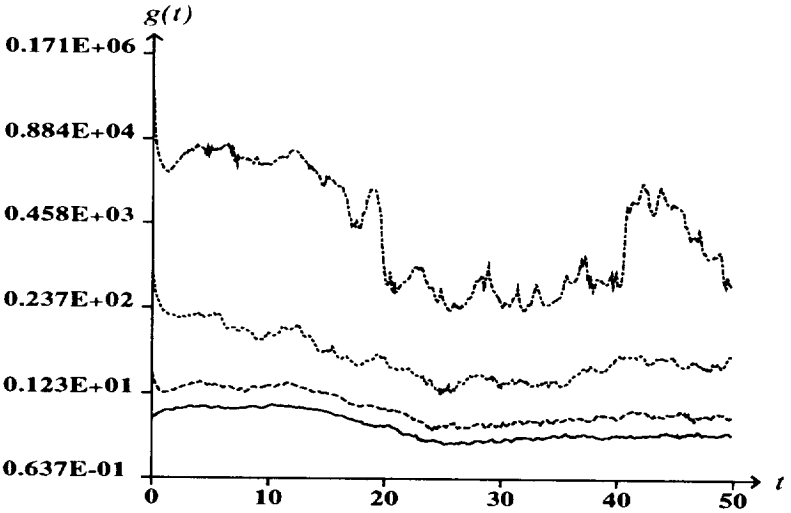

Log. Scale

Figure 39: Time evolution of (resp.) $\nu \mid \Delta \mathbf{z}_{N_1} \mid_2, \mid \dot{\mathbf{z}}_{N_1} \mid_2, \mid Q^N_{N_1} B(\mathbf{y}_{N_1}, \mathbf{y}_{N_1}) \mid_2$, and $\mid Q^N_{N_1} B_{\text{int}}(\mathbf{y}_{N_1}, \mathbf{z}_{N_1}) \mid_2$ for $N_1 = 64,\ 128,\ 256$ and $N_1 = 480$.

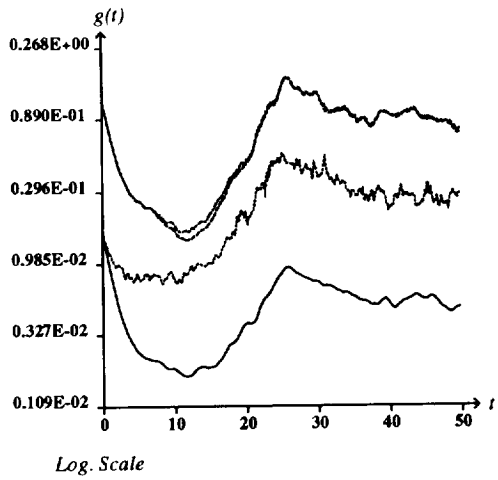

Log. Scale

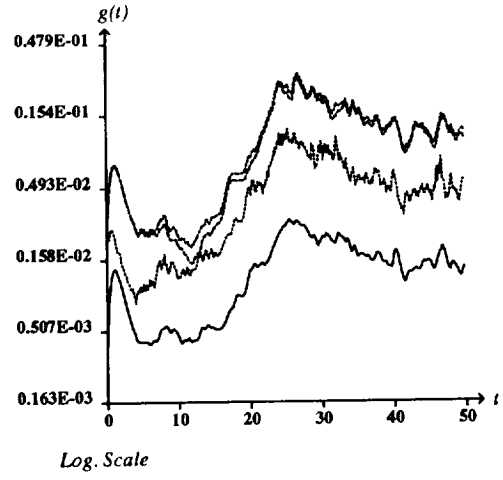

Log. Scale

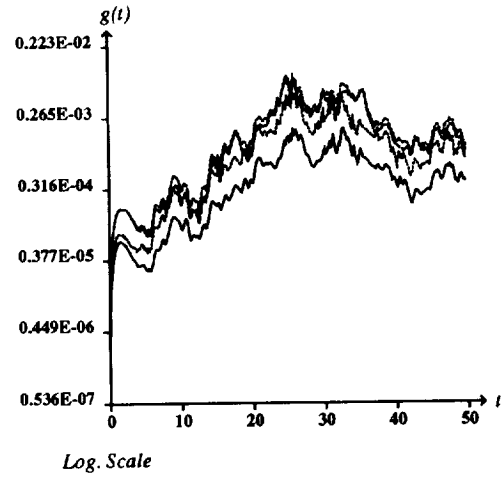

Log. Scale

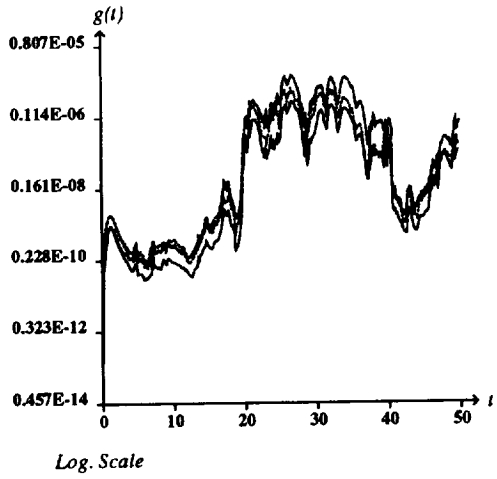

Log. Scale

Figure 40: Vorticity structures at time $t = 30$.

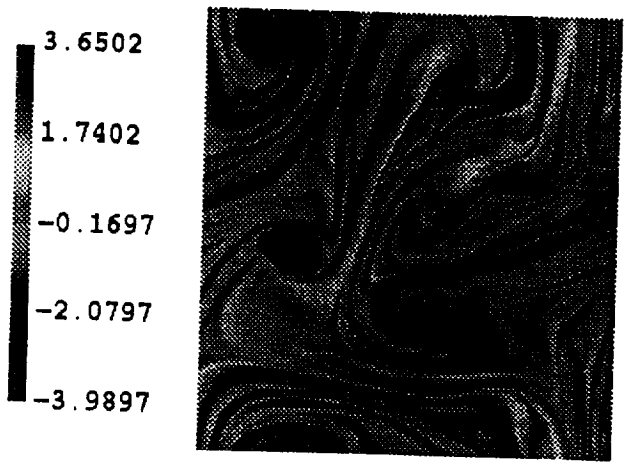

Figure 41: Vorticity structures at time $t = 50$.

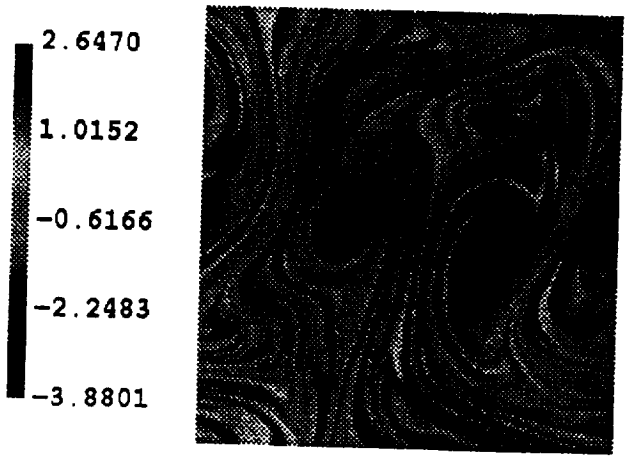

3.3 Simulation of the whole dissipation range with the multiscale method.

In this section, the example is the same as in the Section 3.1. Our purpose is to study the effect of the cut–off value N_{i_1} on the computed solution, so that several numerical experiments have been conducted. We have decreased N_{i_1} so that it is of the order of the dissipation wavenumber k_η ; the whole dissipation range is then modelized by the multiscale strategy described in previous sections. In both simulations, we have noted that the multilevel method allows to recover all the large structures of the flow. Finally, we have made a similar test with the classical method, i.e. we have decreased N in order to estimate the lower level required to recover the large scales.

3.3.1 Analysis of the numerical simulation.

In order to decrease the value of N_{i_1}, the parameter ε has been set to 10^{-2}. In this case, the level N_{i_1} adjusts itself, using the procedure described in Section 2, to the value 24 which is smaller than $N_\eta = 34$. Figure 43 shows the evolution of the two characteristic levels N_{i_1} and N_{i_2}, and Figure 44 shows the evolution of the characteristic time τ_c. The level N_{i_1} is quasiconstant and is equal to 24 while the level N_{i_2} is approximately equal to 128 ; N_{i_2} is chosen to be far inside the dissipation range. On Figures 42, we have represented the energy spectrum of the computed solution at different intermediate times of the interval $[0, 65]$ on which is conducted the computation. There is no energy pile–up at high wavenumbers and the dissipation of the enstrophy is well preserved. By comparing the vorticities obtained with this simulation and the Direct Numerical Simulation performed with the classical Galerkin (pseudospectral) method with a spatial resolution equal to $(256)^2$, we note that all the large scale vortices are well described by the multilevel method. At the times $t = 60$ and $t = 65$, we still have the fusion previously mentioned. We also note that oscillations appear on the domain. They are due to the approximation made on the small scales. They also point out the problem of separation of scales related with a Fourier decomposition. Indeed, Fourier waves oscillate over the whole domain and they can not be directly associated with a scale vorticity. This nonlocal property implies the oscillation appearing on Figures 47. Nevertheless, it appears clearly that all the large

Table 7	$u_1^{GU}(x_1, x_2)$	$u_1^{GNL}(x_1, x_2)$	Difference
$t = 10$	$0.8299845080\ 10^{-1}$	$0.8355520907\ 10^{-1}$	$5.56\ 10^{-4}$
$t = 20$	0.2091267106	0.2087057712	$4.21\ 10^{-4}$
$t = 30$	0.3664263833	0.3652791132	$1.14\ 10^{-3}$
$t = 40$	$0.2926552919\ 10^{-1}$	$0.2587214575\ 10^{-1}$	$3.39\ 10^{-3}$
$t = 50$	0.2458823192	0.2432537325	$2.63\ 10^{-3}$
$t = 60$	0.1573811778	0.1414418124	$1.59\ 10^{-2}$

Table 8	$u_1^{GU}(x_1, x_2)$	$u_1^{GNL}(x_1, x_2)$	Difference
$t = 10$	$-0.7118241214\ 10^{-1}$	$-0.7088992727\ 10^{-1}$	$2.92\ 10^{-4}$
$t = 20$	0.1478691156	0.1470191181	$8.49\ 10^{-4}$
$t = 30$	0.4236670791	0.4264640060	$2.79\ 10^{-3}$
$t = 40$	0.4898684126	0.4800345247	$9.83\ 10^{-3}$
$t = 50$	0.3592114126	0.3480702322	$1.11\ 10^{-2}$
$t = 60$	0.5173406258	0.5179894219	$6.48\ 10^{-4}$

structures are captured with the multilevel method.

The total CPU time required for this simulation is about 4796 seconds and the difference in L^2 (or energy) norm with the solution obtained with the previous DNS is of the order of $3.6\ 10^{-3}$ at $t = 50$. The upper level N_{i_2} of the multilevel procedure is approximatively equal to 128 during the whole computation. The small scale energy on this level is less than 10^{-8} and then much less than ε. Hence, the level N_{i_2} can be decreased to at least 64 as we can see on Figure 16 ; in that case, the CPU time will be reduced.

On tables 7 and 8, we have compared the solutions obtained here with the one obtained by direct simulation. It appears that the difference between the two solutions is of the order of 10^{-2} and hence, of the order of ϵ. The oscillations, appearing on Figures 45, 46,and 47 are probably due to the fact that the intermediate scales, lying in the inertial range and corresponding to wavenumbers larger than $k_{N_{i_1}}$, are not relaxed at each time iteration. A

better understanding of the effects of the multilevel procedure on these scales must be done in order to improve the results presented here.

3.3.2 Comparison with a low resolution Galerkin simulation.

Finally, in order to show the efficiency of the multilevel method on such simulations, we have performed an additional test with the classical method. Indeed, we have first fixed the total number of modes to 32 and we have integrated the system over $50,000$ time iterations, which corresponds to the time interval $[0, 50]$. The solution obtained is different than the one obtained when a Direct Simulation is done, i.e. with 256 modes. Figure 47 shows the vorticity structures obtained with this simulation at time $t = 50$. The number of modes is not sufficiently large so that the large scales can not be computed. The vorticity looks like a non-structured quantity. Figure 48 shows the energy spectrum at different time of the interval $[0, 50]$. By fixing the resolution to $(32)^2$, it seems that we do not allow the appearance of small scales and their dissipation mechanism occuring in the viscous range, the dynamic of the flow is drastically modified. We note that this simulation is stable in the sense that no quantity grows artificially. A similar simulation has been done with $N = 48$ instead of $N = 32$. The picture of the flow (see Figures 47, 49) is more realistic than in the previous case. The large scales of the flow are almost well captured. Nevertheless, the simulation performed with the multilevel method with a lower level $N_{i_1} = 24$ gives a better qualitative result. The CPU time required by this simulation is 2730 seconds and the difference with the DNS is of the order of $3.1\ 10^{-3}$ in L^2 norm. Hence, the accuracy recovered here is the same as the one obtained with the multilevel level method when $N_{i_1} = 24$. The result obtained here confirms the fact that, in the previous computation, the level N_{i_2} can be decreased to 48 ; in such a case, the CPU time required by the multilevel method will be at least two times less than 2730 seconds.

To conclude, we have proved with these experiences that the multilevel method allows to modelize the whole dissipation range and the end of the inertial range without disturbing the large scales of motion. Moreover, we have shown that if the small scales lying in the dissipation range can be modelized, as well as their interaction with the large scales, they are essential

to describe the evolution of the flow.

Figure 42: Energy spectrum at $t = 5,\ 20,\ 35,$ and 50.

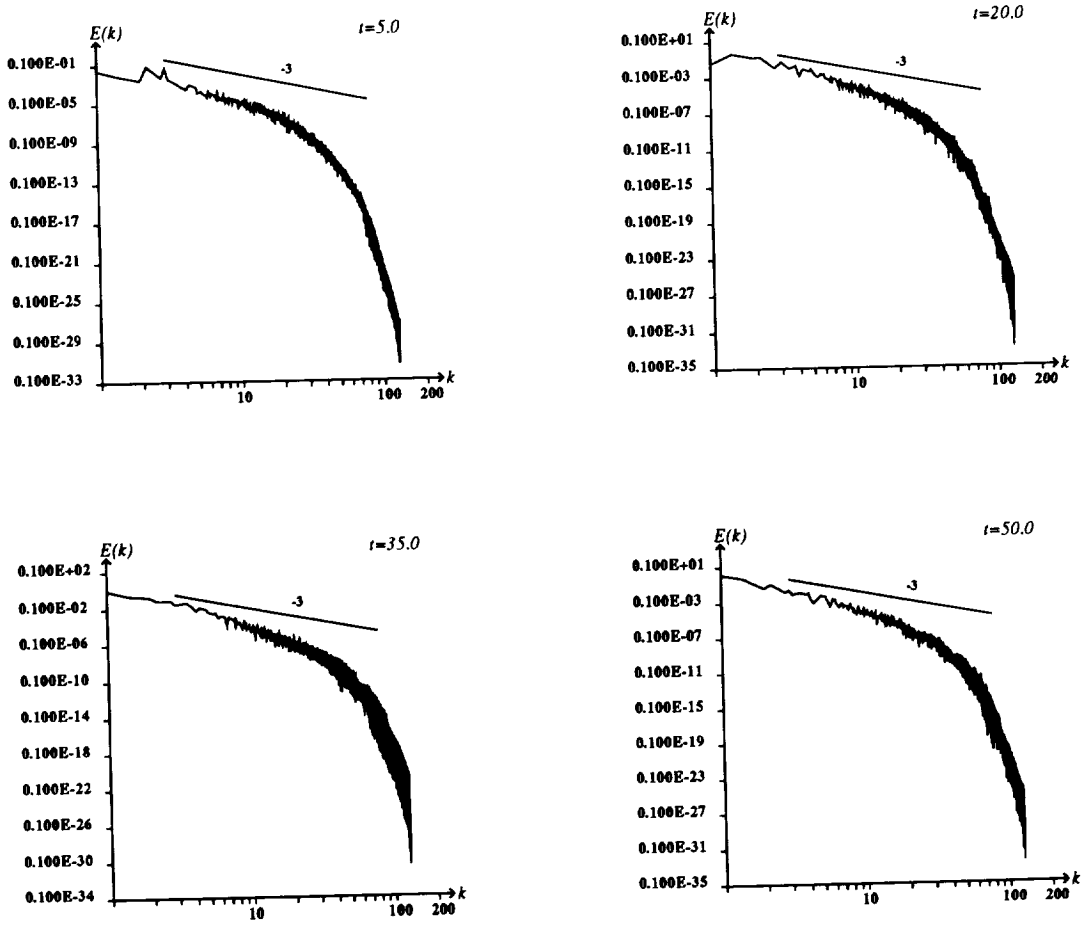

Figure 43: Time evolution of the levels N_{i_1} and N_{i_2}.

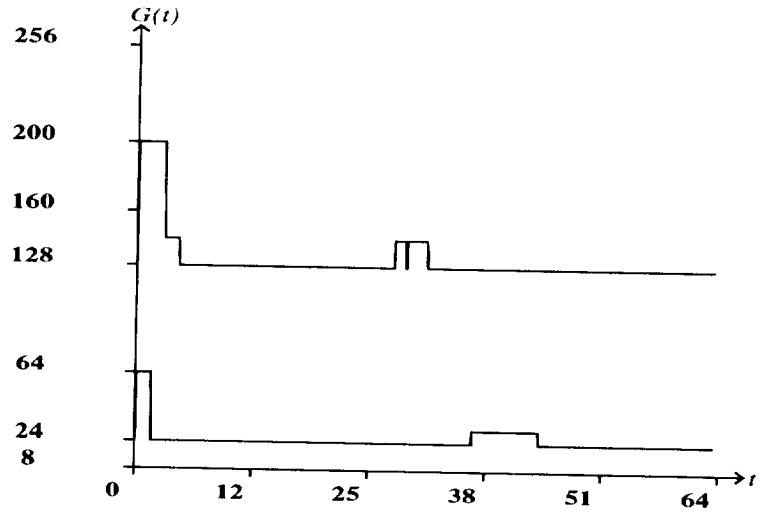

Figure 44: Time evolution of the characteristic length of cycles.

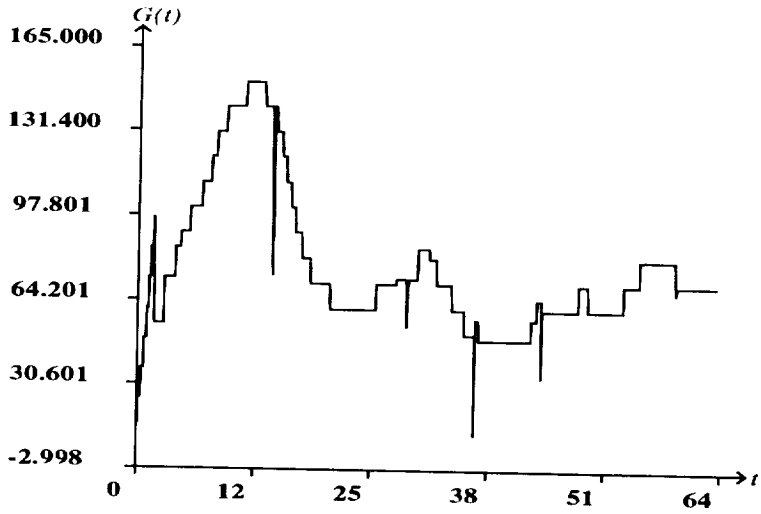

Figure 45: Comparison of the vorticity structures at time $t = 60$.

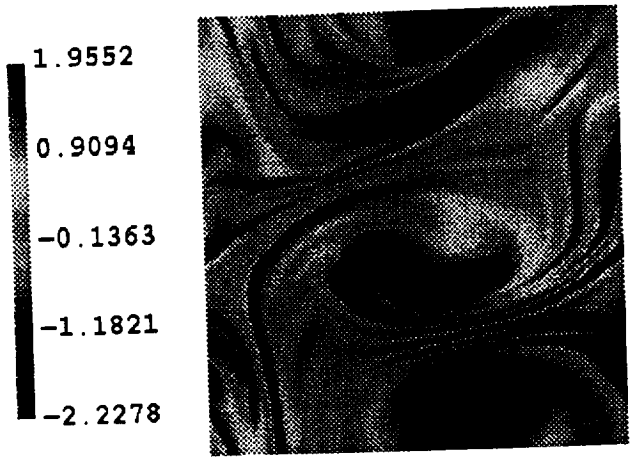

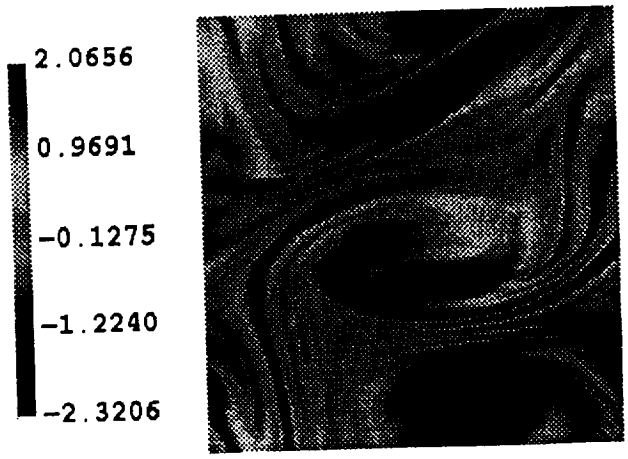

Figure 46: Comparison of the vorticity structures at time $t = 65$.

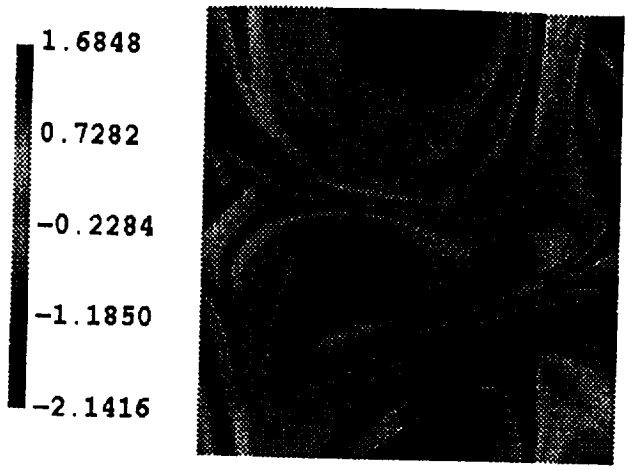

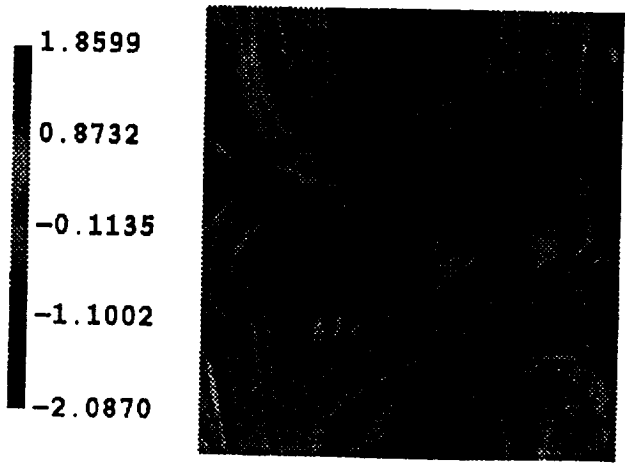

Figure 47: Comparison of the vorticity structures obtained with the classical Galerkin method for $N = 256$ and $N = 32$, at time $t = 50$.

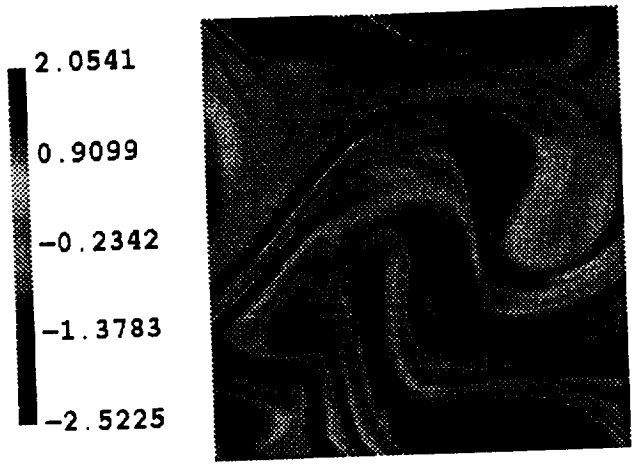

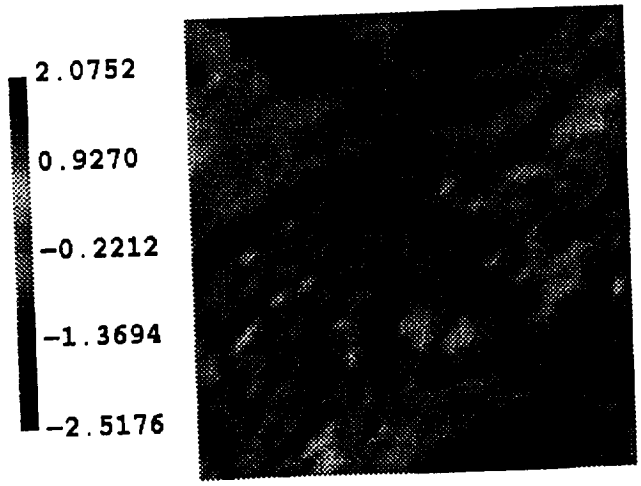

Figure 48: Energy spectrum at $t = 5,\ 20,\ 35,$ and 50.

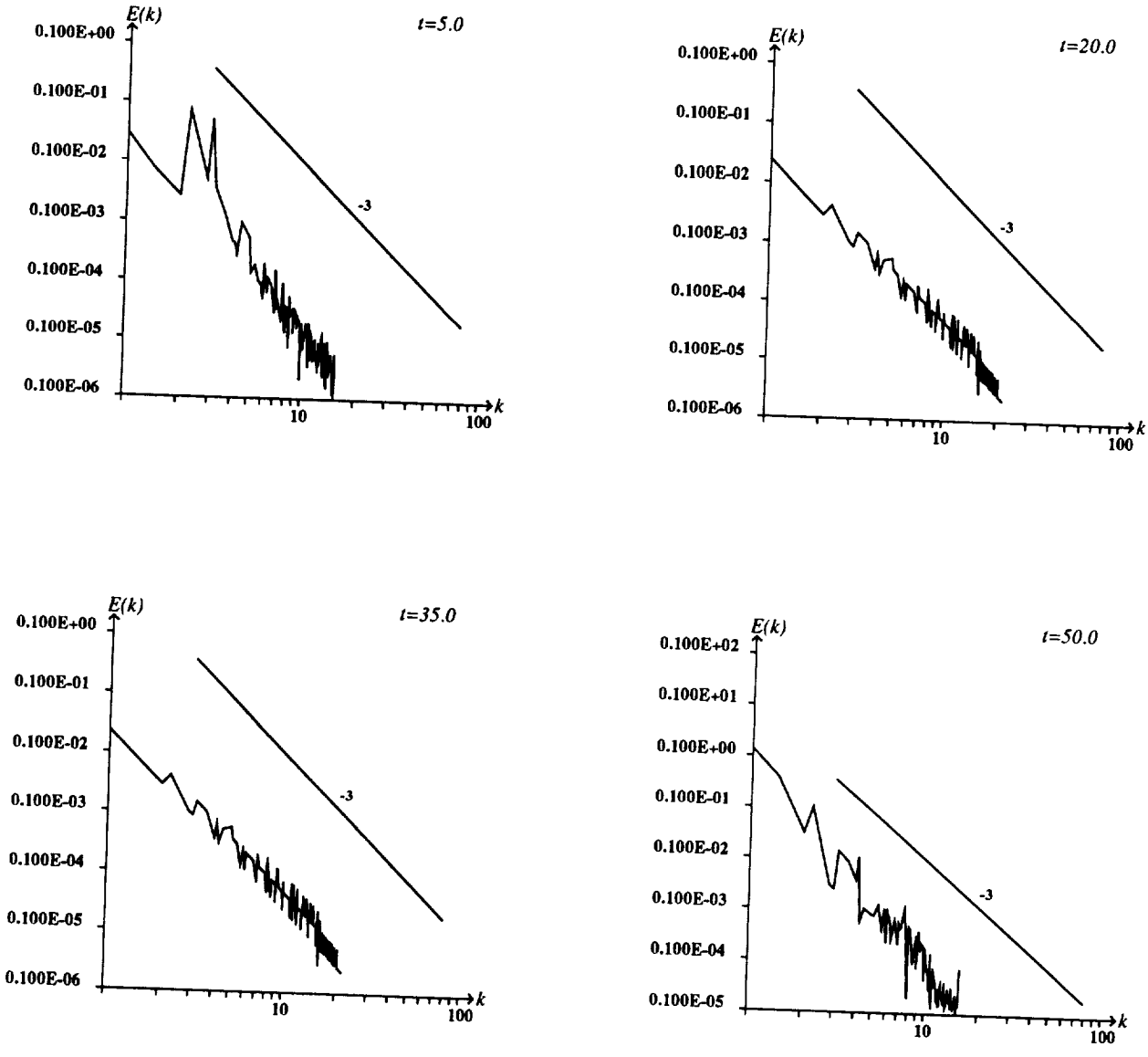

Figure 49: Comparison of the vorticity structures, between results obtained with the classical method for $N = 256$ and $N = 48$, at time $t = 50$.

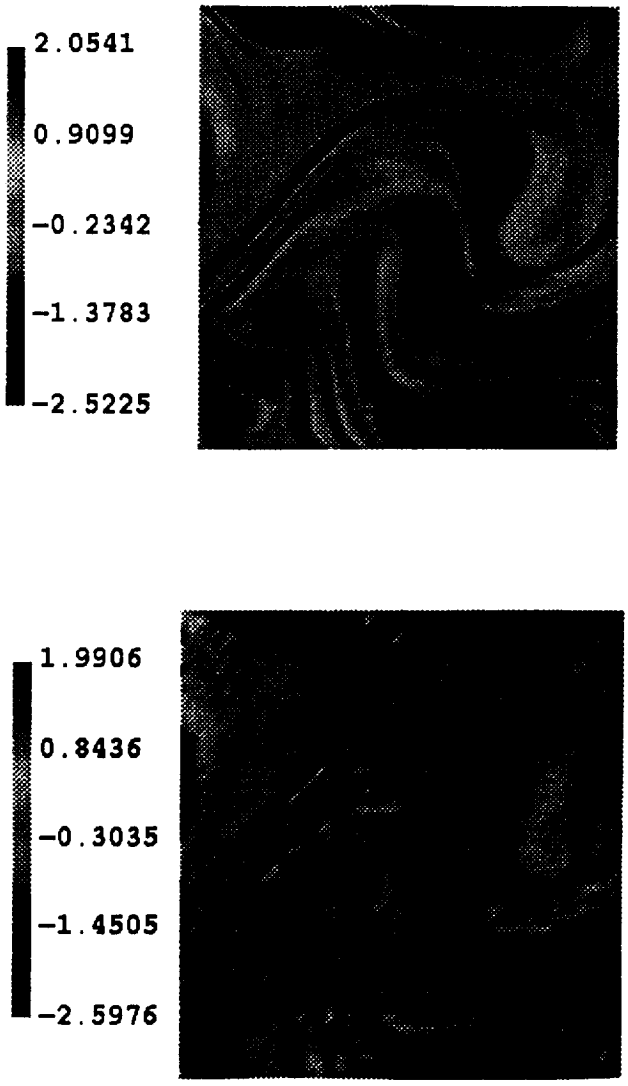

Figure 50: Energy spectrum at $t = 5,\ 20,\ 35,$ and $50.$

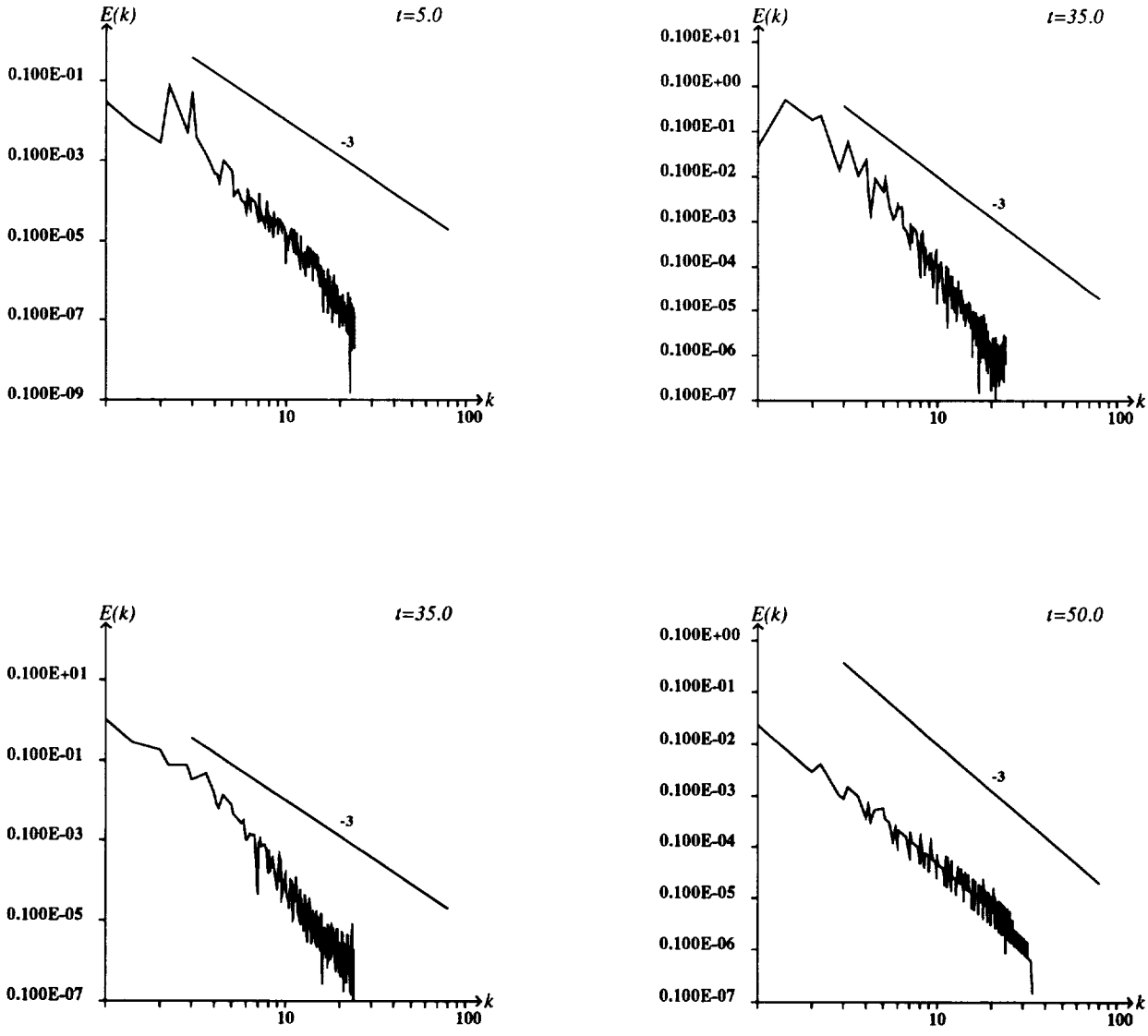

Conclusions

In this article, we have proposed a multilevel method which treats differently the large and the small scales of homogeneous isotropic flows. Moreover, we have derived mathematical estimates for all the parameters (cut-off level, time scales) involved in this dynamical procedure leading to a completely self-adaptive procedure. Firstly, several computations have been conducted in the context of DNS, i.e. the whole spectrum up to the dissipative scale was simulated. In such case, the multi-level method is able to recover a velocity field with the same spatial resolution than the Galerkin method, but with a substantial speed-up of at least 2 in CPU time.

Secondly, in an approach similar to LES, we have decreased the number of modes retained for the resolved scales and used the same algorithm to modelize the interaction between the low and high frequencies. In such case, we have seen that when the resolved scales are larger than the dissipative ones, but of the same order of magnitude (1/12 as compared to 1/17), the large eddies of the flow are captured correctly; this is not the case when the pseudo-spectral Galerkin method is used with only 32^2 modes, i.e. with a larger scale of the order of 1/16.

Although, we only presented computational for moderately large Reynolds numbers, where the small scales are strongly dependent on the energy-containing eddies, we think that these results are very promising. Indeed, we can reasonably hope that the multilevel (nonlinear Galerkin) method can be used efficiently for Large Eddy Simulations. Results on this point will be presented elsewhere, in the case of two and three dimensional homogeneous isotropic flows.

Finally, we want to observe that, by opposition with LES methods, no assumptions on the energy spectra or on the velocity correlations are made here. Therefore the method can be applied to the simulation of non-homogeneous flows. First attempts have been made in this direction, for the channel flow problem. Our efforts will be concentrated on this problem in the near future.

Acknowledgments

The work was partially supported by NFS grant DMS 9024769 and DOE DE-FG02 – 92ER25120. The computations were made on the Cray2 of the

National Center for Supercomputing Applications (NCSA, Illinois) and the Cray2 of the Centre de Calcul Vectoriel pour la Recherche (CCVR, Palaiseau).

References

[1] C.Foias, O.Manley and R.Temam, *Modelling of the interaction of small and large eddies in two dimensional turbulent flows*, M^2AN, **Vol. 22**, p. 93, (1988).

[2] M.Marion and R.Temam, *Nonlinear Galerkin Methods*, SIAM J. Num. Anal., **Vol. 26**, p. 1139, (1989).

[3] M.Marion and R.Temam, *Nonlinear Galerkin Methods : The Finite Elements case*, Numerische Mathematik, **vol 57**, (1990), pp. 205 – 226.

[4] R. Temam, *Inertial Manifolds and Multigrid Methods*, S.I.A.M. J. Math. Anal., **vol 21**, (1990), pp. 154 – 178.

[5] F.Jauberteau, C.Rosier and R.Temam , *A Nonlinear Galerkin Method for the Navier-Stokes equations*, Computer Meth. in Appl. Mechanics and Engineering, **Vol. 80**, p. 245,(1990).

[6] F.Jauberteau, C.Rosier and R.Temam , *The Nonlinear Galerkin Method in computational fluid dynamics*, Applied Numerical Mathematics, **Vol. 6**,p. 361,(1989/90).

[7] T. Dubois, F.Jauberteau et R.Temam, *Solution of the incompressible Navier–Stokes equations by the nonlinear Galerkin method*, to appear in Journal of Phys. Computation.

[8] T.Dubois and R.Temam *Separation of Scales in Turbulence Using the Nonlinear Galerkin Method*, Advances in Computational Fluid Dynamics , W.G.Habashi et M.Hafez ed., Gordon and Breach Publishers, 1993.

[9] C.Foias, O.Manley and R.Temam, *Approximate inertial manifolds and effective viscosity in turbulent flows*, Phys. Fluids A3, 1991.

[10] F.Jauberteau, *Résolution numérique des équations de Navier-Stokes instastionnaires par méthodes spectrales. Méthode de Galerkin nonlinéaire*, Thèse Université de Paris-Sud, 1990.

[11] C.Canuto, Y.Hussaini, A.Quarteroni and T.Zang, *Spectral Methods in Fluid Dynamics*, Springer Verlag, New York (1988).

[12] R. Temam, *Navier-Stokes equations*, North Holland, 1977.

[13] R. Temam, *Infinite dimensional dynamical systems in mechanics and physics*, Applied Mathematical Sciences 68, Springer Verlag, 1988.

[14] R.H.Kraichnan, *Inertial ranges in two-dimensional turbulence*, Phys. Fluids, **Vol. 10**, p. 1417, (1967).

[15] R.H.Kraichnan and D.Montgommery, *Two-dimensional turbulence*, Rep. Prog. Phys., **Vol. 43**, 1980.

[16] P.Constantin, C.Foias, M.Manley and R.Temam, *Determining modes and fractal dimension of Turbulent flows*, J. Fluid Mech., **Vol. 150**, (1985), pp. 427 – 440.

[17] C.Badevant and F.Pascal, *Nonlinear Galerkin method and subgrid scale model for 2D turbulent flows*, to appear in Theoritical and Computational Fluid Dynamics.

[18] R.Temam, *Induced trajectories and approximate inertial manifolds*, Math. Mod. and Num. Anal. (M^2AN), **Vol. 32**, p. 163, (1988).

[19] R.Temam, *Attractors for the Navier-Stokes equations, localization and approximation*, J. Fac. Sci., Tokyo, Sec. IA, **Vol. 36**, p. 629, (1989).

[20] A.Debussche and R.Temam, *Convergent families of approximate inertial manifolds*, to appear in J. Math. Pures Appl.

[21] A.Debussche and T.Dubois, *Approximation of exponential order of the attractor of the Navier-Stokes equations*, to appear in Physica D, 1994.

[22] M.Lesieur, *Turbulence in fluids. Stochatics and numerical modelling*, Klurver Academic Publishers, $2^{\underline{nd}}$ revised edition.

[23] S.A.Orszag, in Proc. 5^{th} Intl. Conf. on Numerical Methods in Fluids Dynamics, Lecture Notes in Physics, **Vol. 59**, p. 32 (1977).

[24] M.E.Brachet, M.Meneguzzy, H.Politano and P.L.Sulem, *The dynamics of freely decaying two-dimensional turbulence*, J. Fluid Mech., **Vol. 194**, pp. 333 – 349 (1988).

REPORT DOCUMENTATION PAGE

Form Approved
OMB No. 0704-0188

1. AGENCY USE ONLY(Leave blank)	2. REPORT DATE	3. REPORT TYPE AND DATES COVERED
	December 1993	Contractor Report

4. TITLE AND SUBTITLE
THE NONLINEAR GALERKIN METHOD: A MULTI-SCALE METHOD APPLIED TO THE SIMULATION OF HOMOGENEOUS TURBULENT FLOWS

5. FUNDING NUMBERS
C NAS1-19480
WU 505-90-52-01

6. AUTHOR(S)
A. Debussche
T. Dubois
R. Temam

7. PERFORMING ORGANIZATION NAME(S) AND ADDRESS(ES)
Institute for Computer Applications in Science
and Engineering
Mail Stop 132C, NASA Langley Research Center
Hampton, VA 23681-0001

8. PERFORMING ORGANIZATION REPORT NUMBER
ICASE Report No. 93-93

9. SPONSORING/MONITORING AGENCY NAME(S) AND ADDRESS(ES)
National Aeronautics and Space Administration
Langley Research Center
Hampton, VA 23681-0001

10. SPONSORING/MONITORING AGENCY REPORT NUMBER
NASA CR-191581
ICASE Report No. 93-93

11. SUPPLEMENTARY NOTES
Langley Technical Monitor: Michael F. Card
Final Report
Submitted to Theoretical and Computational Fluid Dynamics

12a. DISTRIBUTION/AVAILABILITY STATEMENT
Unclassified–Unlimited

Subject Category 34

12b. DISTRIBUTION CODE

13. ABSTRACT *(Maximum 200 words)*

Using results of DNS in the case of two-dimensional homogeneous isotropic flows, we first analyze in detail the behavior of the small and large scales of Kolmogorov like flows at moderate Reynolds numbers. We derive several estimates on the time variations of the small eddies and the nonlinear interaction terms; those terms play the role of the Reynolds stress tensor in the case of LES. Since the time step of a numerical scheme is determined as a function of the energy-containing eddies of the flow, the variations of the small scales and of the nonlinear interaction terms over one iteration can become negligible by comparison with the accuracy of the computation. Based on this remark, we propose a multilevel scheme which treats differently the small and the large eddies. Using mathematical developments, we derive estimates of all the parameters involved in the algorithm, which then becomes a completely self-adaptive procedure. Finally, we perform realistic simulations of (Kolmorov like) flows over several eddy-turnover times. The results are analyzed in detail and a parametric study of the nonlinear Galerkin method is performed.

14. SUBJECT TERMS
Multi-Resolution Method; Nonlinear Galerkin Computational Fluid Mechanics; Modelling of Turbulence

15. NUMBER OF PAGES
87

16. PRICE CODE
A05

17. SECURITY CLASSIFICATION OF REPORT	18. SECURITY CLASSIFICATION OF THIS PAGE	19. SECURITY CLASSIFICATION OF ABSTRACT	20. LIMITATION OF ABSTRACT
Unclassified	Unclassified		